Comprehensive evaluation of oxidative capacity of ambient air with new detection technique of HOx (OH, HO_2) radical production rate

（HOx (OH, HO_2) ラジカル生成速度の新規測定法による、実大気が持つ酸化能の包括的な評価）

Tsurumaru Hiroshi

鶴丸　央

Doctor of Global Environmental Studies

Comprehensive evaluation of oxidative capacity of ambient air with new detection technique of HOx (OH, HO_2) radical production rate

Kyoto University Graduate School of Global Environmental Studies

Tsurumaru Hiroshi

Academic Adviser: Yoshizumi Kajii

January, 2015

Abstract

ROx (OH, HO_2, and RO_2) radical play an important role as oxidant agent. ROx radical can oxidize atmospheric trace species such as CO, NOx (NO and NO_2), and VOCs (Volatile Organic Compounds), and generate photochemical oxidant, O_3, and SOA (Secondary Organic Aerosol) as oxidation products. O_3 and SOA are harmful to human body, and vegetation, also these can affect the radiation budget by absorption or reflection of sunlight. It is necessary to understand behavior of ROx radicals for elucidation of the effect to the environment. ROx radical production process can be divided to two pathways, photolysis and ozonolysis. Photolysis can occur only in daytime, when sunlight is available. Whereas ozonolysis driven by ozone during daytime and also nighttime whenever O_3 is exist. Ozonolysis is important throughout a day. O_3 can react with olefins, which is unsaturated VOCs, and generates HOx mainly. Even though HOx production from ozonolysis is well-understood by laboratory measurement for several species of olefins, existence of many kinds of unidentified VOCs are reported, and much complex schemes of O_3 and olefin reaction are predicted. It suggests that comprehensive measurement underestimate HOx production in atmosphere. In this research, we developed a new direct measurement technique of HOx radical production rate from ozonolysis. O_3 is added to ambient air, and generated ROx concentration within reaction tube is measured by PERCA/LIF (PEroxy Radical Chemical Amplification / Laser Induced Fluorescence) technique. Generated ROx concentration is measured as function of added O_3 concentration. To avoid underestimation at high O_3 period, slope of ROx concentration at close to O_3 = 0 ppb, is divided by reaction time to calculate HOx production rate from ozonolysis, PHOx. For measuring fundamental experiments of PHOx, isoprene, which is most abundant olefin in the atmosphere was used. Generated ROx concentration from isoprene and O_3 reaction is measured under several O_3 concentration and also several isoprene concentration are measured. To assess heterogeneous loss in reaction tube, instrument function, K was estimated with MCM model calculation. Measured PHOx value was corrected according to K. PHOx measurement of ambient air has been held with tedlar bag. In the PERCA/LIF technique, ambient NO_2 and O_3 are counted as background signal. To avoid over/underestimation of background signal caused by fluctuation of ambient NO_2 and O_3 concentration, first ambient air was sampled in tedlar bag, then injected to reaction tube with added O_3. Ambient PHOx was measured at Kyoto University and Wakayama Research Forest with several comprehensive measurement technique for other trace species such as NOx, VOCs and aerosols.

Table of Contents

Table of figures

Tables

1. Introduction

In the atmosphere, many kinds of chemical species are emitted. From middle of 18 century, utilization of significant amount of fossil fuel was started. Some of the released trace species have characteristic property, for example greenhouse effect.

Chemical species released to atmosphere from biogenic, and anthropogenic source was oxidized in the atmosphere then form secondary products or removed from gas phase (Fig.1-1). In the case of this oxidant rich condition, earth's atmosphere has a capacity of the oxidation. Without an efficient oxidation process, concentrations of emitted species elevated up then produce significant change of the condition of atmosphere and biosphere and climate through the greenhouse effect such kinds of CH_4 or N_2O. This cleaning process in atmosphere is controlled by oxidants and estimated by using "oxidation capacity".

Cheng et al. (2008) described quantitative oxidation capacity as below. When trace specie C react with oxidant X (Eq(1-1)), time dependence of C can describe as Eq (1-2).

$$C + X \rightarrow C';k \qquad (1\text{-}1)$$

$$\frac{dC}{dt} = -k[C][X] \qquad (1\text{-}2)$$

The removal of C is assessed as a pseudo-first order reaction, then k[X] is defined as the rate constant of this reaction expressed as K_{por}, which is inverse of lifetime of C in the atmosphere. When C reacts with more than one kind of oxidants, Eq(1-1) can be described as follow

$$C + X_1 \rightarrow C_1';k_1$$
$$C + X_2 \rightarrow C_2';k_2$$
$$C + X_3 \rightarrow C_3';k_3$$
$$\cdots$$
$$C + X_n \rightarrow C_n';k_n \qquad (1\text{-}1)'$$

Then time dependence of C can be expressed in Eq(1-2)'

$$\frac{d[C]}{dt} = \sum_{i=1}^{n} -k_i[C][X_i] \qquad (1\text{-}2)'$$

And also other compounds C_1, C_2… C_n can react with several oxidant. Finally Total reaction rate constant can be represent as Eq(1-3)

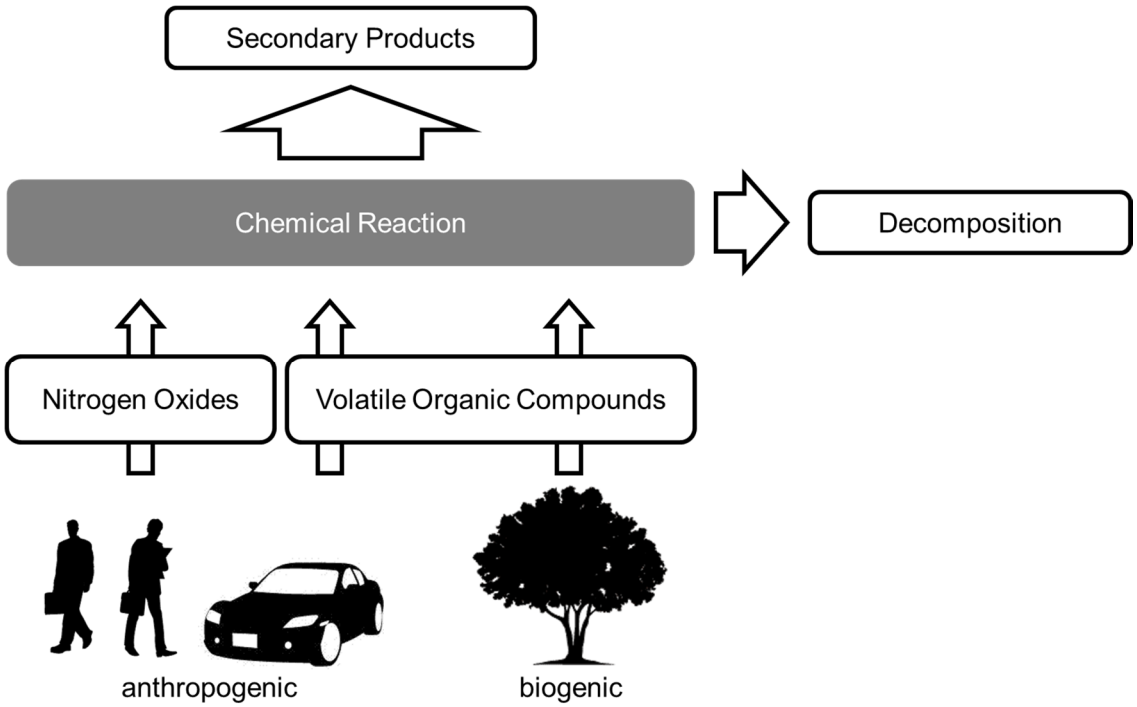

Fig.1-1 Oxidation process in the atmosphere

$$K_{\mathrm{por,T}} = \frac{\sum_{j=1}^{m}\left\{[C_j]\sum_{i=1}^{n} k_{ij}[X_i]\right\}}{\sum_{j=1}^{m}[C_j]} \qquad (1\text{-}3)$$

It is needed to measure oxidant and reactant concentration, also reaction rate constant when oxidation capacity which can determine lifetime of trace species in atmosphere is estimated. In this research, we focused on oxidant, especially generation process of it in new method.

1.1 ROx radical chemistry in atmosphere

ROx (OH, HO_2, and RO_2) radicals have an important role in atmosphere as oxidizing agent. VOC (Volatile Organic Compounds), or NOx species can be oxidized by ROx radicals, and determined life time in atmosphere. In this section, role and behavior of ROx radical species will be discussed.

1.1.1 OH radical

Hydroxyl radical, OH, plays most important role as main oxidant agent in atmosphere. Weinstock (1969) suggests the oxidation of CO by reaction with OH radical. OH radical

can react with most of species in atmosphere and determine life time of compounds except for CO_2, N_2O or CFCs (Chloro Fluoro Carbons). Many species of VOCs are emitted to atmosphere significantly, and OH radical can react with most of items, such as paraffin, olefin, alkynes so on.

General reaction of paraffin and OH radical is indicated in Fig.1-2. First OH removes hydrogen atom from paraffin then form H_2O. Hydrogen-subtracted paraffin forms alkoxy radical, and react with oxygen in the atmosphere quickly then form peroxy radical, RO_2, explained in detail in section 1.1.3.

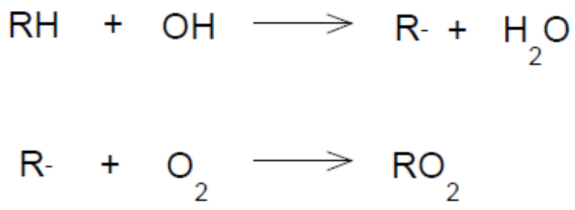

Fig.1-2 Reaction scheme of paraffin and OH radical.

The reaction scheme of olefin and OH radical is shown in Fig.1-3. First OH radical approaches to carbon-carbon double bond, then form intermediate. In the presence of third body, energy rich intermediate collisionally stabilized then form alkoxy radical.

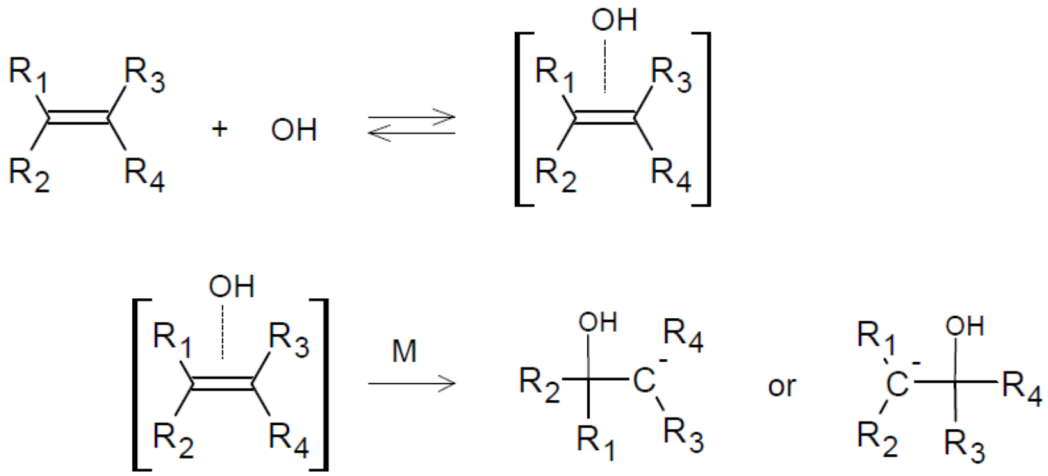

Fig.1-3 Reaction scheme of olefin and OH radical

Also OH radical can react with aromatic compounds. Reaction scheme is shown in Fig.1-4. The reaction scheme can be divided two pathways, hydrogen absorption and OH addition. In the case of hydrogen absorption, alkoxy radical formed same as the case of

the reaction of paraffin and OH radical. In the case of OH addition, ambient O_2 absorb hydrogen atom from intermediate and forms HO_2 radical.

As explained above, OH radical can react with several VOCs and determine the lifetime of each VOCs.

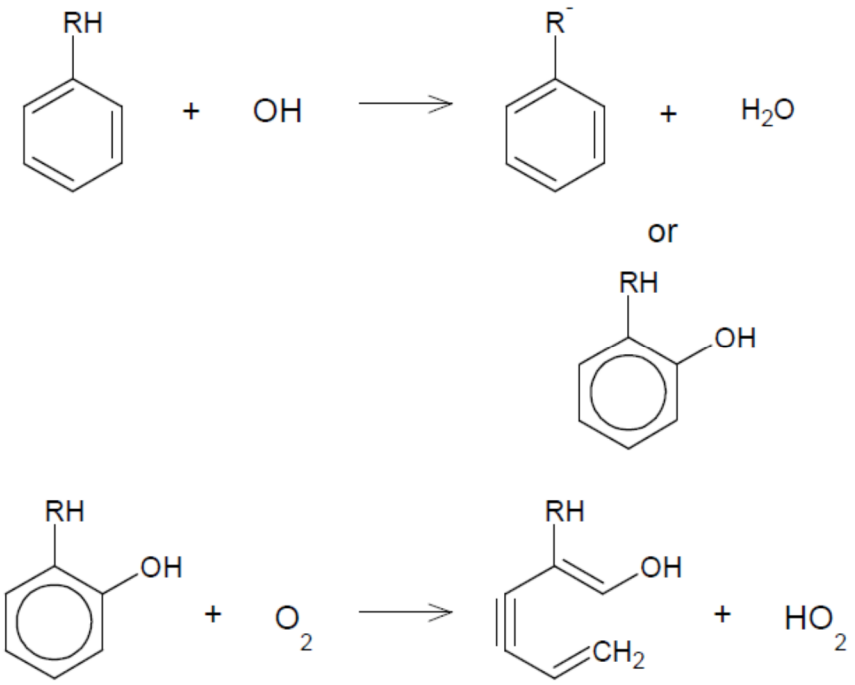

Fig.1-4 Reaction scheme of aromatics and OH radical

1.1.2 HO_2 radical

Hydroperoxy radical, HO_2 also plays important role in troposphere along with OH by constructing chain reaction cycle among them. Weinstock (1969) suggested HO_2 generation from reaction of CO and OH, then Levy (1971) suggested OH regeneration from the reaction of HO_2 and NO (Eq (1-4)). In subsequent reaction, photolysis of NO_2 produce O_3 (Eq (1-5), (1-6)). Dew to this recycle process of OH radical, VOC removal process enhanced in atmosphere.

$$HO_2 + NO \rightarrow OH + NO_2 \quad (1\text{-}4)$$

$$NO_2 + h\upsilon(<398nm) \rightarrow NO + O(^3P) \quad (1\text{-}5)$$

$$O_2 + O(^3P) + M \rightarrow O_3 + M \quad (1\text{-}6)$$

And HO_2 can react with formaldehyde (HCHO) which is the secondary photooxidation product from

VOCs ((1-7) to (1-9)) (Su et al., 1979, Morrison and Heicklen, 1981)

$$HO_2 + HCHO \rightarrow O_2CH_2OH \quad (1\text{-}7)$$

$$2O_2CH_2OH \rightarrow 2OHCH_2O + O_2 \quad (1\text{-}8)$$

$$O_2CH_2OH + HO_2 \rightarrow O_2 + HOCH_2OOH \rightarrow H_2O + HCOOH \quad (1\text{-}9)$$

1.1.3 RO_2 radical

Alkylperoxy radical, RO_2 also oxidize NO to NO_2, then produce HO_2. RO_2 is defined by the species of R group (R = CH_3, C_2H_5, C_2H_4OH, etc). R group with more than five carbon numbers containts many structural isomers.

RO_2 radical also oxidize NO to NO_2, then produce O_3 in subsequent photolysis of NO_2. Additionally, RO_2 self-reaction and cross-reaction cause to production of low-volatile compounds which contribute to formation of aerosol nucleation (Eq (1-10)).

$$RO_2 + RO_2 \rightarrow ROOR + O_2 \quad (1\text{-}10)$$

1.2 Measurement technique of ROx radicals

ROx radical concentration in ambient air is extremely low because of their high reactivity. Rapid reaction with NO or self/cross-reaction cause difficulty in measurement. Several measurement technique of ROx radicals were developed. In this chapter, techniques and characteristics is shown.

1.2.1 OH measurement technique

Among ROx species, OH has the highest reactivity in the ambient air, consequently exists in low concentration. Commonly spectroscopic technique was used because of high time resolution and lower detection limit.

1.2.1.1 LIF

LIF (Laser Induced Fluorescence) technique is used for detection of OH radical mainly. (Hard et al., 1984) Sample air which included OH radicals was injected from pinhole nozzle to low pressure detection cell. 308 nm laser was exposed to excite OH radical in Q_1 2 line ($A^2\Sigma^+$. v=0, $X^2\Pi$, v=0). Detection cell kept low pressure (<5 Torr) to avoid quenching of excited OH radical by third body. Florescence from excited OH radical was measured and converted to concentration with result of calibration.

1.2.1.2 DOAS

DOAS (Differential Optical Absorption Spectroscopy) technique was used for the measurement of OH radical. OH concentration was obtained by difference of light intensity before/after transmission through air sample at OH rotational line at 308 nm (Perner et al., 1976).

Advantage of DOAS, absorption technique is that it is self-calibration by Lambert-Beer law. Disadvantage of DOAS technique is that spatial resolution is low. According to Lambert-Beer law, OH concentration was calculated with light source intensity, concentration and cross-section of target species, and light path length. Because of extremely low concentration of OH, longer light path length is achieved for DOAS technique, generally few kilo meters. Meanwhile, Absorption is features from all atmospheric compounds except for OH should be subtracted as background. Aerosols, or other species, such as SO_2, CH_2O and naphthalene present in atmosphere can absorb UV laser absorption, and lead to larger uncertainty.

1.2.1.3 CIMS

CIMS (Chemical Ionization Mass Spectrometry) technique which is non-spectrometric method was developed by Eisele and Tanner (1991). Ambient OH radical titrated into H_2SO_4 through rapid reaction with SO_2 (10-20 ms), then detected by using selected-ion chemical ionization mass spectrometry.

After, Reiner improved to PerCIMS for measurement of ROx radicals with chemical amplifier technique with high concentration of NO and SO_2.

Advantage of CIMS technique ignore background fluorescence or absorption.

1.2.1.4 ^{14}CO oxidation

^{14}CO oxidation technique was first attempted by Campbell et al., (1979). With assumption of 1) ^{14}CO exclusively reacted with OH, 2) ambient $^{14}CO_2$ concentration is negligible than generated $^{14}CO_2$ and 3) ^{14}CO was not consumed within reaction tube, 4) ^{14}CO and $^{14}CO_2$ were dispersed at equal rate in reaction tube, 5) depletion of OH by surface of reaction tube, the introduction of ^{14}CO, or UV radiation attenuation is negligible. Then time dependence of ^{14}CO can be explained as Eq (1-11).

$$\frac{d[^{14}CO_2]}{dt} = k[^{14}CO][OH] \qquad (1\text{-}11)$$

Where k is reaction rate constant with CO and OH. Then OH concentration can be calculated as Eq (1-12).

$$[OH] = \frac{[^{14}CO_2]}{[^{14}CO]kt} \quad (1\text{-}12)$$

Where t is reaction time of ^{14}CO and OH. Sampled ^{14}CO and $^{14}CO_2$ were analyzed in the Washington State University radiocarbon dating laboratory with gas proportional countor.

1.2.1.5 Scrubbing using salicyclic acid

Scrubbing using salicyclic acid technique is developed by Chen and Mopper (2000). Ambient air is drawn into the solution of salycyclic acid (o-hydroxybenzoic acid, OHBA) then rapid reaction of OH and OHBA produced a stable fluorescent product, 2,5-dihydroxybenzoic acid. Produced 2,5-dihydroxybenzoic acid was determined by reverse-phase HPLC and fluorescence detection. The advantage of this technique is simplicity, portability and low expense.

1.2.1.6 ESR-GCMS

ESR-GCMS (Electron Spin Resonance and Gas Chromatography / Mass Spectroscopy) technique was developed by Watanabe et al., (1982). OH radical was trapped in a α-4-pyridyl-N-tert-butylnitrone α-1-oxide (4-POBN) then form OH adducted 4-POBN in situ. After sampling, OH radical was analyzed with Electron Spin Resonance (ESR).

1.2.2 HO_2 measurement technique

HO_2 radical also important oxidant in atmosphere which can oxidize NO to NO_2, then it re-from OH radical. Because of the less reaction partner compared to OH radical, atmospheric lifetime is much longer and concentration is higher.

1.2.2.1 LIF technique with conversion HO_2 to OH

Addition to the basement of OH-LIF instrument, by adding NO just after pinhole nozzle, HO_2 was converted to OH and detected. (Hard et al., 1995, Mather et al., 1997, Kanaya et al., 2001) Some of RO_2 also can be converted to OH radical and detected, but by controlling NO concentration and reaction time, interference of RO_2 radical was ignored.

1.2.2.2 MIESR

MIESR (Matric Isolation and Electron Spin Resonance) technique was developed by Mihelcic et al. (1978). This technique was consisted from two steps, trapping of radicals and analysis of radicals. First sampled air was passed over copper finger which was

cooled at liquid nitrogen temperature. After passing jet nozzle, sample air was trapped into stainless steel chamber. After sampling, the matrix has been stored at 77 K for two weeks without loss of signal intensity.

Trapped radical concentration was measured by using Electron Spin Resonance spectroscopy.

Advantage of this technique is able to measure each HO_2, CH_3O_2 and other RO_2 separately at the same time.

Disadvantage of this technique is analysis time. 1 sample analysis took 5 hours.

1.2.2.3 ROXMAS

ROXMAS (ROx chemical conversion MAss Spectroscopy) technique was developed by Hanke et al., (2002). ROXMAS is a novel method for atmospheric speciated measurement of HO_2 and sum of organic peroxy radical (ΣRO_2). Sampled air was exposed high concentration of NO and SO_2 then radical chain reaction between OH and HO_2 occurred as below.

$$RO_2 + NO \rightarrow RO + NO_2 \quad (1\text{-}13)$$

$$RO + O_2 \rightarrow HO_2 + products \quad (1\text{-}14)$$

$$HO_2 + NO \rightarrow OH + NO_2 \quad (1\text{-}4)$$

$$OH + SO_2 \rightarrow HOSO_2 \quad (1\text{-}15)$$

$$HOSO_2 + O_2 \rightarrow HO_2 + SO_3 \quad (1\text{-}16)$$

$$SO_3 + H_2O \rightarrow H_2SO_4 \quad (1\text{-}17)$$

Generated H_2SO_4 was detected by using CIMS. Because of low atmospheric background gaseous H_2SO_4 concentration, amplified H_2SO_4 has been measured accurately with high sensitivity of CIMS. In the presence of O_2, RO_2 was converted HO_2 efficiently, but in absence of O_2, RO_2 was removed from radical chain reaction according to following reaction.

$$RO + NO \rightarrow RONO \quad (1\text{-}18)$$

$$RO + SO_2 \rightarrow ROSO_2 \quad (1\text{-}19)$$

By diluting with either N_2 or O_2, conversion efficiency of RO_2 was controlled, then individual measurement of HO_2 and ΣRO_2 has held. Conversion efficiency of RO_2 to HO_2 cannot be 100 %, so ROXMAS technique measured upper limit of HO_2 and lower limit of ΣRO_2.

1.2.2.4 PERCA

PERCA (PEroxy Radical Chemical Amplification) technique was developed by Cantrell and Stedman (1982). Sample air which was including ROx radicals was exposed to high concentration of CO and NO. HO_2 radical is converted to OH by reaction with NO. Then generated OH radical reacted with CO and generate HO_2 again.

Radical chain reaction was occurred between OH and HO_2 radical, around 100 to 200 times, then same amount of NO_2 is produced. Cantrell and Stedman (1982) detected amplified NO_2 by using chemiluminescence with luminol in liquid phase. More recently, LIF technique is used to detection of NO_2, which has high time resolution (Sadanaga et al, 2004a). Detailed reaction mechanism and instrument construction is shown in section 2.

Miyazaki et al. (2010) developed PERCA technique with denuding method. By using glass-wall denuding cell, HO_2 is easily removed from gas phase then HO_2 and ΣRO_2 can be measured separately. Removal efficiency is affected by relative humidity because removal process is not simple absorption.

1.2.3 RO_2 measurement technique

RO_2 is also important species which can oxidize NO to NO_2, and is a precursor of aerosols. Commonly RO_2 concentration is measured as a total concentration of RO_2, ΣRO_2.

1.2.3.1 ROXMAS with N_2 dilution

As explained in section 1.2.2.3, HO_2 was amplified selectively with NO, SO_2 addition and N_2 dilution. With O_2 dilution, $HO_2 + \Sigma RO_2$ concentration were measured, then by subtracting HO_2 concentration from $HO_2 + \Sigma RO_2$ concentration, total RO_2 concentration were estimated. (Hanke et al., (2002))

1.2.3.2 PERCA technique with denuder cell

As explained in section 1.2.2.4, HO_2 was selectively removed by denuding cell, then ΣRO_2 concentration was measured by PERCA-LIF technique. (Miyazaki et al. (2010))

1.2.4 Summary of ROx measurement techniques

Summary of measurement techniques of ROx species was shown in Table 1-1. In this research, several ROx concentration should be measured and high time resolution is needed to observe time series of short lifetime ROx. As a result, PERCA technique combined with NO_2 LIF technique which can measure total concentration of peroxy radical and has high time resolution is employed.

Table 1-1 Summary of measurement techniques of ROx species

Measument technique	Detection llimit (molecules cm^{-3})		Time resolution	References
OH				
LIF	6.0	$\times 10^5$	30 seconds	Creasey et al., 2002
	3	$\times 10^5$	1 minute	Ren et al., 2003
	1.2	$\times 10^6$	1 minute	Kanaya et al., 2001
DOAS	4	$\times 10^5$	4.5 minutes	Armerding et al., 1995
	5	$\times 10^5$	10 minutes	Mount, 1992
	2	$\times 10^6$		Perner et al., 1987
CIMS	< 1	$\times 10^5$	30 seconds	Tanner and Eisele, 1995
	2.4	$\times 10^5$	30 seconds	Berresheim et al., 2003
^{14}CO oxidation	2	$\times 10^5$	5 minutes	Felton et al., 1988
Scrubbing using salicyclic acid	(3-6)	$\times 10^5$	45-90 minutes	Chen and Mopper, 2000
ESR-GCMS	5	$\times 10^5$	20-30 minutes	Watanabe et al., 1982
HO_2				
LIF with HO_2 to OH conversion	3.0	$\times 10^6$	30 seconds	Creasey et al., 2002
	2.5	$\times 10^6$	1 minute	Ren et al., 2003
	1.2	$\times 10^6$	1 minute	Kanaya et al., 2001
MIESR	2.5	$\times 10^7$	30 minutes	Mihelecic et al., 1978
Chamical Amplification				
ROXMAS	0.5	pptv	1 minute	Hanke et al., 2002
	0.5-1.0	pptv	1 minute	Cantrell et al., 2003
PERCA with denuding method	0.41	pptv	1 minute	Miyazaki et al., 2010
RO_2				
ROXMAS	0.5	pptv	1 minute	Hanke et al., 2002
	0.5-1.0	pptv	1 minute	Cantrell et al., 2003
PERCA with denuding method	-	-	1 minute	Miyazaki et al., 2010

1.3 Ambient air measurement campaign and comparison with model calculation

As listed in 1.2, numerous measurement technique of ROx species was developed. Sometime measured ROx concentration is compared with model calculation to estimate the accuracy of understanding for the behavior of ROx species in atmosphere.

1.3.1 Model Calculation

The degradation of VOCs, and generation of harmful secondary pollutants which ROx chemistry is including in the atmosphere is described mathematically by chemical mechanism to estimate air quality. Highly chemical mechanism model was preferred to represent the chemistry in atmosphere as accurately as possible.

In recent years, parameters about kinetics and mechanism relevant to the oxidation of VOCs in the tropospheric chemistry were improved significantly. But the relative contributions of each VOCs were varying in the mixture. The provision of model

calculation was to describe the degradation of a range of VOCs and the production of secondary photochemical pollutants which had adverse effect on health in the boundary layer by using these parameters. O_3 is one of harmful secondary pollutants in troposphere, which has adverse effect on human health and vegetation, it has higher greenhouse effect higher than CO_2, and it drives the oxidation of trace gas species both directly, and indirectly as a precursor of OH radical.

1.3.1.1 Carbon Bond Mechanism (CB05)

Carbon Bond Mechanism (CB05) was updated by Yarwood et al. (2005) from the version CB4. The updated contents are 1) inorganic reactions are extended to simulate remote and polluted urban environment. 2) two extinctions are available to be added to core mechanism for modeling explicit species and reactive chlorine chemistry.

1.3.1.2 Regional Atmospheric Chemical Mechanism (RACM)

Regional Atmospheric Chemical Mechanism (RACM) (Stockwell et al., 1997) was revised version of Regional Acid Deposition Mechanism (RADM2) (Stockwell et al., 1990) which was developed from the first version of RADM (Stockwell, 1986). First RADM mechanism model is based on chamber experiment especially focus on acid deposition by the reaction products which include nitrogen and sulfur compounds. The specialty of RADM mechanism, it includes the parameter of transportation. Most of chemical model calculation is based on 0-dimentional model, without transportation. Radical species such as OH and HO_2 are included as local photochemical oxidizing agent. RADM2 is improved in the means of treatment of alkenes and aromatics, then accordingly RADM2 can simulate behavior of HNO_3 and H_2O_2, which are important species of radical termination reaction products under a wide variety of environment conditions. Additionally peroxy radical-peroxy radical reaction is more detailed and get more realistic predictions. Improvement of RACM is to get new condensed reaction mechanisms for biogenic compounds, such as isoprene, α-pinene and d-limonene by means of reaction rate constant, and product yields. But still oxidation mechanism of biogenic compounds an aromatics has uncertainty.

1.3.1.3 Master Chemical Mechanism (MCM)

The Master Chemical Mechanism (MCM) was developed by Jenkin et al., (1997) and updated to version 3.1 by Bloss et al. (2005). MCM is a near-explicit chemical mechanism which can describe detailed gas phase degradation of a series of emitted VOCs, and conclusively generated ozone and other products.

MCM ver3.1 includes 21691 reaction of 4351 organic species, and 46 associate inorganic reactions, which has largest number of mechanisms among model calculation above. MCM ver3.1 describes the degradation of 125 initial species, while UK National Atmospheric Emissions Inventory (UKNAEI) currently contains 650 species. Selected compounds cover 70 % of the mass emissions.

1.3.2 Comparison between observation and model calculation

Discrepancy between observed ROx concentration and calculated ROx concentration suggests that there was unexplained mechanism or reaction pathways. Chen et al. (2010) reported that comparison between several model calculation and measurement value, there are some differences, mostly underestimation of the model calculation. And also uncertainty might be from the condition of the reaction. Several laboratory experiments available regarding radical generation and loss process estimation, but it is in controlled condition. No experimental data is reported under atmospheric condition.

1.3.3 Photostationary state deviation

Even though many ROx concentration measurement techniques were developed and performance has been held, in many cases, high-cost instruments and handling skills are needed. By using Photostationary state deviation (Cadle and Johnston, 1952, Leighton, 1961) and assumption of Steady State Calculation (Cantrell et al, 1992), only with comprehensive measurement items, ambient ROx concentration was estimated roughly.

First, Photostationary state deviation is focusing on photochemical equilibrium between NO, NO_2 and O_3.

$$NO_2 + h\upsilon(<398nm) \rightarrow NO + O(^3P) \quad (1\text{-}5)$$

$$O_2 + O(^3P) + M \rightarrow O_3 + M \quad (1\text{-}6)$$

$$NO + O_3 \rightarrow NO_2 + O_2 \quad (1\text{-}20)$$

$$HO_2 + NO \rightarrow OH + NO_2 \quad (1\text{-}4)$$

$$RO_2 + NO \rightarrow RO + NO_2 \quad (1\text{-}13)$$

Then time variation of NO can be expressed from equations above as follows;

$$\frac{d[NO]}{dt} = J_{NO2}[NO_2] - k_{NO+O3}[NO][O_3] - k_{HO2+NO}[HO_2][NO] - k_{RO2+NO}[RO_2][NO]$$

(1-21)

In photostationary steady state deviation, time variations of NO is much smaller than its production rate and loss rate. Then $\frac{d[NO]}{dt}$ is estimated as 0. Eq (1-21) is converted as Eq (1-22).

$$[HO_2]+[RO_2]=\frac{J_{NO2}[NO_2]}{k_{ROx+NO}[NO]}-\frac{k_{NO+O3}}{k_{ROx+NO}}[O_3] \quad (1\text{-}22)$$

To estimate the concentration of total peroxy radicals, HO_2+RO_2, rate constant of the reaction between HO_2 and NO (k_{HO2+NO}), RO_2 and NO (k_{RO2+NO}), measured individually, are averaged as k_{ROx+NO}. The rate constant of total peroxy radicals and NO, k_{ROx+NO} is estimated by assuming that most of peroxy radicals in the atmosphere are HO_2 and CH_3O_2, and taking the average of rate constants of these. By analyzing data from common measurement tools, NOx and O_3 concentration, photolysis frequency of NO_2, total peroxy radical concentration can be calculated.

1.3.4 Steady state calculation

Next, concentration of total peroxy radical was calculated from production rate and loss rate of ROx. The time variation of ROx concentration is assumed as comparatively much smaller than its production or loss rate. Then ROx concentration was assumed as constant (Eq(4-23)).

$$\frac{d[ROx]}{dt}=P_{ROx}-L_{ROx}=0 \quad (1\text{-}23)$$

P_{ROx} indicates production rate of ROx, and L_{ROx} indicates loss rate of ROx. PROx and LROx were estimated as follows;

$$P_{ROx}=\sum_{i=1}^{n}J_i[Ci]+\sum_{j=1}^{m}k_{j+O3}[Cj][O_3] \quad (1\text{-}24)$$

$$L_{ROx}=\sum_{j=1}^{m}k_{ROxj+NO2}[ROx_j][NO_2]+\sum_{k=1}^{l}k_{wall}[ROx_k] \quad (1\text{-}25)$$

In Eq(1-25), C_i and C_j indicate the concentration of ROx precursor, and J_i and k_{j+O3} indicate photolysis frequency and rate constant for individual precursor. And in Eq(1-25), $ROx_{i,\,j,\,k}$ indicate various ROx concentration, and $k_{radical}$ is self or cross-reaction rate constant of ROx, $k_{ROxj+NO2}$ is the rate constant of individual ROx and NO_2, kwall is wall reaction loss rate of ROx_k. Then Eq (1-23) can be assigned as Eq (1-26).

$$[HO_2]+[RO_2]=\frac{\sum_{i=1}^{n}J_i[Ci]+\sum_{j=1}^{m}k_{j+O3}[Cj][O_3]}{k_{ROxj+NO2}[NO_2]+k_{wall}} \quad (1\text{-}26)$$

For the simplification, peroxy radical concentration is calculated as previous chapter. And ROx loss process includes radical-radical self or cross-reaction, but compared to ROx+NO_2 reaction, frequency is much lower. ROx self or cross-reaction is ignored in this chapter and total peroxy radical concentration is calculated as Eq (1-27).

1.4 ROx radical generation process

1.4.1 Photolysis

As discussed in section 1.1, daytime ROx radicals were produced by photolysis in the form of OH and HO_2. Production rate was estimated as multiplication of precursor concentration and photolysis rate. Photolysis rate was calculated by multiplication of cross section, quantum yield and actinic flux (Eq (1-27)) in the case of single wavelength light. Generally photolysis reaction in ambient air occurred at several wavelength. Photolysis rate was calculated by integration at all wavelength Eq (1-28). Mainly OH radical was generated from photolysis of O_3 in troposphere (Eq (1-29)).

$$J(\lambda) = \sigma(\lambda)\Phi(\lambda)I(\lambda) \tag{1-27}$$

$$J = \int_{\lambda_1}^{\lambda_2} \sigma(\lambda)\Phi(\lambda)I(\lambda)d\lambda \tag{1-28}$$

$$O_3 + h\upsilon(<336nm) \rightarrow O_2 + O(^1D) \tag{1-29}$$

Then generated $O(^1D)$ react with water molecule and generate two molecules of OH. (Eq (1-30))

$$O(^1D) + H_2O \rightarrow 2OH \tag{1-30}$$

In the presence of third body, like N_2 or O_2 electronically excited $O(^1D)$ will be deactivated to ground state $O(^3P)$ (Eq (1-31)), and reform O_3 (Eq (1-32)).

$$O(^1D) + M \rightarrow O(^3P) + M \tag{1-31}$$

$$O(^3P) + O_2 + M \rightarrow O_3 + M \tag{1-32}$$

In stratosphere, OH radical is also generated by photolysis of water vapor (Eq (1-33)).

$$H_2O + h\upsilon(<242nm) \rightarrow OH + H \tag{1-33}$$

But it is negligible in earth surface because of O_3 layer in stratosphere. UV region of solar radiation can be absorbed by O_2 or O_3. Consequently lower than 300 nm UV

radiation cannot reach to earth surface.

OH radical is generated also from photolysis of HONO (Atkinson, 2002), H_2O_2.

$$HONO + h\upsilon(< 400nm) \rightarrow OH + NO \quad (1\text{-}34)$$

$$H_2O_2 + h\upsilon(< 350nm) \rightarrow 2OH \quad (1\text{-}35)$$

During daytime, when sunlight is available, OH radical is mainly generated by photolysis. But in nighttime, dominant OH generation process is shifted to ozonolysis, the reaction of O_3 and unsaturated VOCs. General scheme of ozonolysis is showed in Fig.1-5. First O_3 attack to carbon-carbon double bond of VOC and form ozonide. Ozonide dissociate to Cregiee intermediate and carbonyl compound. Criegee intermediate will through three pathways, 1) dissociation 2) isomerization 3) hydrogen transfer. OH radical will be generated by 3) hydrogen transfer.

Generated OH radical react with trace gases in atmosphere, for example CO, NOx (NO and NO_2), SO_2, methane, and other VOCs. Within VOCs, alkane, alkene, alkyne, aromatics are included. Reaction rate constant of OH and several trace species, and reaction products are well-investigated. Main loss process is estimated as reaction with these trace gas species. Reaction with VOC leads to generation of several types of RO_2 (details in section 1.1.3). Recently, direct measurement method of OH radical loss process is developed by Sadanaga et al. (2004b) as OH reactivity. Even Simple photooxidation products of isoprene, there is around 30 % of uncertainty is included (Nakashima et al., 2012).

HO_2 radical is mainly generated from photolysis of carbonyl compounds and ozonolysis similar like OH. In the atmosphere, formaldehyde, acetaldehyde, acetone photolysis is main source of HO_2.

$$HCHO + h\upsilon(< 398nm) \rightarrow H + HCO \quad (1\text{-}36)$$

$$CH_3CHO + h\upsilon(< 321nm) \rightarrow H + CH_3CO \quad (1\text{-}37)$$

$$H + O_2 + M \rightarrow HO_2 + M \quad (1\text{-}38)$$

$$HCO + O_2 \rightarrow HO_2 + CO \quad (1\text{-}39)$$

Loss process of HO_2 is reaction with NO (Eq(1-4)), self-reaction (Eq(1-40)) and cross-reaction with RO_2 (Eq(1-41)). Self-reaction and cross-reaction with RO_2 generates low volatile species, then reaction products lead to SOA (Secondary Organic Aerosol) formation, which affect the radiation budget, by absorbing or reflecting sunlight, and involves nucleation of cloud particles.

$$HO_2 + NO \rightarrow OH + NO_2 \quad (1\text{-}4)$$

$$HO_2 + HO_2 \rightarrow H_2O_2 + O_2 \quad (1\text{-}40)$$

$$HO_2 + RO_2 \rightarrow ROOH + O_2 \quad (1\text{-}41)$$

HO_2 react with NO_2 and form HO_2NO_2, which act as NOx reservoir. It is thermally and photochemicaly dissociated and reproduce HO_2 and NO_2 at transported site (Eq(1-42)and(1-43)).

$$HO_2 + NO_2 + M \rightarrow HO_2NO_2 + M \quad (1\text{-}42)$$

$$HO_2NO_2 + M \rightarrow HO_2 + NO_2 + M \quad (1\text{-}43)$$

1.4.2 Ozonolysis

HOx radical also produced from ozonolysis, which is the reaction of unsaturated VOC and O_3. The simplest olefin, C_2H_4 and O_3 reaction scheme is shown in Fig.1-5 (Atkinson, 1997). First O_3 approaches to carbon-carbon double bond then forms primary ozonide. Primary ozonide dissociate to carbonyl compound and energy-rich biradical, Criegee Intermediate. Excited Criegee Intermediate dissociate and get products as shown in Fig.1-5.

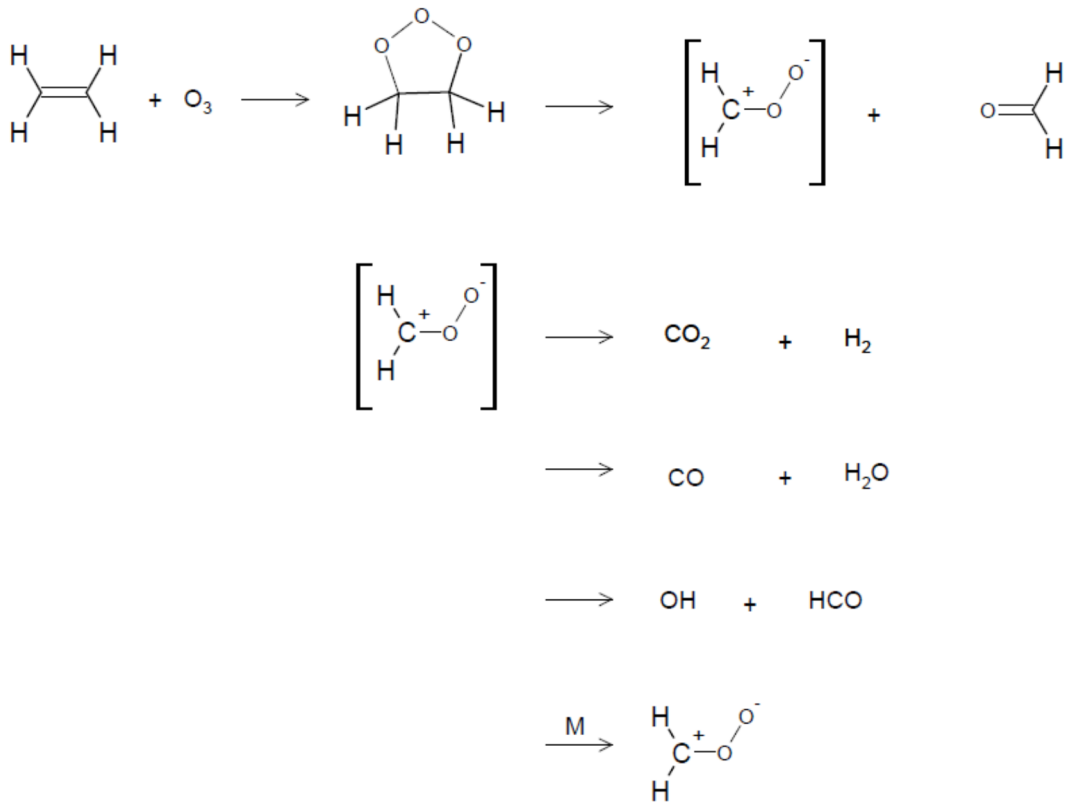

Fig.1-5 Reaction scheme of C_2H_4 and O_3

In the case of higher olefins, such as propene or butene, reaction scheme become much

complicated. Reaction scheme of propene and O_3 is shown in Fig.1-6 (Atkinson, 1997). Same as the reaction of C_2H_4 and O_3, first O_3 approaches to double bond then forms primary ozonide. Since primary ozonide from propene and O_3 reaction is not symmetrical, after dissociation, different type of Criegee Intermediate are produced. From both of Criegee intermediates, OH radical and HO_2 radical are produced.

In the atmosphere, there are many series of olefins which has the potential to generate HOx radiclas. HOx radical yield from several olefins in previous study is shown in Table 1-2. In laboratory studies, some of the HOx yield from single olefin have discrepancy, for example isoprene, which is most dominant VOC in the atmosphere (Guenther et al., 1995). It suggests that uncertainty has been exist during the estimation of ambient HOx radical generation. And reactive olefins from biogenic source has complex structure. Some of olefins have more than two double bond, then it is easily predicted that complicate ozonolysis will be occurred in the atmosphere. Especially in nighttime, when sunlight is not available, radical generation from ozonolysis is important. In the study, HOx radical yield from VOC + O_3 reaction

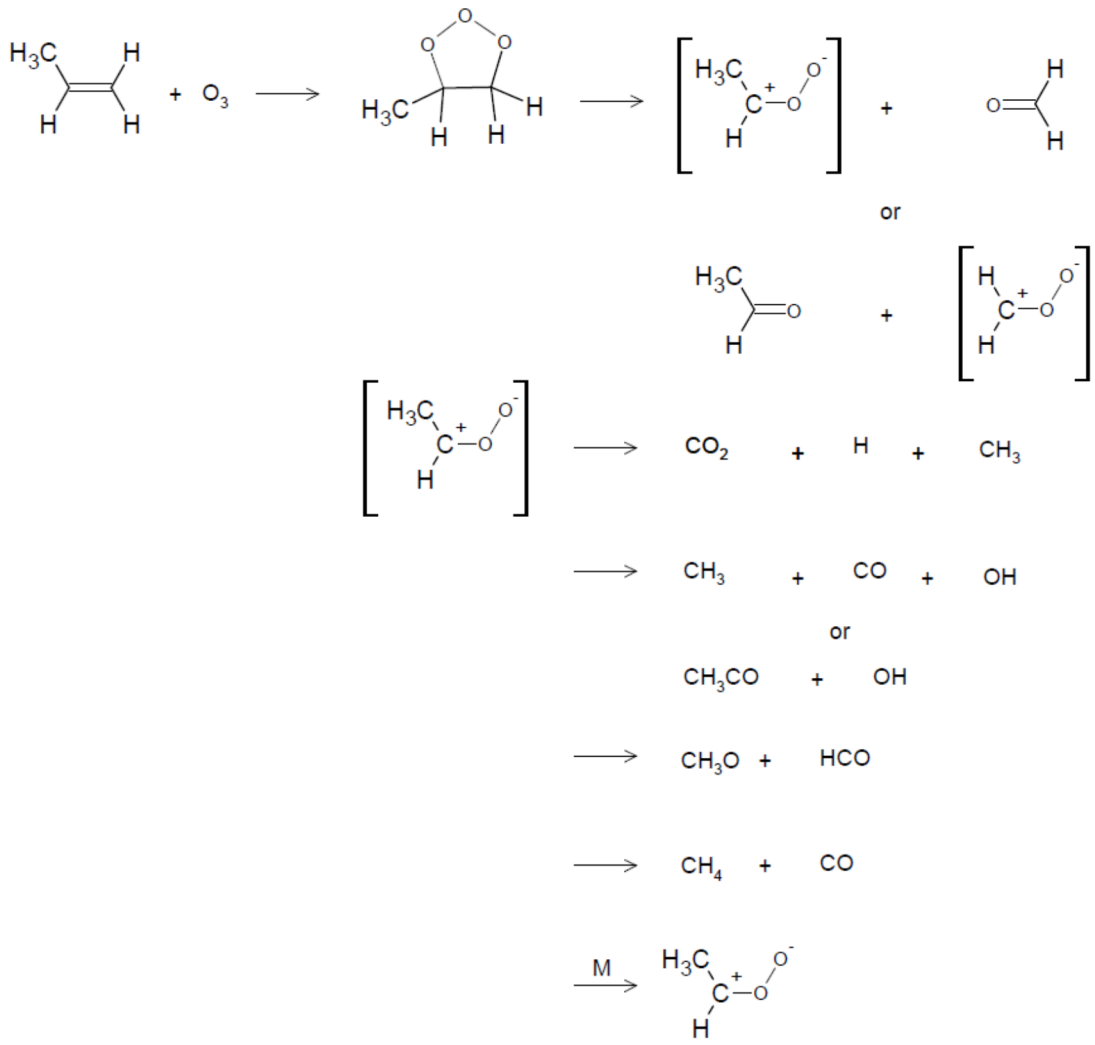

Fig.1-6 Reaction scheme of C_3H_6 and O_3

1.5 PHOx definition

PHOx is defined as HOx radical production rate from ozonolysis, at unit O_3 concentration and unit time. Dimension can be explained as [ppt radicals (ppb O_3)$^{-1}$ s^{-1}]. Measured ROx concentration is divided by added O_3 concentration and reaction time. Detail of PHOx estimation is in section 4.

1.6 Objective of this study

In previous studies, HOx radical which is important oxidant species in ambient air from VOC + O_3 reaction is well understood. But dataset had discrepancy even though within single component due to the difference of experimental condition especially temperature and humidity. These kinds of parameters were varying in ambient air and

cause discrepancy between our understanding and observed value. By measuring produced HOx radical from in situ ozonolysis directly, production process of HOx radical was estimated quantitatively. Observed HOx production rate, PHOx, can be apply for the determination of atmospheric lifetime of trace species, which is important for greenhouse gases, and also improvement of chemical model calculation.

Table1-2 HOx yield from ozonolysis

Species	OH yield	HO_2 yield	reference
Ethene	0.12		Atkinson and Aschmann, 1993
	0.17±0.09	0.10±0.03	Alam et al., 2011
Propene	0.33		Atkinson and Aschmann, 1993
	0.36±0.10		Alam et al., 2013
1-Butene	0.41		Atkinson and Aschmann, 1993
	0.56±0.15	0.18±0.05	Alam et al., 2013
cis-2-Butene	0.41		Atkinson and Aschmann, 1993
	0.26±0.07	0.12±0.03	Alam et al., 2013
trans-2-Butene	0.64		Atkinson and Aschmann, 1993
	0.63±0.17	0.04±0.01	Alam et al., 2013
2-Methylpropene	0.84		Atkinson and Aschmann, 1993
	0.67±0.18	0.34±0.09	Alam et al., 2013
1-Pentene	0.37		Atkinson et al., 1995
2-Methyl-1-butene	0.83		Atkinson and Aschmann, 1993
2-Methyl-2-butene	0.89		Atkinson and Aschmann, 1993
	0.93±0.14		Chew and Atkinson, 1996
1-Hexene	0.32		Atkinson et al., 1995
2,3-Dimethyl-1-butene	0.50		Atkinson et al., 1995
2,3-Dimethyl-2-butene	0.7±0.1		Niki et al., 1987
	1.00		Atkinson and Aschmann, 1993
	0.80±0.12		Chew and Atkinson, 1996
	~0.5		Gutbrod et al., 1996
	0.83±0.22	0.18±0.05	Alam et al., 2013
1-Heptene	0.27		Atkinson et al., 1995
1-Octene	0.45±0.20		Paulson and Sienfield, 1992
	0.18		Atkinson et al., 1995
1,3-Butadiene	0.08		Atkinson and Aschmann, 1993
Isoprene	0.68±0.15		Paulson et al., 1992
	0.27		Atkinson et al., 1992
	0.26	0.26	Malkin et al., 2010
Cyclopentene	0.61		Atkinson et al., 1995
Cyclohexene	0.68		Atkinson and Aschmann, 1993
1-Methylcyclohexene	0.90		Atkinson et al., 1995
Camphene	≦0.18		Atkinson et al., 1992
3-Carane	1.06		Atkinson et al., 1992
Limonene	0.86		Atkinson et al., 1992
Myrcene	1.15		Atkinson et al., 1992
cis-Ocimene	0.63		Atkinson et al., 1992
trans-Ocimene	0.63		Atkinson et al., 1992
β-Phellandrene	0.14		Atkinson et al., 1992
α-Pinene	0.85		Atkinson et al., 1992
	0.76±0.11		Chew and Atkinson, 1996
β-Pinene	0.35		Atkinson et al., 1992
Sabinene	0.26		Atkinson et al., 1992
	0.33±0.06		Chew and Atkinson, 1996
Terpinolene	1.03		Atkinson et al., 1992
α-Cedrene	0.67		Shu and Atkinson, 1994
α-Copaene	0.38		Shu and Atkinson, 1994
	0.32		Shu and Atkinson, 1994
β-Caryophyllene	0.06		Shu and Atkinson, 1994
α-Humulene	0.22		Shu and Atkinson, 1994

2 Instrumentation

In this research, generated ROx concentration was measured by using PERCA/LIF unit. Possible measurement techniques are MIESR, PERCA and CRD, but MIESR and CRD require the detail of several RO_2. It suggests that PERCA and PerCIMS is suitable in the term of measuring several RO_2. PERCA/LIF technique has the advantage of high time resolution and capacity which can measure total concentration of peroxy radicals, HO_2 and several RO_2. In this chapter, construction of PERCA/LIF instrument and optimization of the instrument performance was described.

In Fig.2-1, overview of the PERCA-LIF instrument is shown. This instrument can be divided to three parts, reaction (or calibration) cell, PERCA reaction cell and NO_2-LIF instrument. Instrument setting and optimization of each part will be introduced in individual part.

2.1 NO_2 LIF technique

In this research, amplified NO_2 by using PERCA technique was detected with LIF technique. NO_2 has wide range of absorption spectrum as shown in Fig.2-2, it can absorb longer than 398 nm to ground state (X^2A_1) to excited state (A^2B_2) (Voigt et al., 2002) (Eq (2-1)). Shorter wavelength than 398 nm, NO_2 will be dissociate to NO and O. Most of excited NO_2 collide to third body then be deactivated (Eq(2-2)), but some of them produce fluorescence (Eq(2-3)).

$$NO_2 + h\nu \rightarrow NO_2* \quad (2\text{-}1)$$

$$NO_2* + M \rightarrow NO_2 + M \quad (2\text{-}2)$$

$$NO_2* \rightarrow NO_2 + h\nu' \quad (2\text{-}3)$$

Amount of fluorescence respond to NO_2 concentration linearly, it will be information of NO_2 concentration in sample air. To make minimize effect of deactivation (Eq(2-2)), FAGE (Fluorescence Assay Gas Expansion) technique (George and O'Brien, 1991) is used. Fluorescence cell pump to low pressure (2 Torr) with small orifice in order to make fluorescence lifetime of excited NO_2 longer. A frequency-doubled Nd:YAG LASER is used for light source. Time dependence of excited NO_2 concentration can be define as Eq (2-

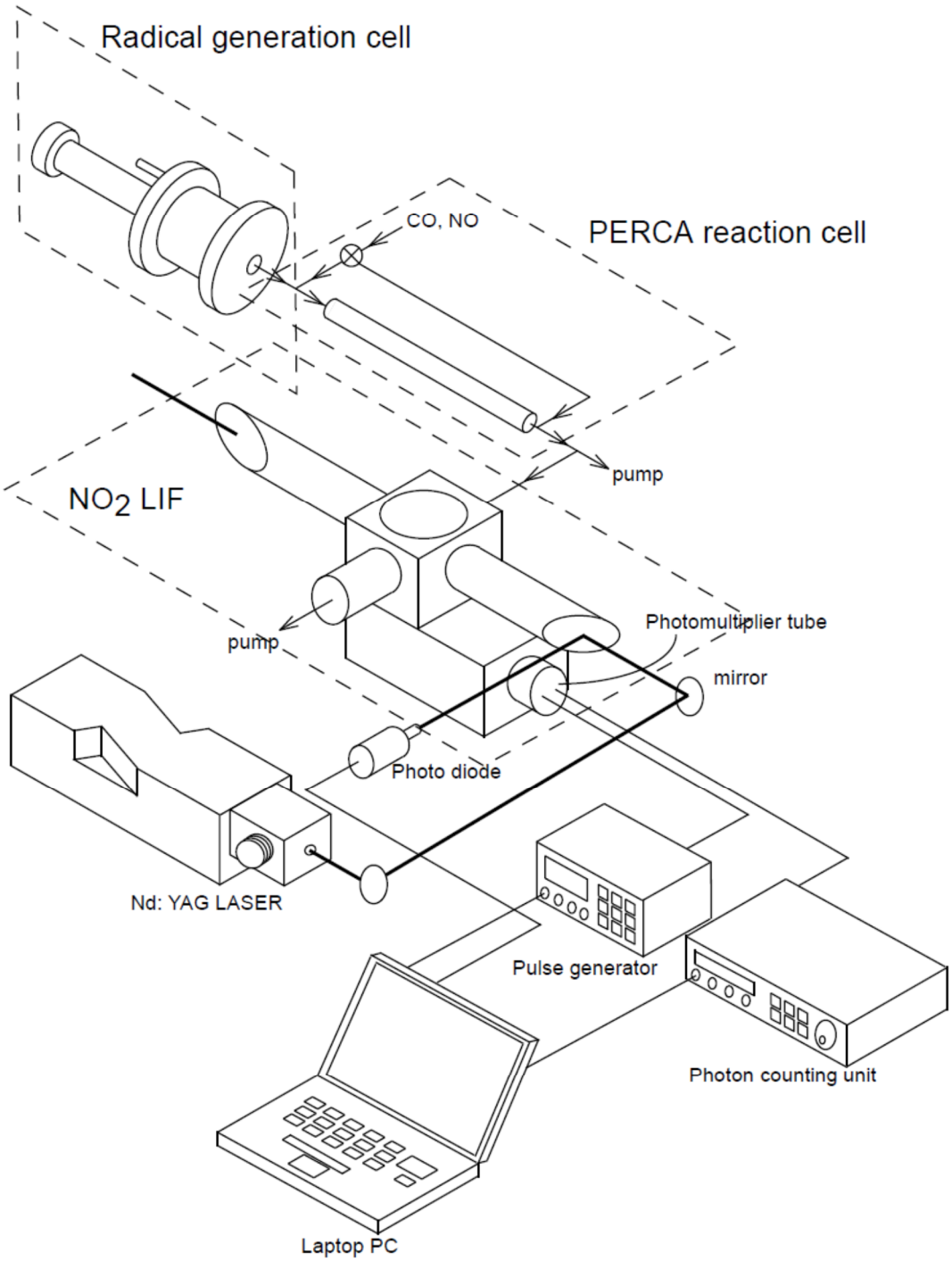

Fig.2-1 Overview of PERCA-LIF instrument

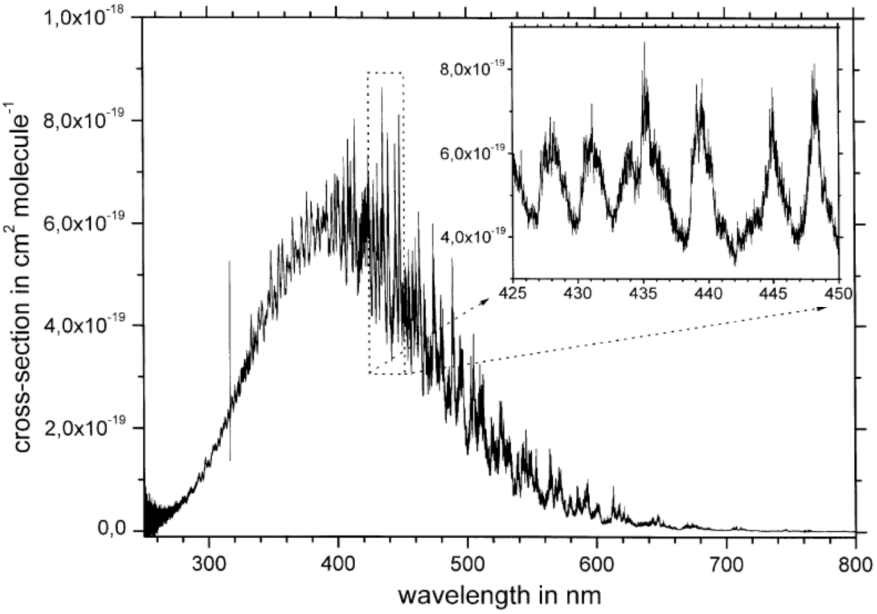

Fig.2-2 NO_2 absorption spectrum from Voigt et al., 2002

4).

$$\frac{d[NO_2*]}{dt} = I\sigma[NO_2] - (k_{rad} + kq[M])[NO_2*] \qquad (2\text{-}4)$$

Here, I is LASER flux (unit: photons s^{-1} cm^{-2}), σ is cross section (unit: cm^2) of NO_2 at 532 nm (=1.49×10^{-19} cm^2. Vandaele et al, 1997). k_{rad} is radiative rate constant of excited NO_2 molecule (=2.3×10^4 s^{-1}, Myers et al, 1966). kq is quenching rate, [M], [NO_2], [NO_2*] are number density of third body, ground state NO_2 and excited state of NO_2, individually. From Eq (2-4), fluorescence signal of NO_2, S canbe indicated as Eq (2-5).

$$S = KI\sigma\times[NO_2]\times\Phi_F \qquad (2\text{-}5)$$

K is LIF instrument function which includes sensitivity of photon detection unit and collection efficiency of photon. Φ_F is fluorescence yield from excited NO_2 molecule. Eq (2-5) can be converted as Eq (2-6) with NO_2 volume mixing ratio, m_{NO2}.

$$S = CKI\sigma m_{NO_2} P\Phi_F \qquad (2\text{-}6)$$

Here C is conversion factor from number density to mixing ratio. P is pressure of LIF cell. In this research, photons are counted with tame-gated photon counting unit for the use of improving signal to noise ratio. Detection of photons are held after each LASER pulse, then Φ_F can be calculated as Eq (2-7).

$$\Phi_F(t_1,t_2) = \Phi_F(t=\infty) \times \int_{t_1}^{t_2} e^{\frac{-t}{\tau}} dt \tag{2-7}$$

$$\Phi_F(t=\infty) \equiv \frac{k_{rad}}{k_{rad} + \sum_i k_i[M_i]} \equiv \frac{k_{rad}}{k} \equiv \frac{1}{1+\sum_i q_i P_{Mi}} \tag{2-8}$$

$$\tau \equiv \frac{1}{k} = \frac{1}{k_{rad}(1+\sum_i q_i P_{Mi})} \tag{2-9}$$

$$q_i = \frac{k_q}{k_{rad}} \tag{2-10}$$

Here t_1 and t_2 are initial and final times of counting gate after the LASER pulse respectively, k_i is rate constant of quenching by third body M_i. krad is the radiative rate constant of the excited NO_2 molecule (2.3×10^4 s^{-1}, Myers et al., 1966). $[M_i]$ is number density of third body M_i. q_i is quenching factor of M_i. P_{Mi} is partial pressure of M_i.

NO_2 sensitivity of LIF instrument, S_{NO2} was calculated with normalized fluorescence signal, S (unit: counts s^{-1}), NO_2 mixing ratio and LASER intensity I as Eq (2-11).

$$S_{NO2} = CK\sigma \frac{P}{1+\sum_i q_i P M_i} \int_{t_1}^{t_2} e^{\frac{-t}{\tau}} dt \tag{2-11}$$

Sensitivity of NO_2 can be affected by instrument function, K, which includes cell pressure, quenching factor and optimization of counting gate.

Calculated fluorescence signal from excited NO_2 can be estimated as Eq (2-12).

$$Fluorescence = \int_{t_1}^{t_1} n \cdot \exp\left(-t \cdot (k_{rad} + k_q[M])\right) \tag{2-12}$$

Where t_1 and t_2 are photomultiplier gate open time and close time individually, n is number density of NO_2. k_{rad} is inverse of radiative lifetime of excited NO_2, 44 μs. Result of the calculation is shown in Fig.2-3. x axis indicates cell pressure at Torr, and y axis indicates fluorescence signal at arbitrary unit. Fluorescence signal has a peak at 1.9 Torr. It is reasonable that fluorescence signal has a peak because too low pressure suppress the number density of NO_2 and too high pressure increases quenching excited NO_2 and third body.

For the optimization of photomultiplier tube gate time, in Fig.2-4, image of counting gate is shown. Blue and red line indicates LASER scatter and fluorescence from excited

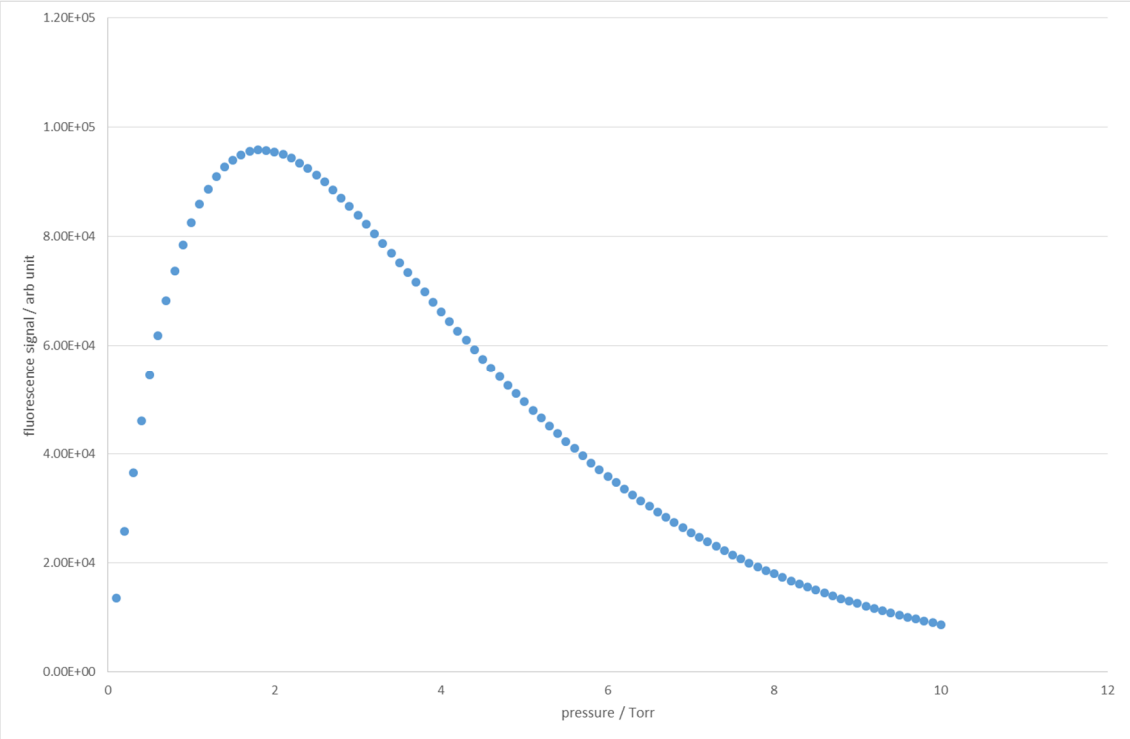

Fig.2-3 Fluorescence signal dependence simulation at various cell pressure

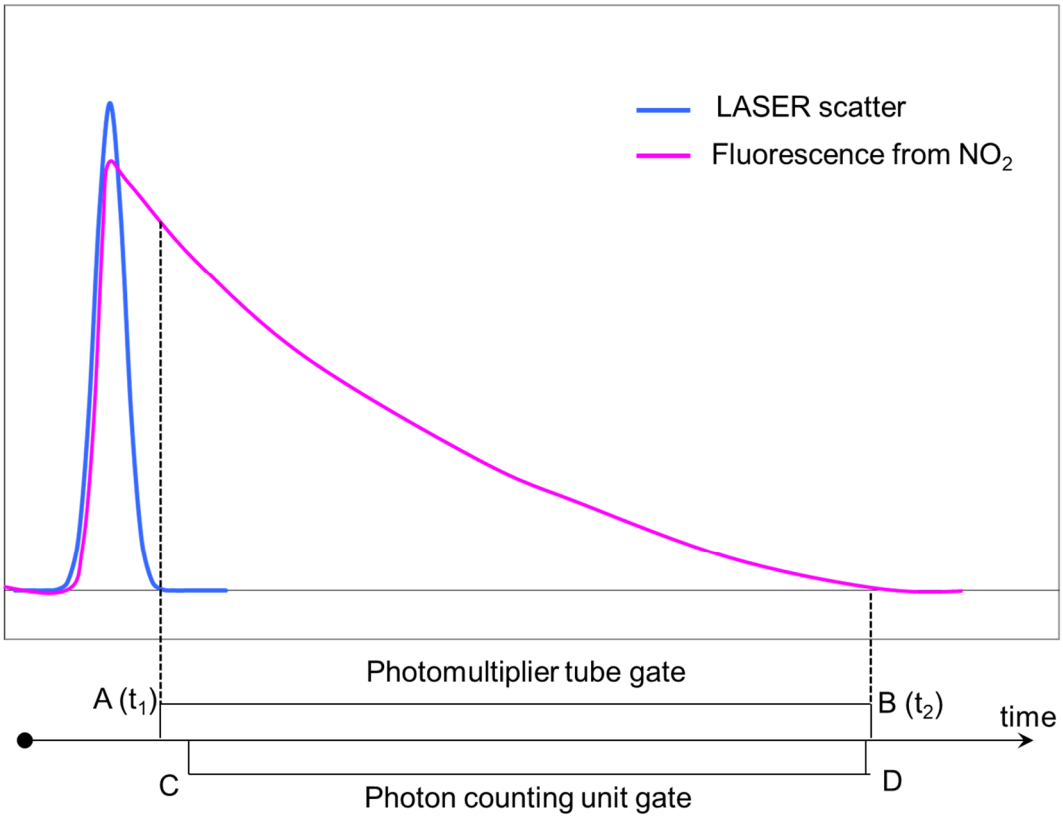

Fig.2-4 Diagram of photomultiplier tube and photon counting gate timing of NO_2 LIF

NO_2 molecules individually. For the improvement signal/noise ratio, gate of photomultiplier tube should start from later as possible, but make gate start time earlier for getting fluorescence signal more as possible. The gate start time A (in Fig.2-4) is optimized as maximize signal/noise ratio. The gate open time A to B preferred as longer as possible. But the duty cycle, which is the capacity of gate open and close frequency is limited. In the case of this instrumental setting (YaG LASER frequency; 10 kHz, Photomultiplier unit HAMAMATSU R928P), the gate open time A to B is fixed as 1900 μs. Then amplified signal by Photomultiplier tube is counted by Photon Counting Unit (STANFORD Research Systems SR400). The gate open time C to D should be within gate open time A to B and optimized. At the beginning of As a result of optimization, NO_2 detection limit is determined as Eq (2-13)

$$LOD_{NO2} = \frac{S/N}{S_{NO2}} \cdot \left(\frac{1}{m} + \frac{1}{n}\right)^{\frac{1}{2}} \cdot \left(\frac{S_{BG}}{I \cdot \Delta t}\right)^{\frac{1}{2}} \qquad (2\text{-}13)$$

Here, LOD_{NO2} is NO_2 Limit Of Detection, S/N is signal to noise ratio which is defined lower limit of the signal hired as data, 2. Then m and n indicate signal and background sampling time, 1 for each. S_{BG} indicates background sensitivity, which is the signal from LASER scatter. I is LASER power intensity, and Δt is accumulation time, 60 seconds in this research. From the optimization of the S_{NO2} and S_{BG} is measured as 543.67 cps ppb^{-1} W^{-1} and 19329 cps W^{-1} individually. Finally LOD_{NO2} is calculated as 61 pptv.

2.2 PERCA technique

Principle of PERCA technique is the chain reaction between OH and HO_2 radical, with NO and CO. Reaction scheme of PERCA is shown in Fig.2-5. First RO_2 and HO_2 react with NO, then through reaction (1-4), (1-13) and (1-14)

$$RO_2 + NO \rightarrow RO + NO_2 \qquad (1\text{-}13)$$

$$RO + O_2 \rightarrow HO_2 + carbonyl \qquad (1\text{-}14)$$

$$HO_2 + NO \rightarrow OH + NO_2 \qquad (1\text{-}4)$$

Then subsequent rapid reaction of generated OH with CO reform HO_2

$$OH + CO + O_2 \rightarrow HO_2 + CO_2 \qquad (2\text{-}14)$$

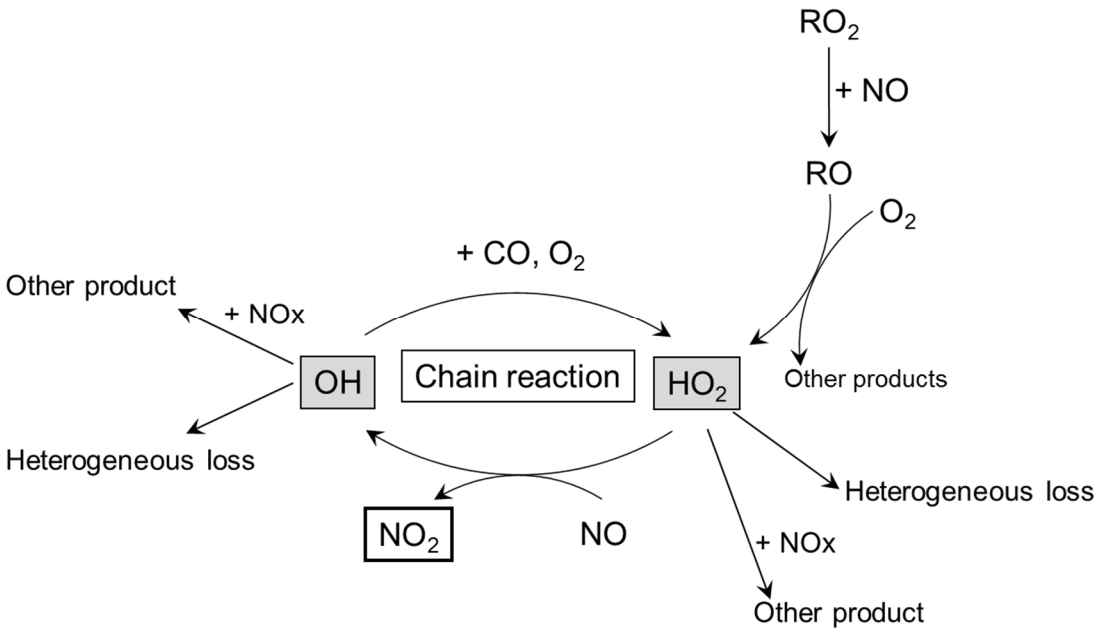

Fig.2-5 PERCA reaction scheme

Equation of 1-17 and 2-3 constitute OH-HO_2 chain reaction which form NO_2 according to Eq (2-4)

$$\Delta NO_2 = k_{1-4}[NO]\int_0^t [HO_2]dt \qquad (2\text{-}15)$$

Here, $k_{1\text{-}17}$ is reaction rate constant of Eq (1-4). The time dependence of HO_2 is determined by reactions which remove OH and HO_2 radical as below.

$$HO_2 + HO_2 \rightarrow H_2O_2 + O_2 \qquad (1\text{-}40)$$

$$OH + NO + M \rightarrow HONO + M \qquad (2\text{-}16)$$

$$HO_2 + NO_2 + M \rightarrow HO_2NO_2 + M \qquad (1\text{-}42)$$

$$HO_2 + NO \rightarrow HNO_3 \qquad (2\text{-}17)$$

$$OH + NO_2 \rightarrow HNO_3 \qquad (2\text{-}18)$$

$$OH + wall \rightarrow heterogeneous\_loss \qquad (2\text{-}19)$$

$$HO_2 + wall \rightarrow heterogeneous\_loss \qquad (2\text{-}20)$$

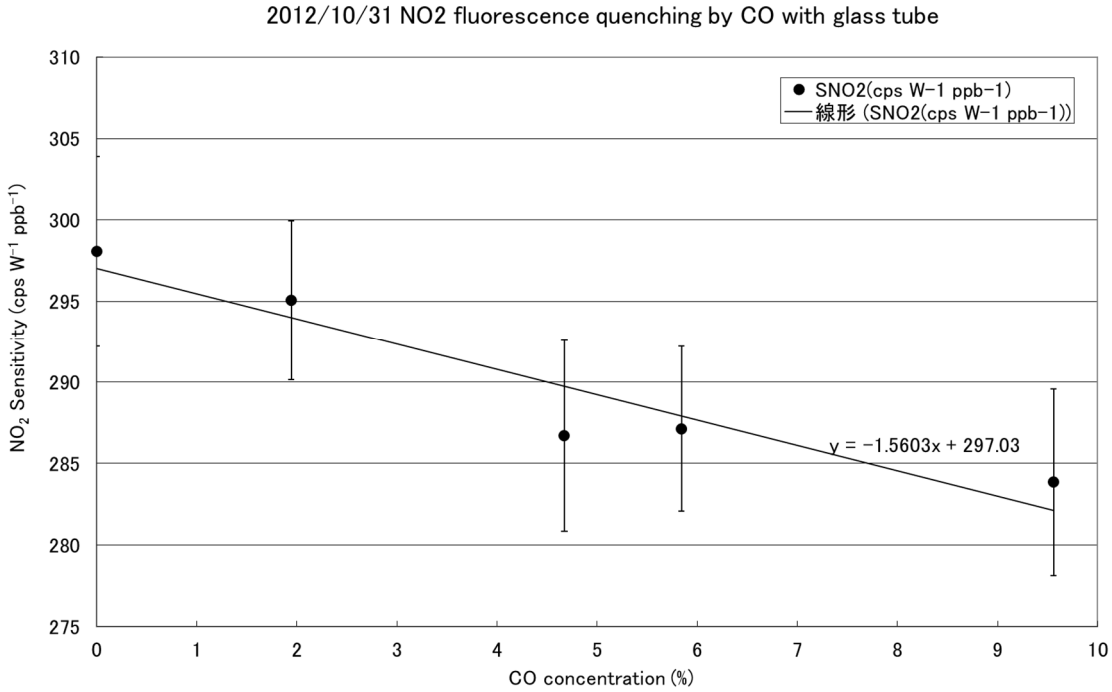

Fig.2-6 NO_2 sensitivity at different CO concentration

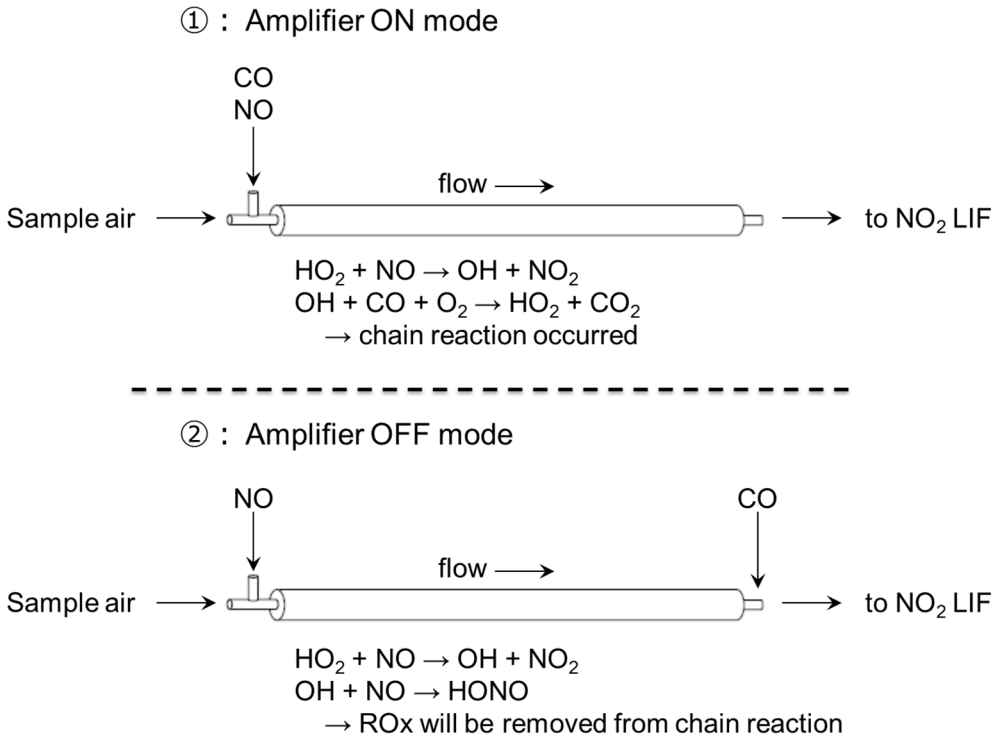

Fig.2-7 Chemical Amplifier ON mode and OFF mode

ΔNO_2 indicates amplified NO_2 concentration. To measure amplified NO_2 concentration accurately, background NO_2 concentration and NO_2 concentration after amplification should be measured. There are two ways to control background mode and amplification mode, 1) Adding nitrogen instead of CO or 2) Change adding point of CO. In the case of 1), sampled air after through PERCA reaction tube had huge difference of CO concentration between background mode and amplification mode. After PERCA technique, LIF technique was used to detect amplified NO_2 concentration. Then huge difference of CO caused deactivation of excited NO_2 and lead to over estimation of amplified NO_2 concentration. Sensitivity of NO_2 at different CO concentration is shown in Fig.2-6. NO_2 sensitivity clearly decreased with increment of CO concentration. Here we employ 2) and configuration of PERCA reaction tube is shown in Fig.2-7. In amplification mode, CO was added with NO at the top of PERCA reaction tube. CO and NO amplified ROx radicals to NO_2. When CO was added at the end of PERCA reaction tube, in background mode, HO_2 and RO_2 were converted to OH by the reaction with NO. Next OH reacted with NO and formed HONO in the absence of CO, then removed from radical chain reaction. Reaction rate constant of OH + NO is fast ($k = 3.3\times10^{-11}$ cm^3 $molecule^{-1}$ s^{-1}, Atkinson and Smith, 1994) and NO concentration was significantly high (4 ppm), most of ROx was converted to HONO within 2 seconds. After PERCA reaction tube, CO is added then sample air is introduced to NO_2 LIF unit. Example of amplifier ON and OFF signal at PERCA-LIF instrument is shown in Fig.2-8.

To minimize loss of HOx radicals by reaction with NO, we did optimization of reaction chain length with varying NO and CO concentration. Reaction chain length can be defined as Eq (2-21).

$$ChainLength = \frac{\Delta[NO_2]}{[HOx]} \qquad (2\text{-}21)$$

Here [HOx] indicates generated HOx radical concentration. Known concentration of HOx radical was generated from HOx calibration cell (at Fig.2-1) by photolysis of water at 184.9 nm of low pressure mercury lump (SEN light corporation SP-3-2H), as Eq (2-22) and (1-38).

$$H_2O + h\upsilon(184nm) \rightarrow OH + H \qquad (2\text{-}22)$$

$$H + O_2 + M \rightarrow HO_2 + M \qquad (1\text{-}38)$$

In this technique, same amount of OH and HO_2 will be generated. But due to high reactivity of OH radical, it can react on the wall of radical calibrator. To avoid OH radical

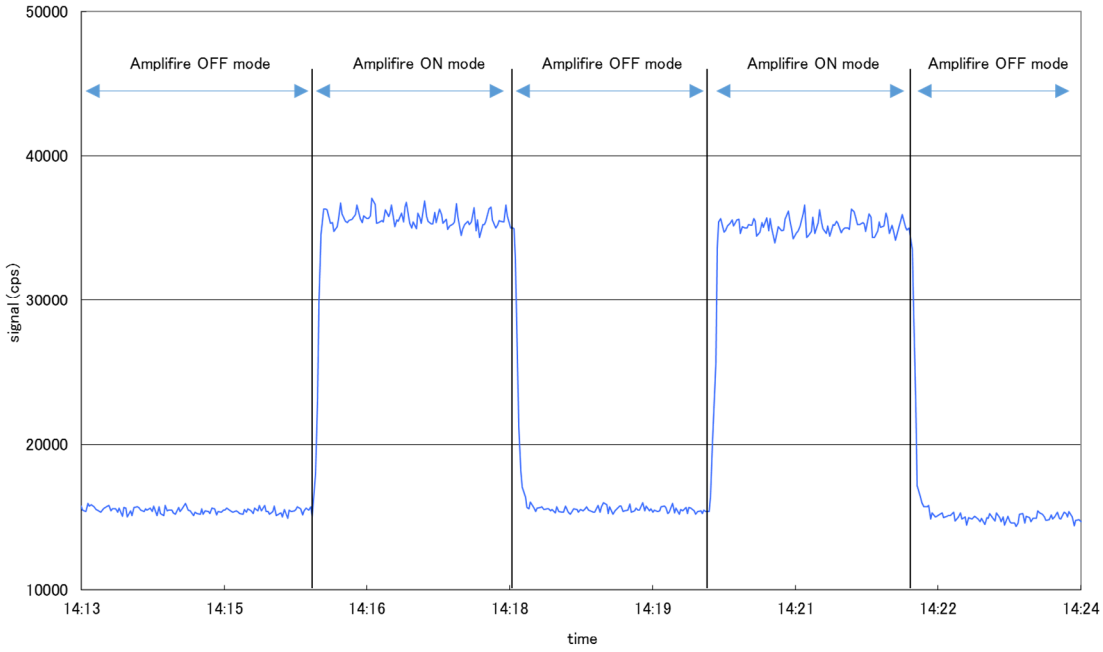

Fig.2-8 Example of amplifier ON and OFF signal at PERCA-LIF instrument

loss in heterogeneous process, CO (1 ppm) was added to purified air to convert OH to HO_2. Purified air was generated by using Zero Air generator (Thermo Model 111), which was using Pt converter to converted most of carbon-containing species to CO_2, and trapped NOx species with purafil and active charcoal. H_2O was added by bubbling water, then introduced radical calibrator with CO. Amount of generate HOx radical can be calculated in Eq (2-23), by using H_2O and O_2 photolysis (Schultz et al., 1995).

$$[OH]=[HO_2]=I_{184.9}\times\sigma_{H2O\_184.9}\times[H_2O]\times t \qquad (2\text{-}23)$$

Here [OH], [HO_2] and [H_2O] indicate concentration of OH, HO_2 and H_2O individually. $I_{184.9}$ and $s_{H2O\_184.9}$ is intensity and cross section of H_2O at 184.9 nm. And t indicates irradiation time of 184.9 nm light. Here, measurement of $I_{184.9}$ and t is difficult due to the fluctuation of $I_{184.9}$ and uncertainty of reaction time. By using formation of O_3, which is occurred at same time as Eq (1-4). Concentration of O_3 which is generated $I_{184.9}$ was calculated as Eq (2-24).

$$[O_3]=2\times I_{184.9}\times\sigma_{O2\_184.9}\times[O_2]\times t \qquad (2\text{-}24)$$

Here $s_{O2\_184.9}$ indicates cross section of O_2 at 184.9 nm. By substituting Eq (2-24) into (2-23), Eq (2-23) can be explained as (2-25).

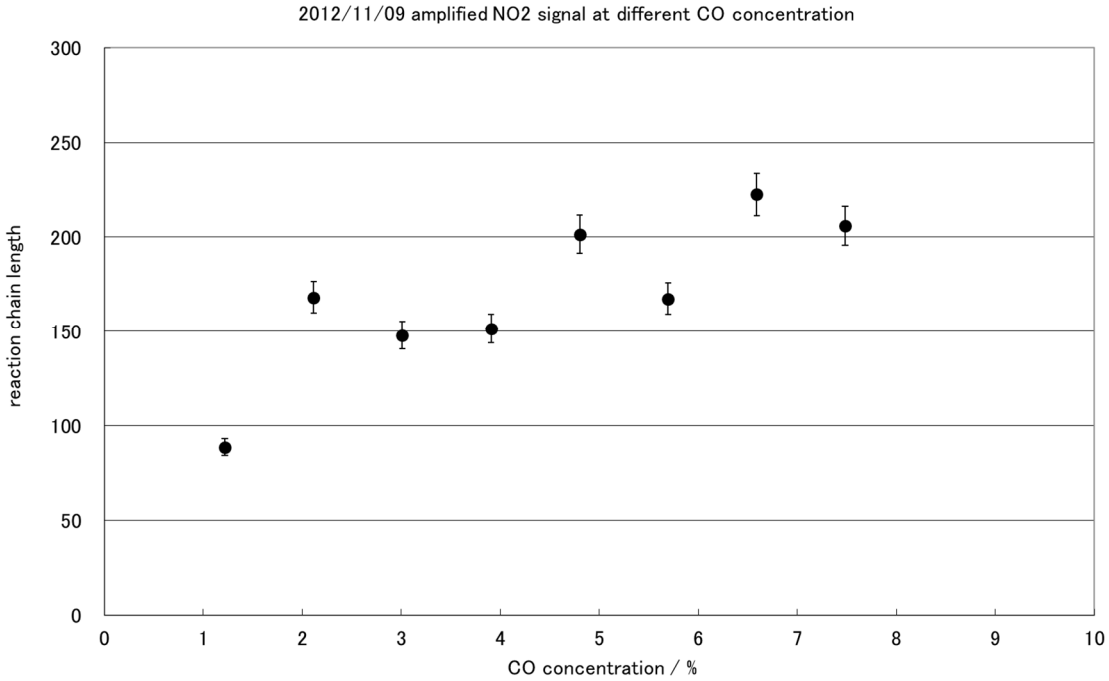

Fig.2-9 Reaction chain length at different CO concentration

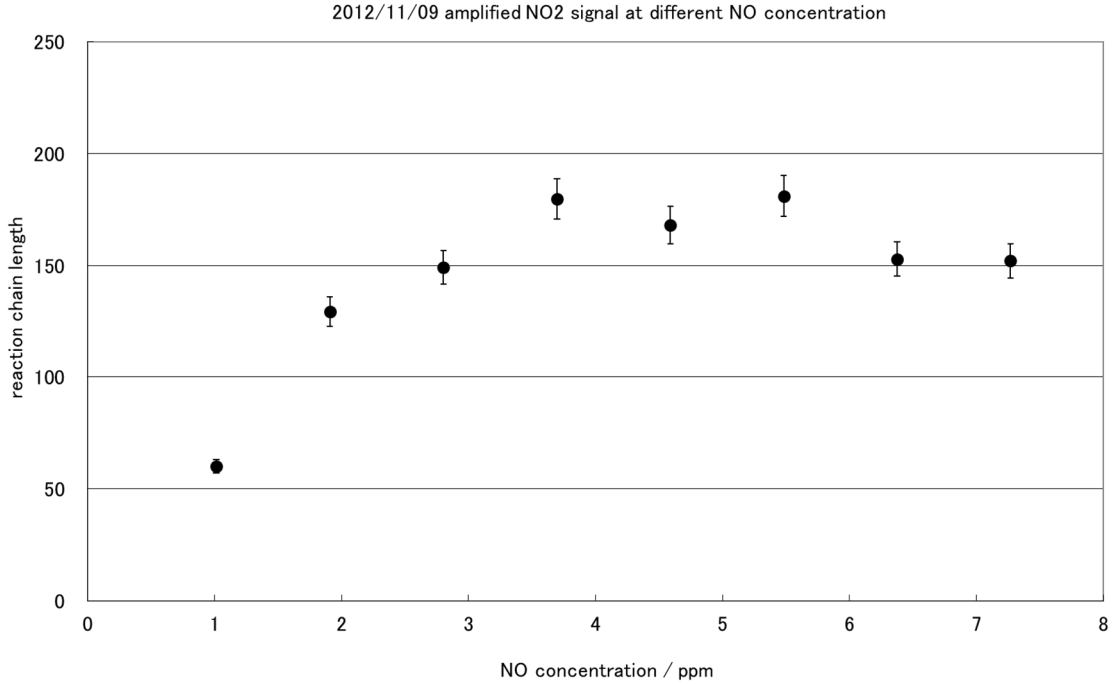

Fig.2-10 Reaction chain length at different NO concentration

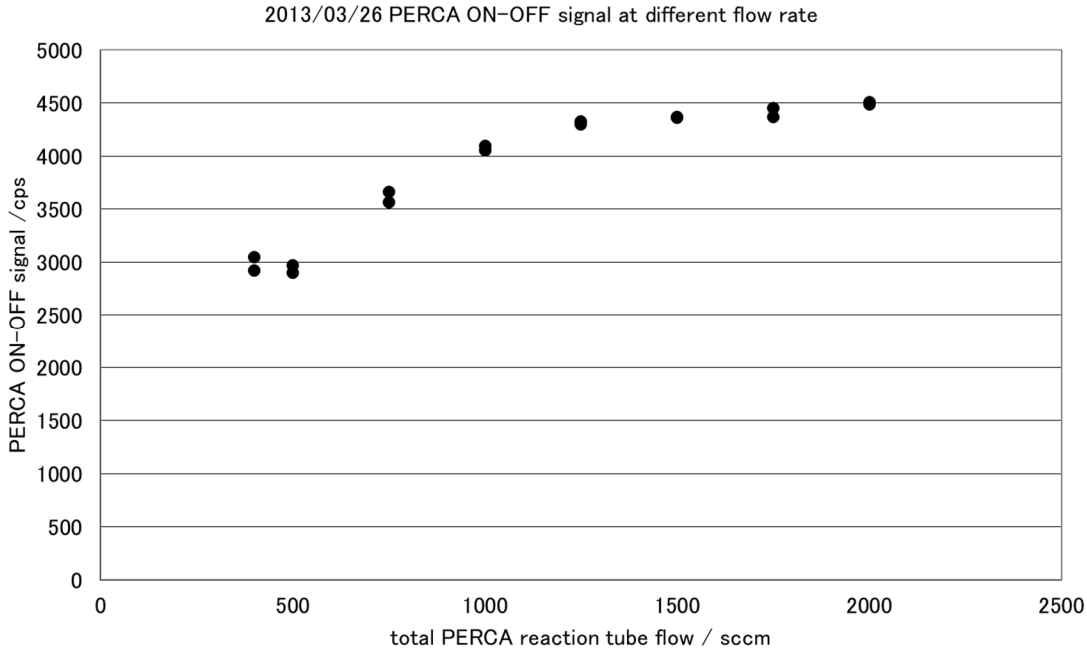

Fig.2-11 PERCA ON-OFF signal at different PERCA reaction flow rate

$$[OH]=[HO_2]=\frac{1}{2}\times\frac{\sigma_{H2O\_184.9}}{\sigma_{O2\_184.9}}\times\frac{[H_2O]\times[O_3]}{[O_2]} \qquad (2\text{-}25)$$

Result of chain length at different CO concentration is shown in Fig.2-9. Here, to make flow rate in PERCA reaction tube same, nitrogen was added instead of CO when CO concentration was low. Chain length was simply increasing with increment of CO concentration because there is no experiment was reported about radical loss process with CO. But it is needed to increase CO flow when we make CO concentration was high, sample air was more diluted and chain length will be low. Additionally, lower explosion limit of CO is 12.5 %. To keep distance from explosion limit, CO concentration was set to 10 %.

Result of chain length at different NO concentration is shown in Fig.2-10. Here also nitrogen is used to control NO concentration without changing flow rate. From Fig.2-10, reaction chain length was increasing until 4 ppm NO concentration, then after it started decreasing because of the effect of reaction (2-16), OH loss by reaction with NO become dominant. To maximize reaction chain length, NO concentration was set to 4 ppm.

Next, flow rate of PERCA reaction tube was fixed. At same concentration of CO and NO, flow rate of PERCA reaction tube was changed from 300 sccm to 2000 sccm. Result is shown in Fig.2-11. Result w divided to two part, 300 to 1000 sccm and over 1000 sccm.

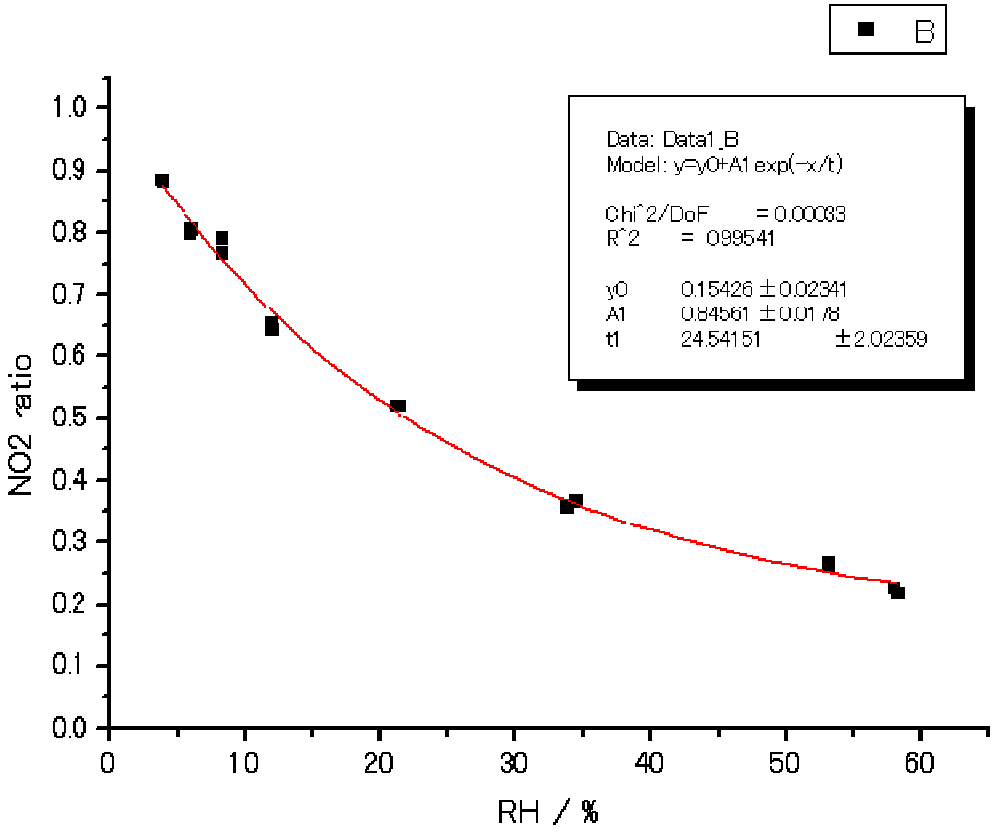

Fig.2-12 Relative chain length ration at different relative humidity

At the part of 300 to 1000 sccm, PERCA ON-OFF signal was increasing dew to longer reaction time. And over 1000 sccm, PERCA ON-OFF signal got stable because of HOx radical chain reaction was finished dew to loss of OH and HO_2. In this research, to save CO and NO and maximize reaction chain length, flow rate of PERCA reaction tube was set to 1000 sccm.

Mihele and Hastie (1998) reported that reaction chain length was getting lower in high relative humidity condition because of increment of wall loss of HO_2. Different concentration of water was added to sample air, then measured reaction chain length. Result is shown in Fig.2-12. Rection chain length decreases with increment of relative humidity.

Reaction chain length was also affected by O_3 concentration. After HOx generation from H_2O photolysis, O_3 which is generated another low pressure mercury lump is added, then introduced to PERCA reaction tube. Result is shown in Fig.2-13. Reaction chain length decreased correlated with O_3 concentration.

As a conclusion, PERCA reaction tube flow set to 1000 sccm, and CO and NO

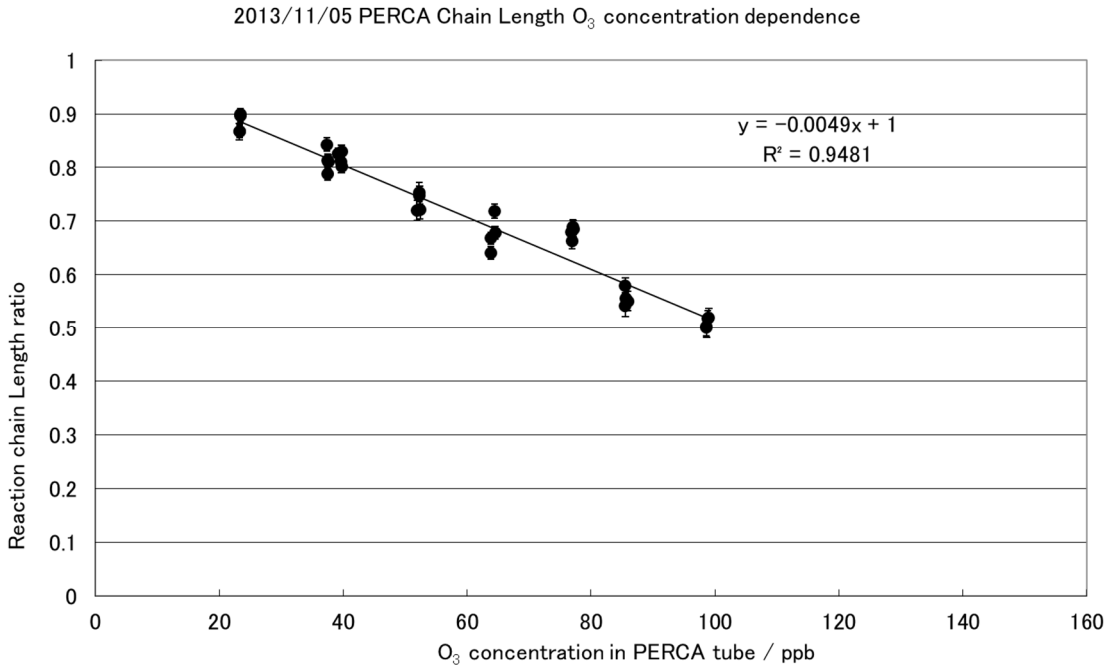

Fig.2-13 Reaction chain length at different O_3 concentration

concentration set to 10 % and 4 ppm individually. Reaction chain length was estimated as 174, at 0 % relative humidity and 0 ppb O_3 concentration. Then ambient relative humidity and O_3 concentration were measured, and used to the revision of reaction chain length. Here, LOD of HOx was calculated with LOD of NO_2 and reaction chain length as below:

$$LOD_{HOx} = \frac{LOD_{NO2}}{CL_{dry}} \qquad (2\text{-}26)$$

At 0 % relative humidity and 0 ppb O_3 concentration, LOD of HOx is calculated as 0.35 pptv.

2.3 Instrument configuration with tedlar bag

In ambient air measurement, because of high concentration of NO (4 ppm) in PERCA reaction tube, ambient O_3 is converted to NO_2, and then detected as background. Amplified signal is indicated as NO_2 and ambient NO_2 and O_3 is fluctuating, so background signal during PERCA ON is possibly not confirmed to background signal

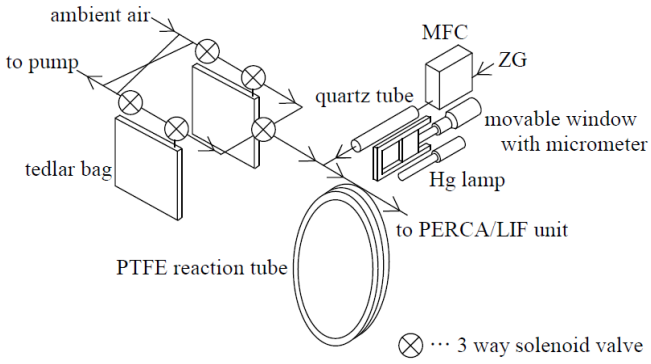

Fig.2-14 Tube configuration of ambient PHOx measurement with tedlar bag. MFC: Mass flow controller, ZG: Zero Gas produced by purified air by Thermo Model 111.

during PERCA OFF, it could lead to over/underestimating of amplified NO_2 concentration. We proposed that at first we took sample air to tedlar bag, and then measured PHOx. Configuration of the PHOx measurement system with tedlar bag is showed in Fig.2-14. By measuring O_3, NO_2 concentration normalized air through PERCA ON and OFF mode, amplified NO_2 concentration was measured accurately.

Sampling to tedlar bag, and PHOx measurement scheme are showed in Fig.2-15. Top of Fig.2-15, measurement scheme can be divided to 4 modes, a, b, c, d. and bag-pump connection is showed. Measured typical signal from tube connection is showed in middle of Fig.2-15. And at bottom of Fig.2-15 shows that each scheme is in which process. In mode a and c, to avoid remaining sample in last measurement, air was subtracted by diaphragm pump (ENOMOTO, MV-6005VP) at 4 L/min^{-1} to make bag empty before start sampling. For sampling to tedlar bag at scheme b and d, 3 L min^{-1} sampling was held by using diaphragm pump (IWAKI BA-230TN). Continuous measurement is worked out by using 2 bags, sampling and measuring at same time. During sampling air to tedlar bag, to avoid contamination of ambient ROx which leads to overestimation of produced HOx concentration, teflon filter (GL Science PF060) at the head of the inlet. Same O_3 concentration within reaction tube was preferred, but because of fluctuating O_3 concentration in ambient air, added O_3 concentration to set same concentration within ambient air was difficult. Then always 100 ppb O_3 was added in ether 0 ppb O_3 concentration or high O_3 concentration. Reaction time within reaction tube was 30 seconds. Here, Limit of detection of PHOx, LODPHOx was calculated as Eq (2-27).

$$LOD_{PHOx} = \frac{1}{t} \cdot \sqrt{\left(\frac{LOD_{ROx}}{O_{3add}} \right)^2 + \left(\frac{LOD_{ROx}}{(O_{3add})^2} \cdot LOD_{O3} \right)^2} \qquad (2\text{-}27)$$

Here, LOD_{ROx} and LOD_{O3} denote the limit of detection of ROx and O_3 concentration,

which is 0.21 pptv, 1 ppbv individually in this experiment. O_{3add} denotes added O_3 concentration (100 ppb). From Eq (2-27), LOD_{PHOx} is calculated as 1.85×10^{-5} pptv radicals $(ppbv\ O_3)^{-1}\ s^{-1}$. t denotes reaction time, 60 seconds. PERCA ON mode and OFF mode switched every 60 seconds, and removed first 30 seconds off for waiting stabilization of PERCA ON/OFF signal. PERCA ON/OFF signal were measured one time for each tedlar bag, PHOx value was taken every 2 minutes. Residence time of sample gas within reaction tube was 60 seconds, which same time as PERCA ON/OFF measurement time, and first 30 second data is removed, effect of previous (remaining) air sample was ignored.

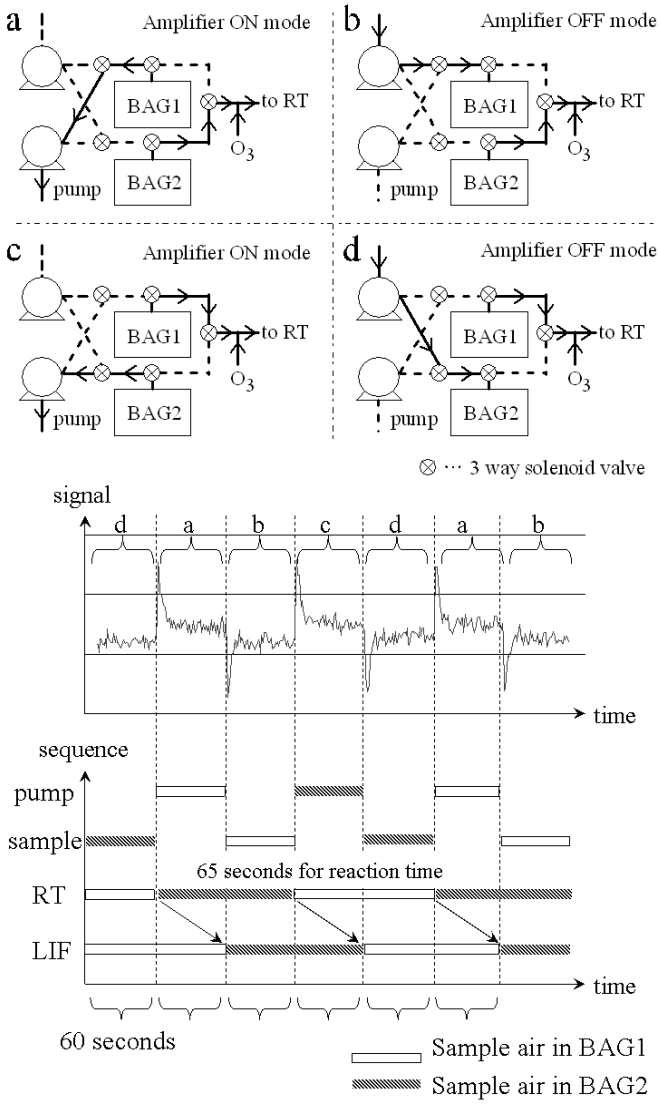

Fig.2-15 Cycle of ambient PHOx measurements sampling via a tedlar bag. Top: Tube configuration for each of the 4 modes, Middle: Typical PERCA/LIF signal for each mode, Bottom: measurement scheme of each air sample. RT: reaction tube.

3 Fundamental experiment by the reaction of single VOC and O_3

3.1 Generated ROx concentration from single VOC and O_3 concentration

For the fundamental measurement of radical production from VOC + O_3 reaction, single VOC and O_3 reaction experiment was derived. For the single VOCs, propene, isoprene, cyclohexene, and limonene were chosen. Propene was chosen for the simple olefin experiment. Ethylene is the simplest olefine, but reaction rate constant is much lower compare than other olefins. And propene is exist meaningful amount in troposphere from anthropogenic source. Isoprene is typical biogenic VOC, which is abundant within VOC in the atmosphere. By using isoprene which takes account of 44 % (Guenther et al., 1995) of BVOC as model VOC, this fundamental experiment is close to real atmospheric condition. And Cyclohexene was chosen for the fundamental experiment of simple cyclic olefin. It is said that the mechanisms of ozonolysis of cyclic olefins are still including uncertainties. Limonene is one of the monoterpene species, which has high carbon number, 10, mainly emitted from plants and has high reactivity with O_3 and OH, then high OH and HO_2 yield. Limonene was used for advanced fundamental experiment. By measuring produced ROx concentration from single VOC and O_3, with varied O_3 and VOC concentration for checking response to added O_3 and VOC concentration.

3.1.1 Propene experiment

The result of produced ROx concentration O_3 concentration dependence from several propene concentration is shown in Fig.3-1. Produced ROx concentration is showed in y axis, and added O_3 concentration is showed in x axis. Measured ROx concentration increased similar as increment of O_3 concentration, but not respond linearly. Least square fit described increment of ROx concentration as power-exponential. The reason produced HOx concentration respond non-linearly, radical-radical reaction is possibly occurred as equation below.

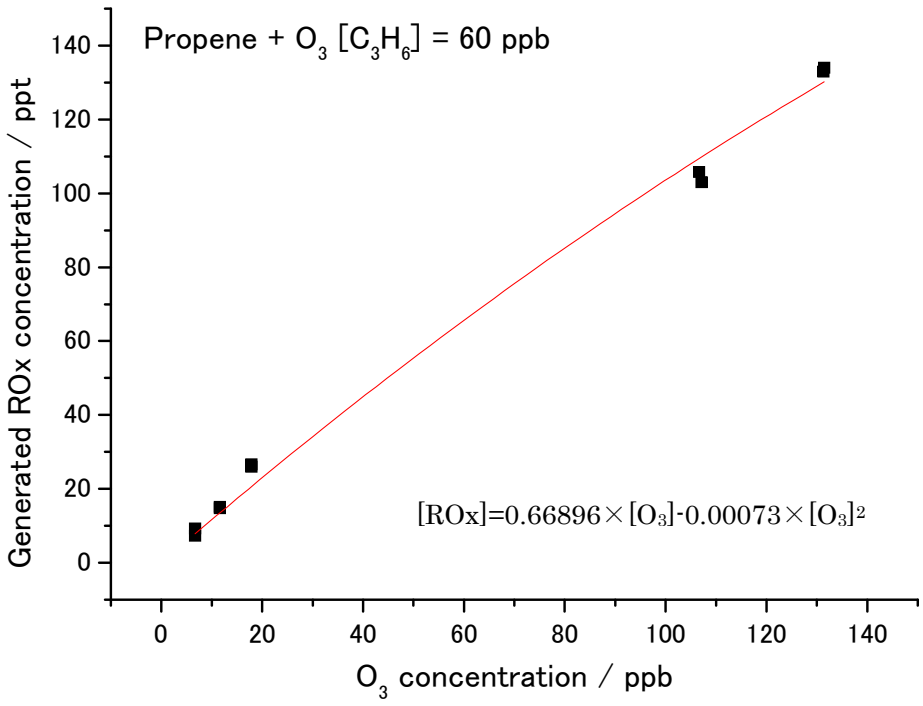

Fig.3-1 Generated ROx concentration from propene and O_3 at several O_3 concentration

$$HO_2 + HO_2 \rightarrow H_2O_2 + O_2 \qquad (1\text{-}40)$$

$$HO_2 + RO_2 \rightarrow ROOH + O_2 \qquad (1\text{-}41)$$

$$RO_2 + RO_2 \rightarrow ROOR + O_2 \qquad (1\text{-}10)$$

$$OH + HO_2 \rightarrow H_2O + O_2 \qquad (3\text{-}1)$$

In low O_3 condition, produced ROx concentration is less compare than high O_3 condition, so radical-radical reaction is less occurred. By calculating the slope of fitting curve at O_3 concentration close to o ppbv, (∂ [ROx]/ ∂ [O_3]), only produced HOx concentration is estimated.

From fitted curve at Fig.3-1, produced ROx concentration can be expressed as added O_3 concentration as Eq (3-2).

$$[ROx] = 0.66896 \times [O_3] - 0.00073 \times [O_3]^2 \qquad (3\text{-}2)$$

Here, coefficient, 0.66896 is assumed that is relating to isoprene concentration, Eq (3-

2) can be described as general Eq (3-2)'. Then the experiment within same O_3 concentration and varied propene concentration is worked out.

$$[ROx] = \alpha \times [O_3] - \beta \times [O_3]^2 \qquad (3\text{-}2)'$$

The result of propene and O_3 reaction at various propene concentration is shown in Fig.3-2. Generated ROx concentration from propene and O_3 reaction respond to linearly with added propene concentration.

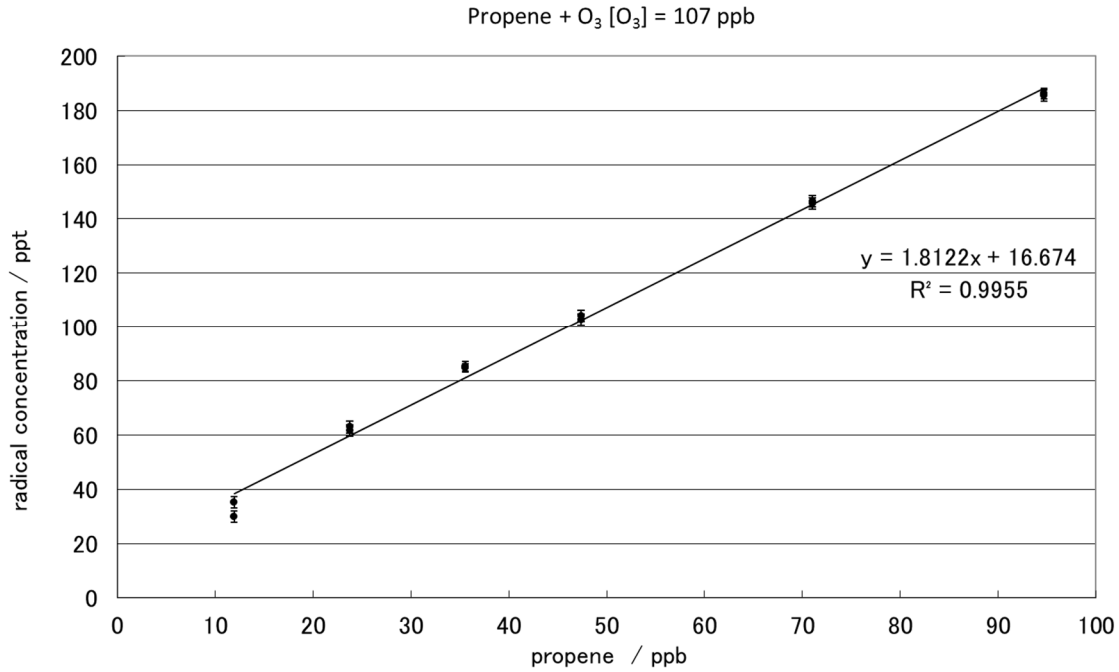

Fig.3-2 Generated ROx concentration from propene and O_3 reaction at several propene concentration

3.1.2 Isoprene experiment

The result of produced ROx concentration of 47 ppb isoprene and varied O_3 reaction is showed at Fig.3-3. Same as 4.1.1.1 Propene experiment, generated ROx concentration from isoprene and O_3 reaction increase regards to added O_3 concentration.

Fig.3-4 showed that produced ROx concentration is respond linearly to isoprene concentration. If VOC concentration is changed in ambient air, produced ROx concentration respond linearly, PHOx is simply estimated.

3.1.3 Cyclohexene experiment

The result of fundamental experiment for the cyclic olefin with cyclohexene is shown

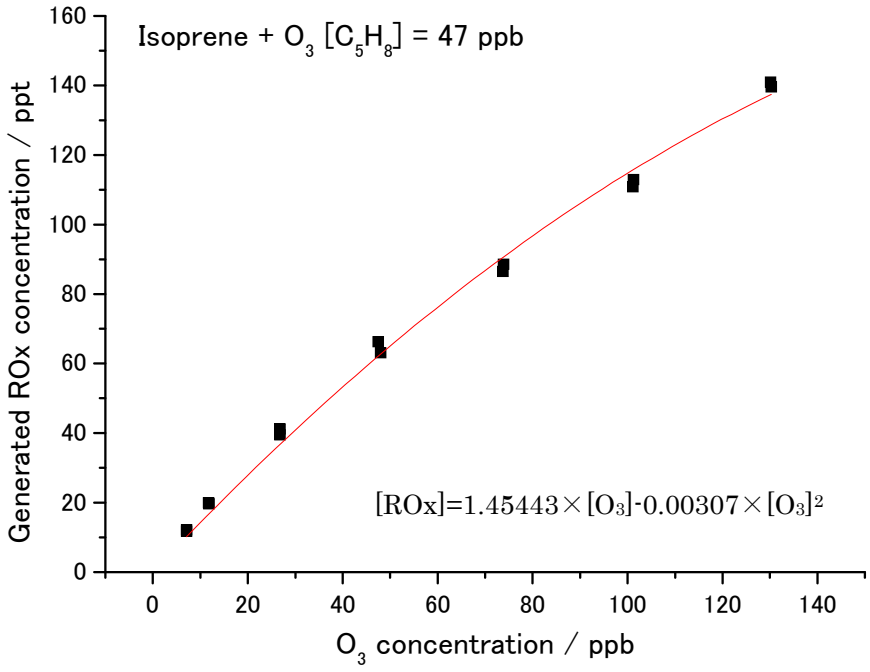

Fig.3-3 Produced ROx concentration at different O_3 concentration

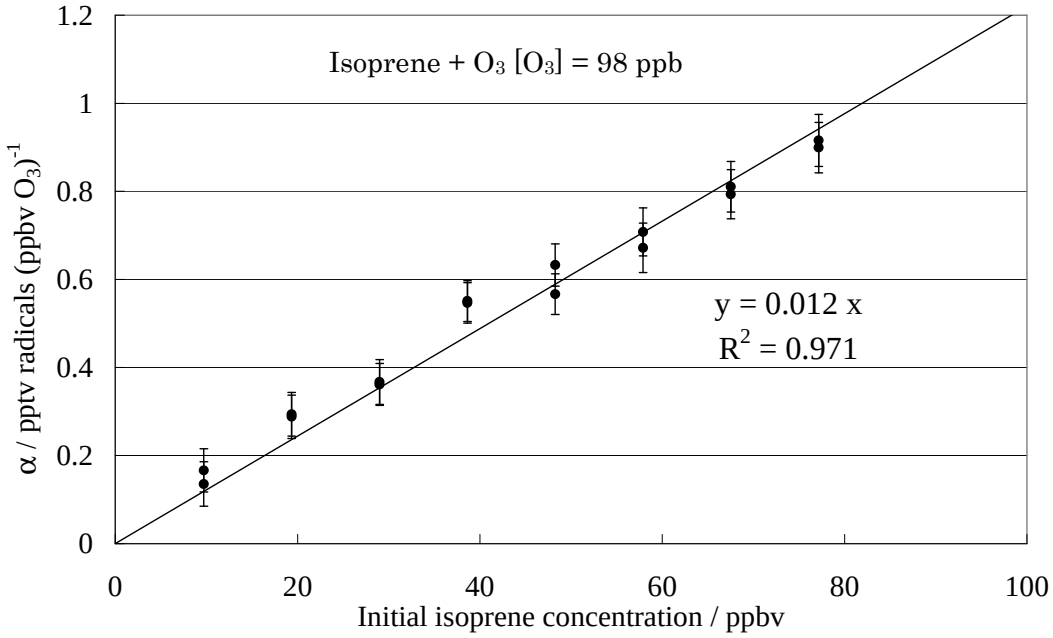

Fig.3-4 Produced ROx concentration from the experiment of same concentration of O_3 and varied concentration of isoprene reaction. Normalized produced radical concentration α, which is in equation is showed in y axis

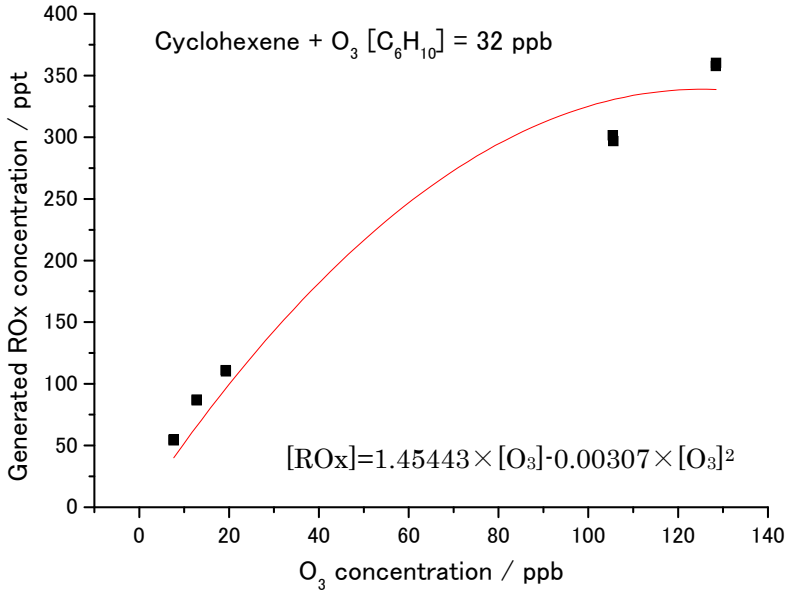

Fig.3-5 Generated ROx concentration from cyclohexene and O_3 reaction at several O_3 concenration

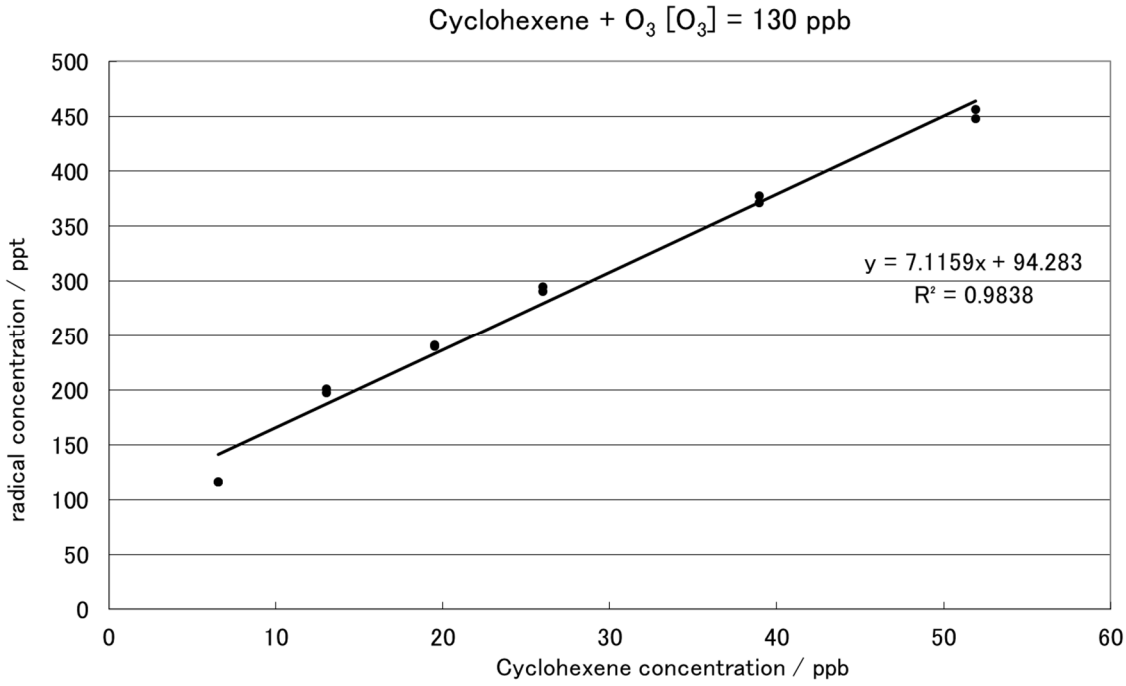

Fig.3-6 Generated ROx concentration from cyclohexene and O_3 reaction at several cyclohexene concentration

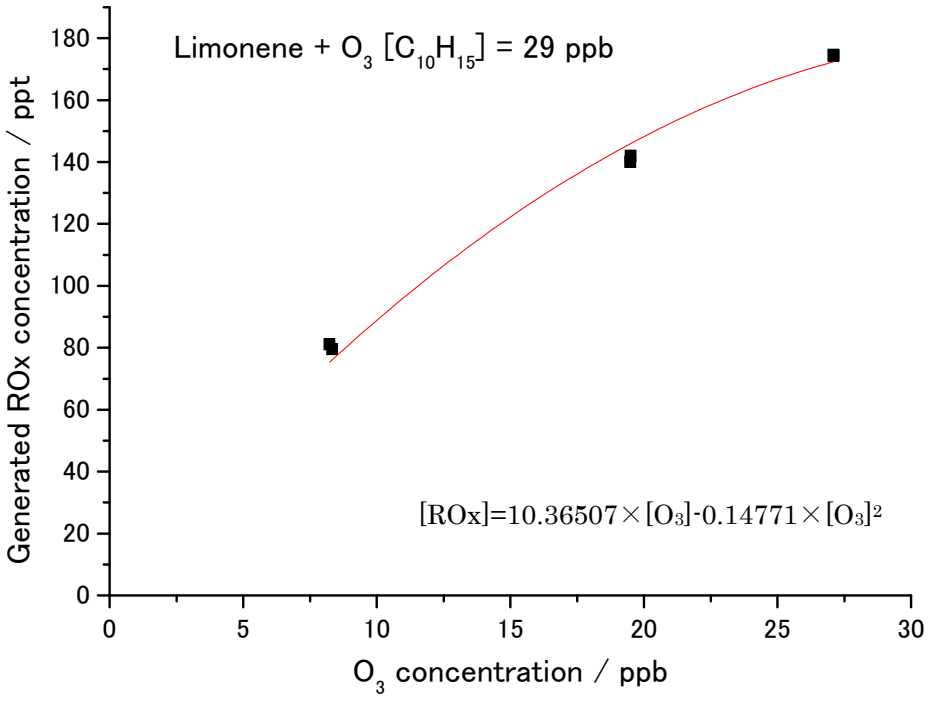

Fig.3-7 Generated ROx concentration from limonene and O_3 reaction at several O_3 concentration

in Fig.3-5. Generated ROx concentration from cyclohexene also increased non-linearly. Generated ROx concentration with various cyclohexene concentration is shown in Fig.3-6. Generated ROx concentration respond to linearly with cyclohexene concentration. This result shows that cyclic olefins possibly act same as other simple olefins.

3.1.4 Limonene experiment

The result of advanced fundamental experiment with limonene is shown in Fig.3-7. Generated ROx concentration from limonene and O_3 reaction respond to linearly with added O_3 concentration.

For the summary of generated ROx concentration from single VOC and O_3, αβ, multiplied parameter of α and β from the fitting curve of Eq(4-2)' versus each VOC concentration is shown in Fig.3-8. αβ includes reaction rate constant with O_3 and VOC, and HOx yield for each VOC species. Fig.3-8 indicates each VOC has own tendency.

Fig.3-9 indicates correlation between slopes of the formula of each VOC in Fig.3-8 vs calculated reaction rate constant and HOx yield for each VOC. Each plot correlates linearly. It indicates that fundamental experiments get reasonable result compare with

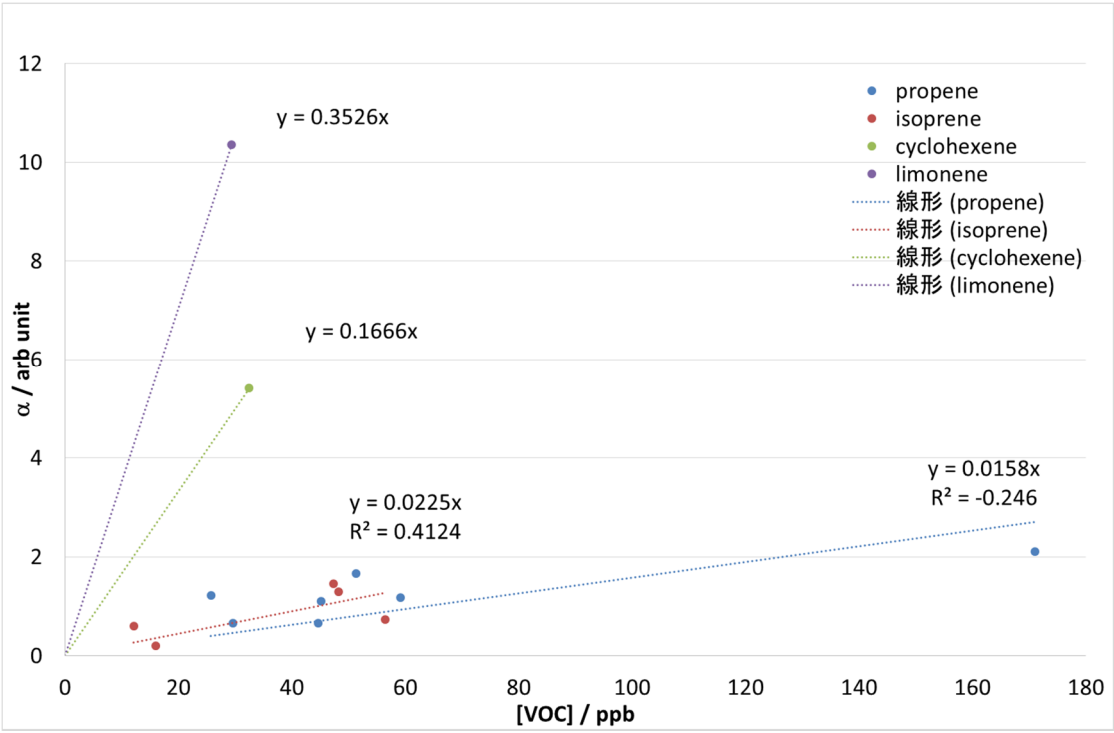

Fig.3-8 VOC concentration dependence of fitting parameter αβ

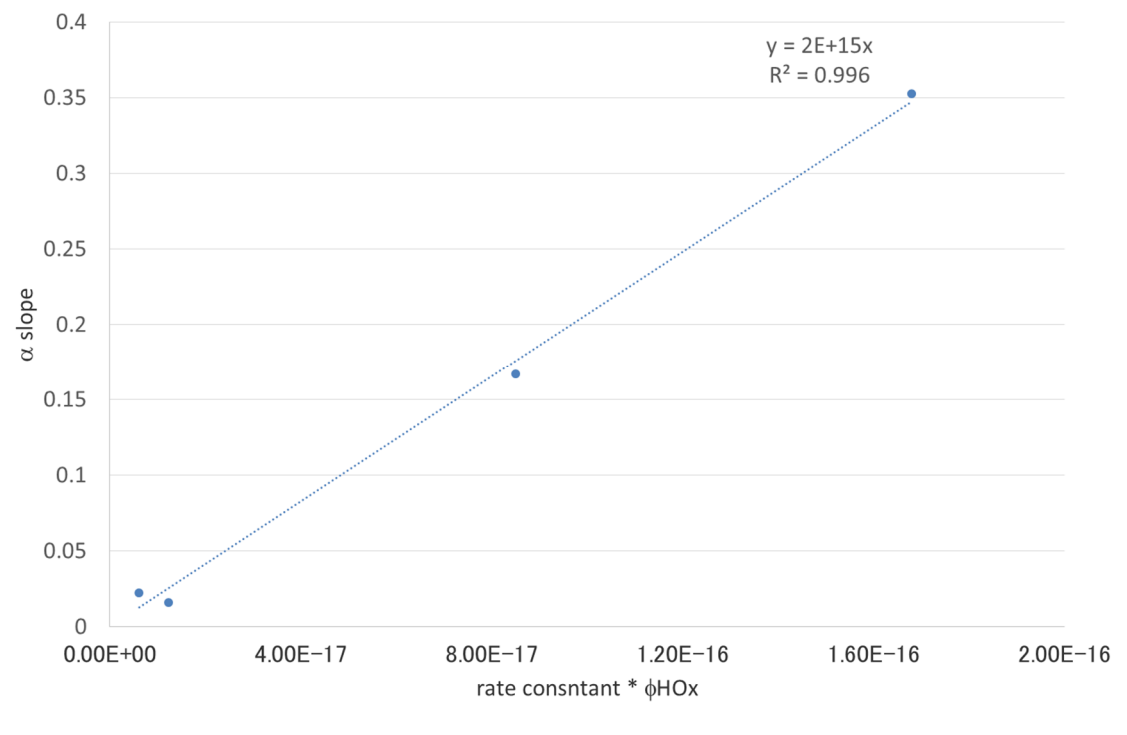

Fig.3-9 αβ slope vs multiplication of reaction rate constant with O_3 and HOx yield for each VOC species

previous experiment. By fixed with Eq(4-2)', HOx production rate in ambient air measured accurately.

3.2 Chemical interferences

Generated ROx from VOC+O_3 reaction within reaction tube will be decreased by several loss process, for example reaction of ROx and NOx, heterogeneous loss of ROx. In this section, effect of possible ROx loss process were estimated, and observed PHOx value was revised.

3.2.1 Wall loss rate determination with MCM model calculation

4 cm diameter glass tube is used as reaction tube in this experiment. Measured ROx concentration might be underestimating than actually generated HOx concentration because of the heterogeneous loss process of ROx species at the wall of reaction tube. Therefore, by comparing measured ROx concentration with calculated ROx concentration with model calculation, instrument function, K, which is correcting influence of wall loss of ROx species, is estimated.

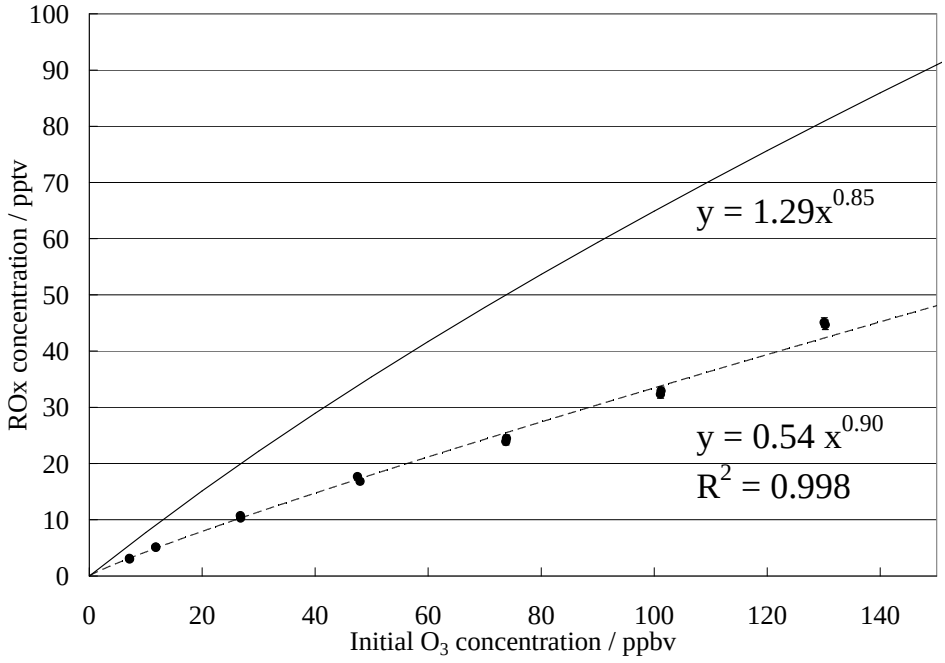

Fig.3-10 Comparison of observed ROx concentration and calculated ROx concentration

$$PHOx = \frac{d}{dt}\left(\frac{\partial[RO_x]}{\partial[O_3]}\right)\cdot K \qquad (3\text{-}3)$$

Comparison between measured ROx concentration and Modeled ROx concentration is showed in Fig.3-10. MCM Model calculation version 3.1 (Bloss et al. 2005) is used for calculation of modeled ROx concentration. Modeled ROx concentration calculated by MCM respond to similar behavior with measured ROx concentration. Modeled ROx concentration respond to power-exponential. Whereas MCM calculation did not include heterogeneous reaction, wall loss of ROx species, it excess than measured ROx concentration. Instrument function K is estimated by dividing the slope of modeled ROx concentration at O_3 concentration at 1 ppbv by the slope of measured ROx slope by measured ROx, as 2.26. Definition of PHOx, is fixed as Eq (3-3)'.

In the reaction tube, generated OH react rapidly with many kinds of VOC, and several RO_2 are generated and the rate constant of wall loss might be depend on each VOC (Miyazaki et al., 2010). Instrument function K in this experiment is assessed by using isoprene, which is abundant species in the atmosphere, rate constant of wall reaction of several RO_2 which are generated in the atmosphere. The effect of loss reaction of other RO_2 is future subject.

3.2.2 Chemical interference of NOx

In the presence of NOx (NO, NO_2), O_3 and ROx radicals can react with ambient NOx species and removed from gas phase. Generated ROx concentration from VOC + O_3 reaction at various concentration of NOx species is checked in this chapter.

3.2.2.1 Interference of NO

NO can react with O_3 rapidly then it cause decrement of initial O_3 concentration for the use of VOC + O_3 reaction. Generated ROx concentration from isoprene and O_3 reaction at various NO concentration is showed in Fig.3-11. Isoprene and ozone concentration is constant, 50 ppb and 100 ppb individually. Observed ROx concentration is normalized by added O_3 concentration same as Fig.3-11. Added NO concentrations changed from 0 to 27 ppb. Generated ROx concentration decays exponentially. Least square fitting calculates generated RO_2 decrement as Eq (3-4). Interference of NO can be calculated from ambient NO concentration.

$$\alpha = 0.21 + 0.27\exp\left(-\frac{[NO]}{9.63}\right) \qquad (3\text{-}4)$$

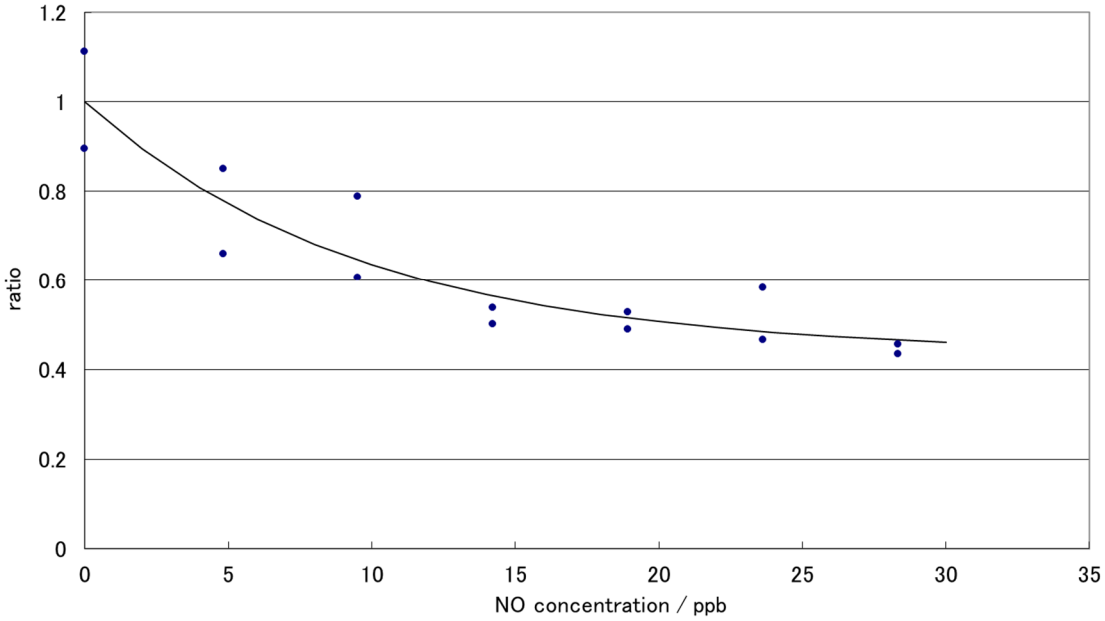

Fig.3-11 Ratio of generated RO_2 radical concentration at various NO concentrations

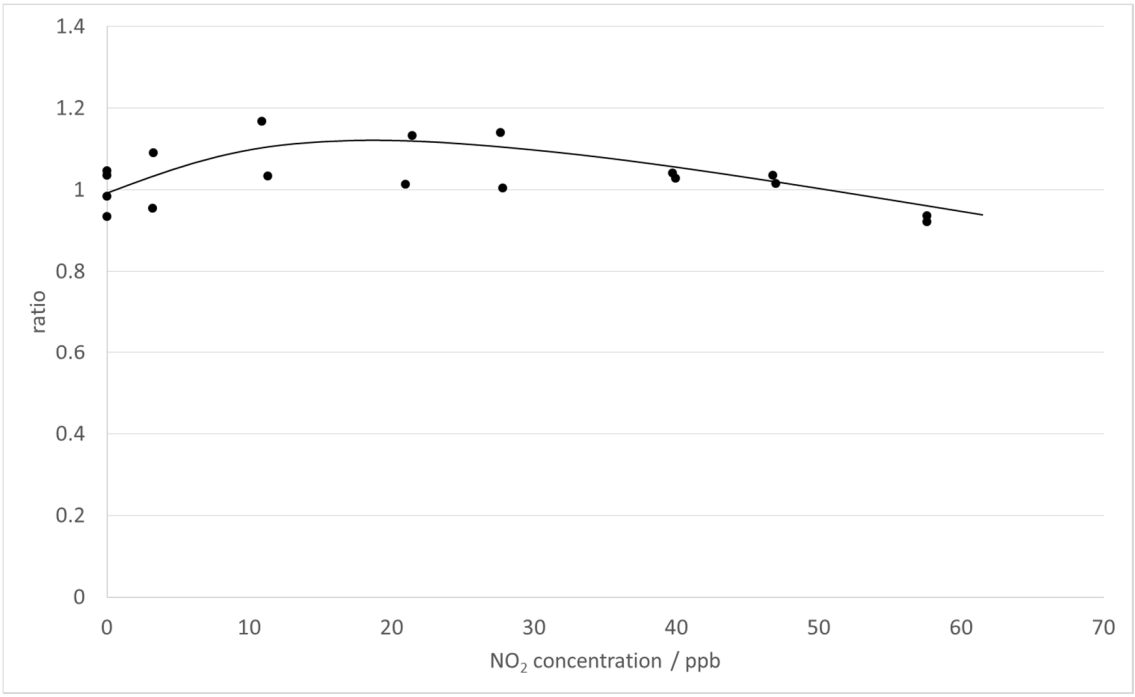

Fig.3-12 Ratio of generated ROx radical concentration at various NO_2 concentrations

3.2.2.2 Interference of NO_2

To check the effect of NO_2 during ozonolysis of VOC, isoprene and O_3 reaction is held with various NO_2 concentrations. NO_2 concentration is changed from 0 to 60 ppb. Isoprene and ozone concentration is constant, 50 ppb and 100 ppb individually. The result of generated RO_2 concentration at various NO_2 concentrations is showed in Fig.3-12. Generated RO_2 concentration has two distinct, increasing during 0 to 10 ppb and decreasing over 20 ppb of NO_2 concentration. At 0-10 ppb NO_2 period, NO_3 radical which is generated from $NO_2 + O_3$ reaction react with isoprene then formed RO_2 attributed to increment of measured RO_2 concentration. Generated RO_2 radical from reaction of NO_3 and isoprene, nitrooxyalkyl peroxy radical, can react with NO and generate HO_2 (Berndt and Boge, 1997, Fun and Zhang, 2004) so that contribute to ROx increment.

Whilst in the presence of NO_2, OH react with NO_2 to form HNO_3, HO_2 and RO_2 react and form peroxynitric acid, organic nitrate individually which can dissociate and re-form HO_2 and RO_2. This loss process influenced to over 20 ppb NO_2 period. Here, Generated ROx concentration have not been approximated by fitting because of high uncertainty of mechanisms, but NO_2 concentration during ambient air measurement was below than 20 ppb and effect of NO_2 interference is within experimental errors. PHOx value includes 10 % uncertainty when NO_2 concentration is high.

3.2.2.3 Interference of NO_3

In the section 4.1.4.2, effect of NO_3 radical is suggested. There are many uncertainty about RO_2 radical from NO_3 with VOC reaction. And also ROx from NO_3 radical is not actually HOx radical generation from ozonolysis (Berndt and Boge, 1997, Fan and Zhang, 2004). In this chapter, detail of NO_3 photolysis cell constraction which can remove the ROx generation from NO_3 radical only will be explained.

NO_3 can photolyze by absorbing light (Eq (3-5) and (3-6))

$$NO_3 + h\upsilon \rightarrow NO_2 + O \qquad (3\text{-}5)$$

$$NO_3 + h\upsilon \rightarrow NO + O_2 \qquad (3\text{-}6)$$

Experimental configuration is shown in Fig.3-13. Artificially NO_3 is generated as $NO + O_3$ reaction, then introduced to NO_3 photolysis cell. For the NO_3 photolysis cell, 5 cm diameter and 25 cm length PYLEX tube is used. As shown in Fig.3-14, 30 LEDs (Opto Supply OSM5XME3C1S) which wavelength is 595 ± 5 nm is set and irradiated from both side and top of the PYLEX tube (Fig.3-14).

After photolysis cell, NO_3 concentration is measured by BB-CEAS (Broad Band – Cavity Enhanced Absorption Spectroscopy) technique (Berdent and Meijer, 2000, Ball et al., 2004). Result of experiment is summarized in Table 3-1. Result indicates the difference between LED ON and OFF. Photolysis rate of NO_3 by LED is lower than 10% at all experiments. Higher intensity LED or longer

residence time is required to photolyze NO3 efficiently.

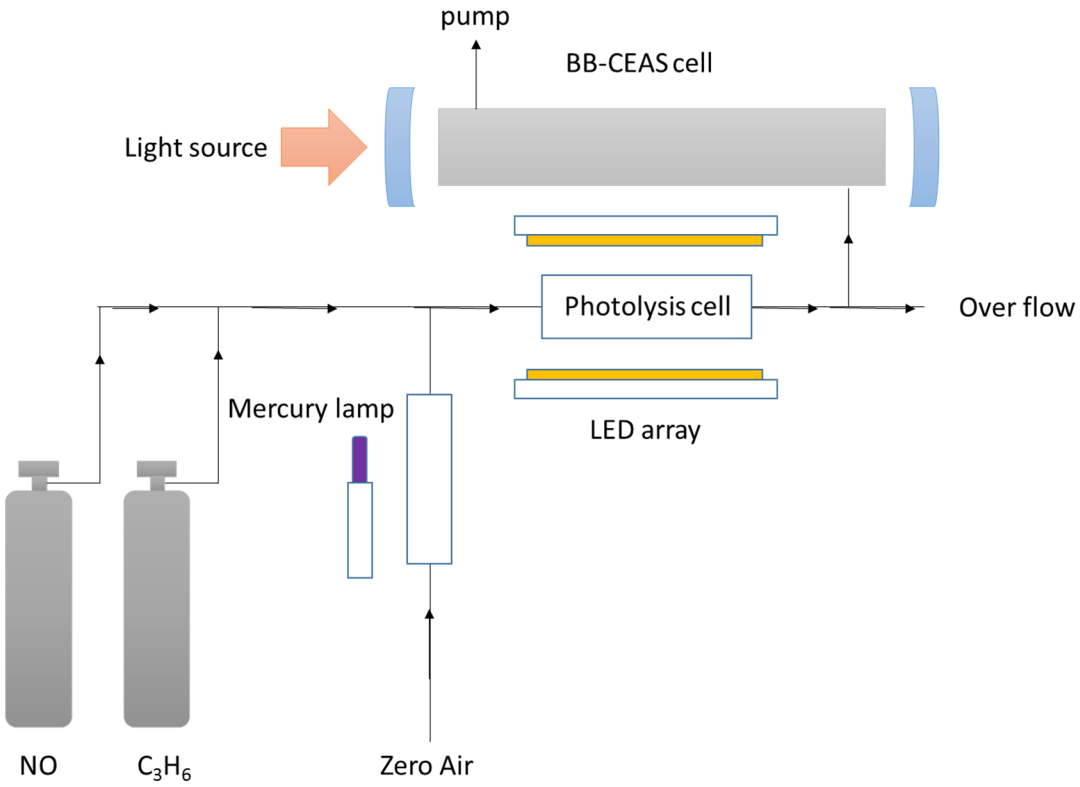

Fig.3-13 Construction of NO_3 photolysis cell

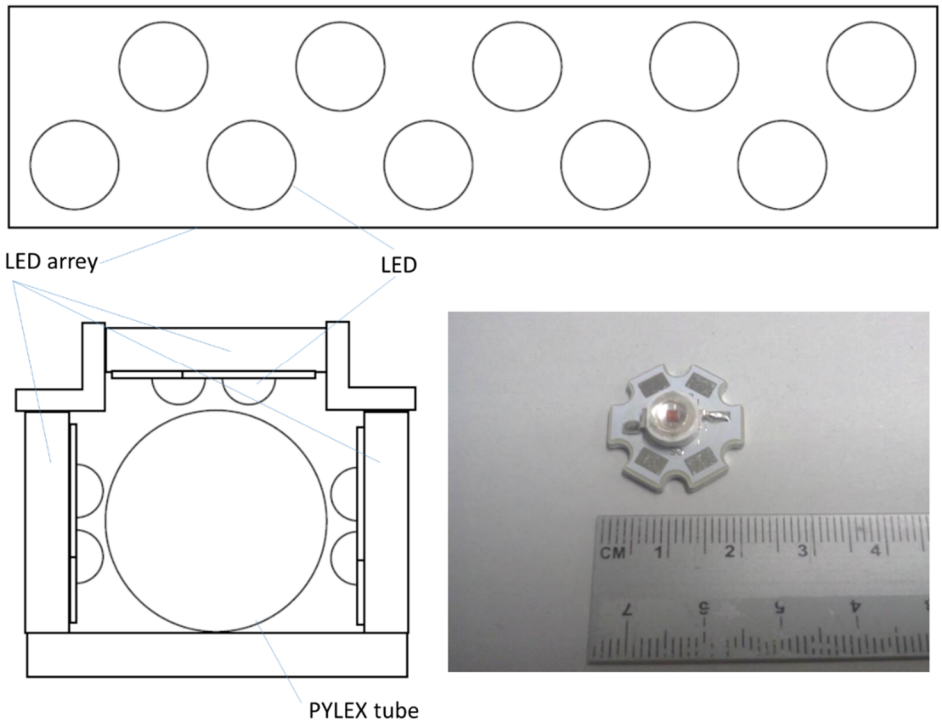

Fig.3-14 Configuration of LED array for NO_3 photolysis

Table 3-1. Result of experiment with NO_3 photolysis cell

	remained NO3 radical
4/4	
1st time	89.4%
2nd time	91.2%
3rd time	89.7%
4th time	89.4%
5th time	91.2%
6th time	89.7%
4/5	
1st time	96.3%
2nd time	92.1%
3rd time	90.7%
4/6	
1st time	80.1%
without inlet	98.6%
less O3	86.0%
higher O3	99.1%
with C3H6 1st	52.8%
with C3H6 2nd	32.6%
4/7	
1st time	100.5%
2nd time	91.5%
with C3H6 1st	83.3%
with C3H6 2nd	103.9%
with C3H6 3rd	73.3%
4/8	
1st time	96.6%
2nd time	94.0%
with C3H6 1st	75.4%
with C3H6 2nd	79.9%

4 Ambient PHOx measurement

4.1 Ambient air measurement

Ambient PHOx measurement was held with comprehensive measurement. Mainly with Thermo O_3 analyzer (Model 49C, UV absorption tecnique), NOx analyzer (Model 42iTL, NO+O_3 chemiluminescence) and CO analyzer (Model 48i, Non Dispersive Infrared Spectroscopy). Ambient ROx concentration also measured by using PERCA technique.

4.1.1 2013/07/10 to 2013/07/12 at Kyoto University Yoshida South Campus

First ambient PHOx measurement was held during 2013/07/10 to 2013/07/12 in Kyoto University Yoshida-South campus. Measurement side is shown in Fig.4-1. Orange line indicates main road of Kyoto city with heavy traffic, Higashi-Oji Street and Imadegawa Street. Anthropogenic VOC and NOx emission are expected. Green line indicates Mt. Yoshida. Biogenic emission from plants is expected during north-east wind event. Inlet is set at 3rd floor and placed in front of cortile with many series plants which can emit biogenic VOCs. At same time period, ROx concentration by PERCA technique, and O_3, NOx concentration measurement are held.

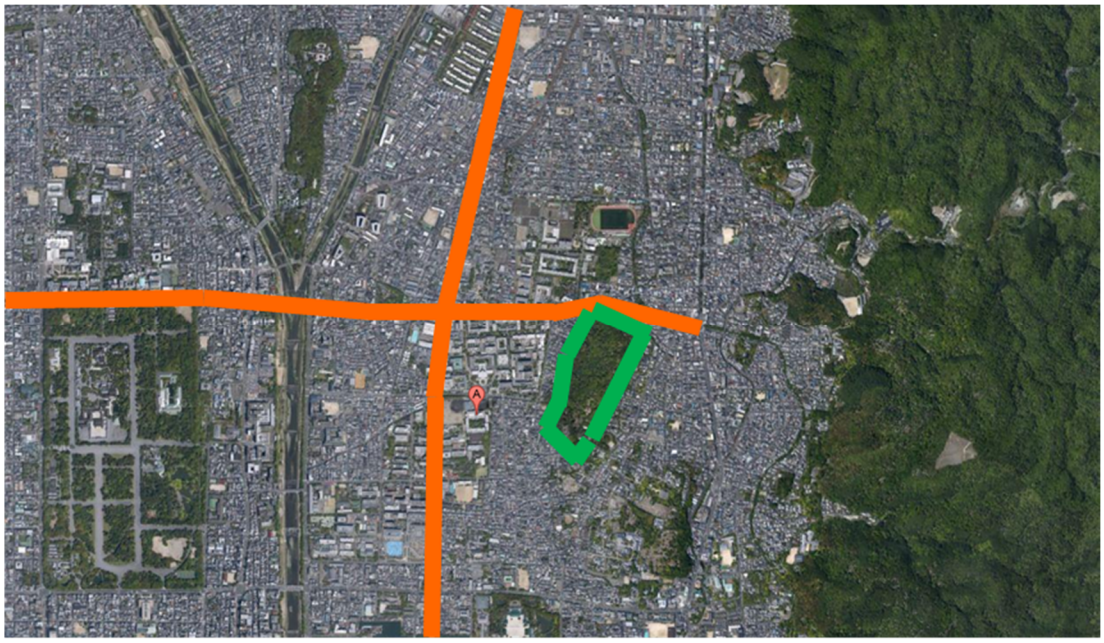

Fig. 4-1 Ambient PHOx measurement site during 2013/07/10 to 2013/07/12

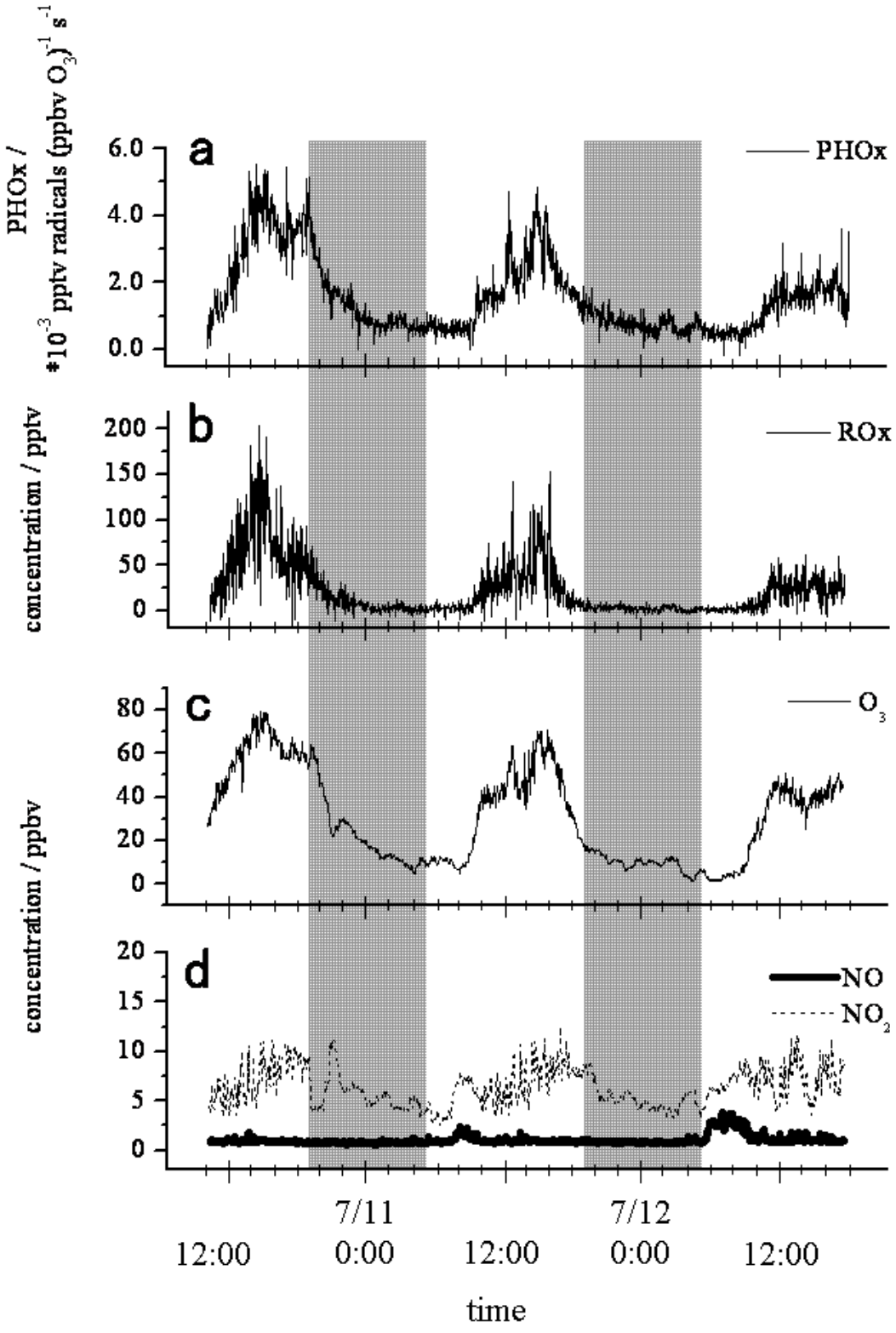

Fig.4-2 Ambient PHOx and ROx, O_3, NOx concentration measurement during 2013/07/10 to 2013/07/12. Gray mesh indicate nighttime

Successfully ambient PHOx value is measured, and tend to high during daytime, low during nighttime. PHOx value has similar trend with ROx concentration and O_3 concentration. Biogenic VOC such as α-pinene, β-pinene and limonene has high reactivity with O_3 and high HOx yield from VOC and O_3 reaction. Gray mesh in Fig.4-2 indicates nighttime, which after sunset and before sunrise. At 7/10 night, small amount of ROx concentration is measured but not in 7/11 night. During 7/10 night, PHOx value and O_3 concentration is higher than 7/11 night. This tendency is consistent with previous research about nighttime radical production from VOC and O_3 reaction, and concept of PHOx measurement. The comparison between observed PHOx value and VOC concentration is needed to evaluate direct measurement of HOx production rate.

4.1.2 2013/08/19 to 2013/09/13 at Kyoto University Yoshida South Campus

Ambient PHOx measurement with NO_3 photolysis cell is held in 2013/08/19 to 2013/09-13 in Kyoto University Yoshida South Campus. This PHOx measurement is held as comprehensive measurement for assessment of radical behavior in atmosphere. In Table. 4-1, instrument list is shown. ROx concentration and PHOx values are measured by PERCA technique showed in this research. To estimate HOx production rate from photolysis, photolysis rate constant, J value are measured by spectroradiometer. This instrument can measure 32 species, and 34 pathways photolysis rate constant. OH reactivity measurement which can measure OH radical loss rate in ambient air is held by using LASER pump-probe technique. Especially terminal productions from radical chain reaction, several nitrate compounds and aerosols are measured in wide techniques particularly.

Result of PHOx and ROx concentration is shown in Fig.4-4. Similar as ambient PHOx measurement campaign during 2013/07/10 to 2013/07/12, PHOx and ROx, O_3 concentrations tend to high during daytime and low during nighttime. Diurnal average of PHOx and ROx concentration are shown in Fig.4-5. Here, by comparing with O_3 concentration during measurement campaign, it suggests nighttime PHOx strongly enhance ROx concentration.

Concentration of VOCs are measured successfully during 2013/08/20 to 2013/08/22. Time dependence of VOC concentration is shown in Fig.4-7. In contrast to PHOx measurement, diurnal variation is not clear. For the estimation of VOC contribution to PHOx value, PHOx value is calculated by using measured VOC concentration, reaction rate constant and HOx yield which is summarized at Table 4-2. PHOx from measured VOCs are calculated by following Eq (4-1)

$$PHOx_{calc} = k_{VOC1+O3}[VOC_1][O_3] + k_{VOC2+O3}[VOC_2][O_3] + \ldots + k_{VOCn+O3}[VOC_n][O_3]$$

Table.4-1 Instrument list of ambient PHOx measurement campaign during 2013/08/19 to 2013/09/13

Measurement Items	Measurement Methods	Institution
RO_x (OH, HO_2, RO_2) concentration	PERCA technique	Kyoto University
PHOx	PERCA technique	Kyoto University
OH reactivity	Laser pump-probe technique	Kyoto University
Photolysis rate	Spectroradiometer	Kyoto University
VOC concentration	GC-FID	Kyoto University
	Fast GC	National Institute for Environmental Studies
	GC-MS with absorption tube	Kyoto University
	PTR-MS	Tokyo Metropolitan University
CO concentration	NDIR Absorption	Kyoto University
	Mid IR Laser Absorption	Kyoto University
O_3 concentration	UV Absorption	Kyoto University
SO_2 concentration	Pulsed UV Fluorescence	Kyoto University
N_2O_5 concentration	Cavity Enhanced Absorption Spectroscopy	Tokyo University of Agriculture and Technology
PAN concentration	GC-MS with absorption tube	Osaka City Environmental Bureau
Aerosol size distribution	Scanning Mobility Particle Sizer	Nagoya University
	Optical Particle Counter	Nagoya University
SOA production rate form VOC+O_3 reaction	Scanning Mobility Particle Sizer	Nagoya University
NO_2, peroxy and organic nitrate, HNO_3 concentration	Thermal Dissociation NO_2 LIF	Nagoya University
Nitric acid concentration	Scrubber difference / Chemiluminescence	Osaka Prefecture University
NO_2 concentration	NO_2 LIF	Teikyo University of Science
	Cavity Attenuated Phase Shift Spectroscopy	Osaka Prefecture University
	Photolytic conversion / Chemiluminesecne	Kyoto University

$$= \sum_{i=1}^{n} k_{VOCi+O3}[VOC_i][O_3] \qquad (4\text{-}1)$$

Time dependence calculated PHOx and contribution from VOCs are shown in Fig.4-8. Calculated PHOx during measurement period is averaged and shown in Fig.4-9. Through this measurement period, trans-2-pentene has highest contribution. Next highest contribution is from one of the biogenic VOC, α-pinene. After that, cis-2-butene, b-pinene, 1-pentene and trans-2-butene follow. Main expected biogenic VOC, isoprene contribution contributes only 3 %. It suggest that terpene emitter, needle leaf tree has dominant effect compare than broad-leaf tree in this site, in this season.

Comparison between observed PHOx and calculated PHOx in the means of time series is shown in Fig. 4-10. Absolute value is not in same magnitude but trend of observed and calculated looks similar. Scatter plot of observed PHOx and calculated PHOx is shown in Fig.4-11 Clear positive correlation can be seen between observed PHOx and calculated

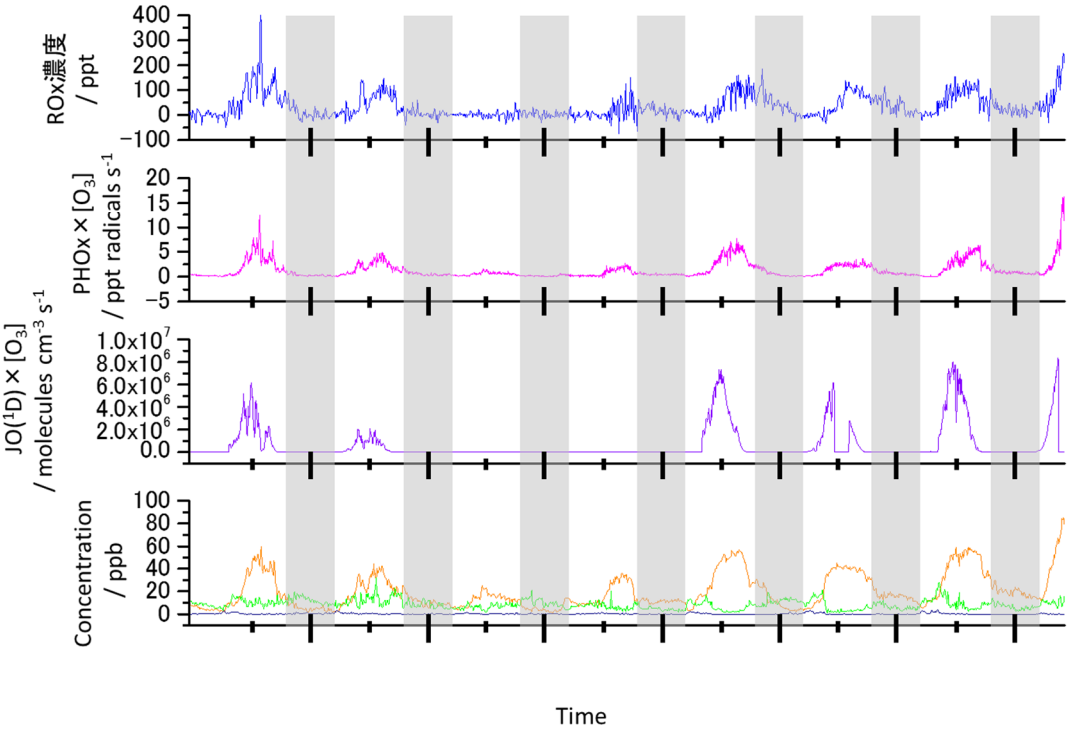

Fig.4-3 Observed value during 2013/08/19 to 2013/09/13

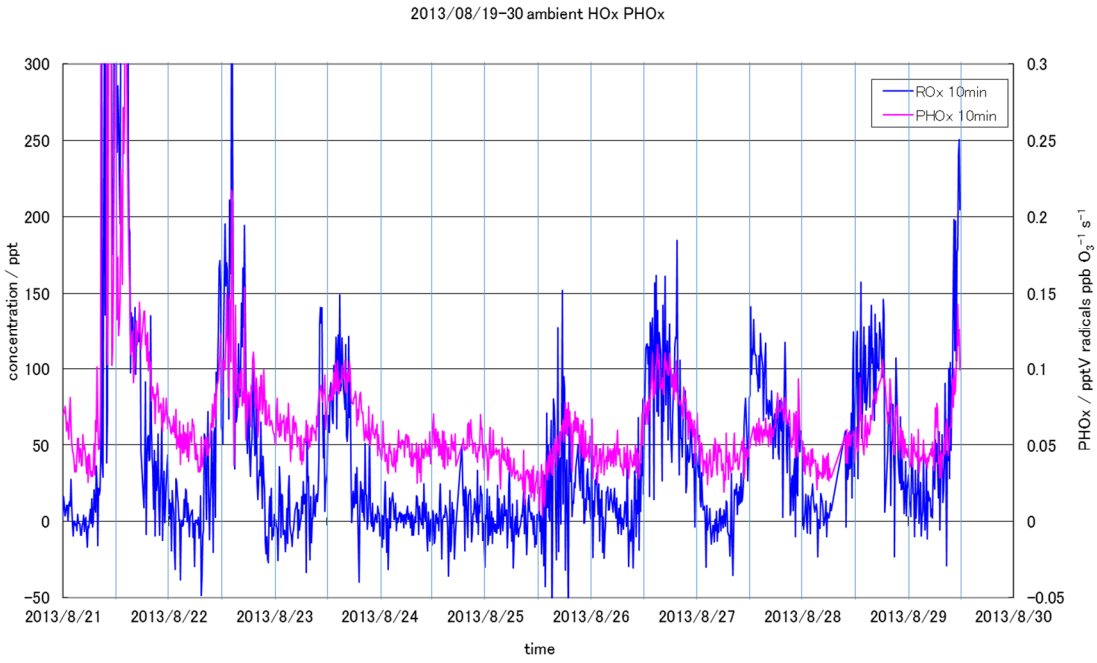

Fig.4-4 Ambient PHOx and ROx concentration during 2013/08/21 to 2013/08/29

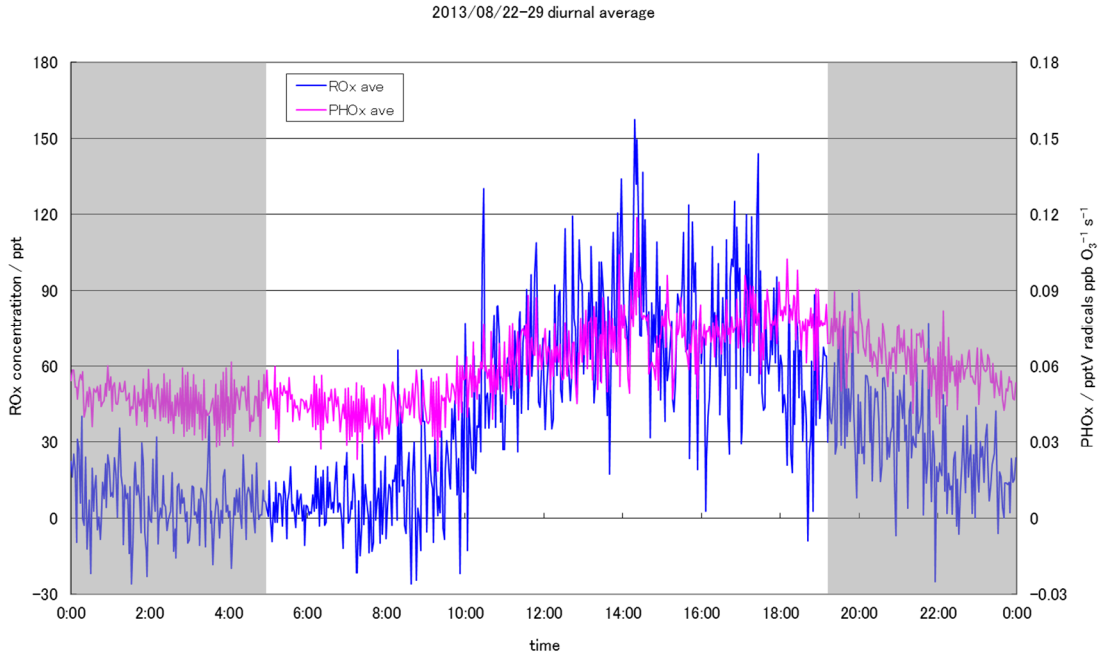

Fig.4-5 Diurnal average of PHOx and ROx concentration

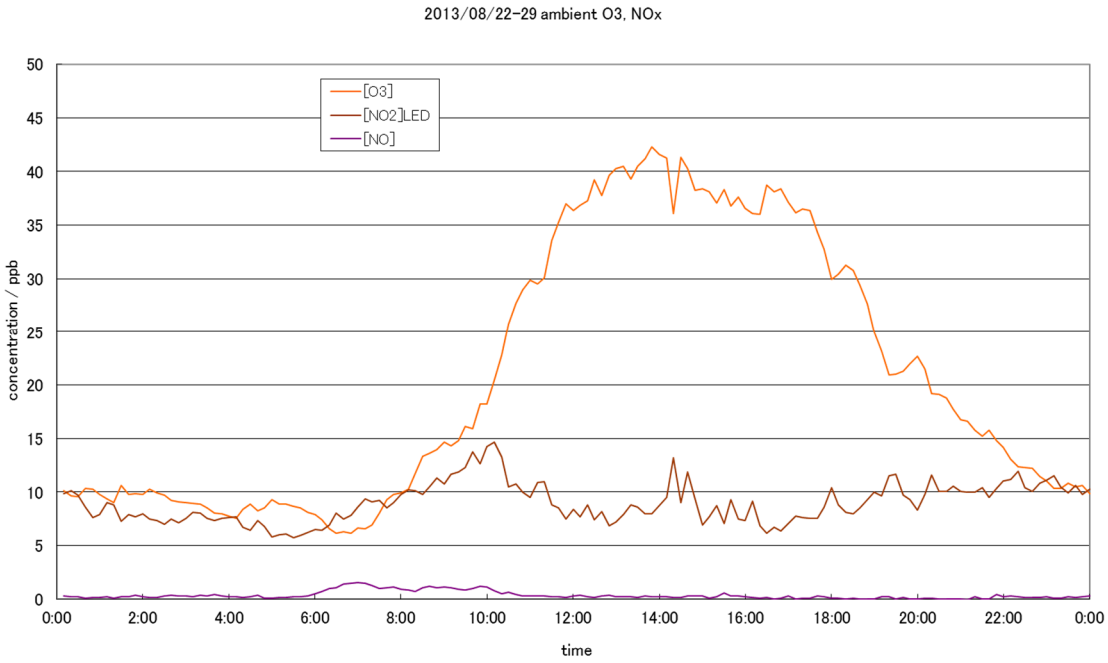

Fig.4-6 Diurnal average of O_3, NOx concentration

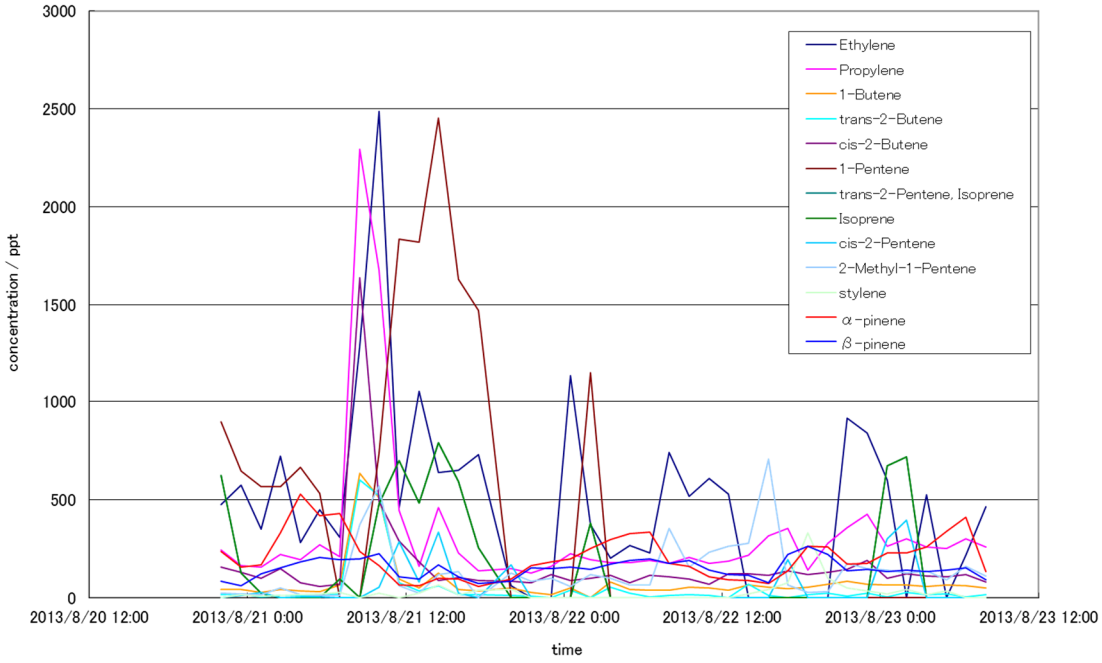

Fig.4-7 VOCs concentration during 2013/08/20 to 2013/08/23

Table 4-2 Reaction rate constant and HOx yield of each VOC and O_3

VOC	Rate constant with O_3 (cm^3 $molecule^{-1}$ s^{-1})	ϕHOx	reference
Ethylene	1.45×10^{-18}	0.44	Alam et al., 2010
Propene	1.13×10^{-17}	0.33	Atkinson et al., 1984(rate) Atkinson et al., 1993(yield)
1-butene	1.10×10^{-17}	0.41	Atkinson et al., 1984(rate) Atkinson et al., 1993(yield)
trans-2-butene	2.00×10^{-16}	0.64	Atkinson et al., 1984(rate) Atkinson et al., 1993(yield)
1-pentene	0.87×10^{-17}	0.37	Avzianova et al., 2002(rate) Rickard et al., 1999(yield)
cis-2-pentene	1.32×10^{-16}		Avzianova et al., 2002(rate)
Isoprene	1.17×10^{-17}	0.52	Malkin et al., 2010
a-pinene	9.71×10^{-17}	0.68	Atkinson et al., 2004(rate) Berndt and Stratmann, 2003
Limonene	2.10×10^{-16}	0.86	Atkinson et al., 1993(yield)

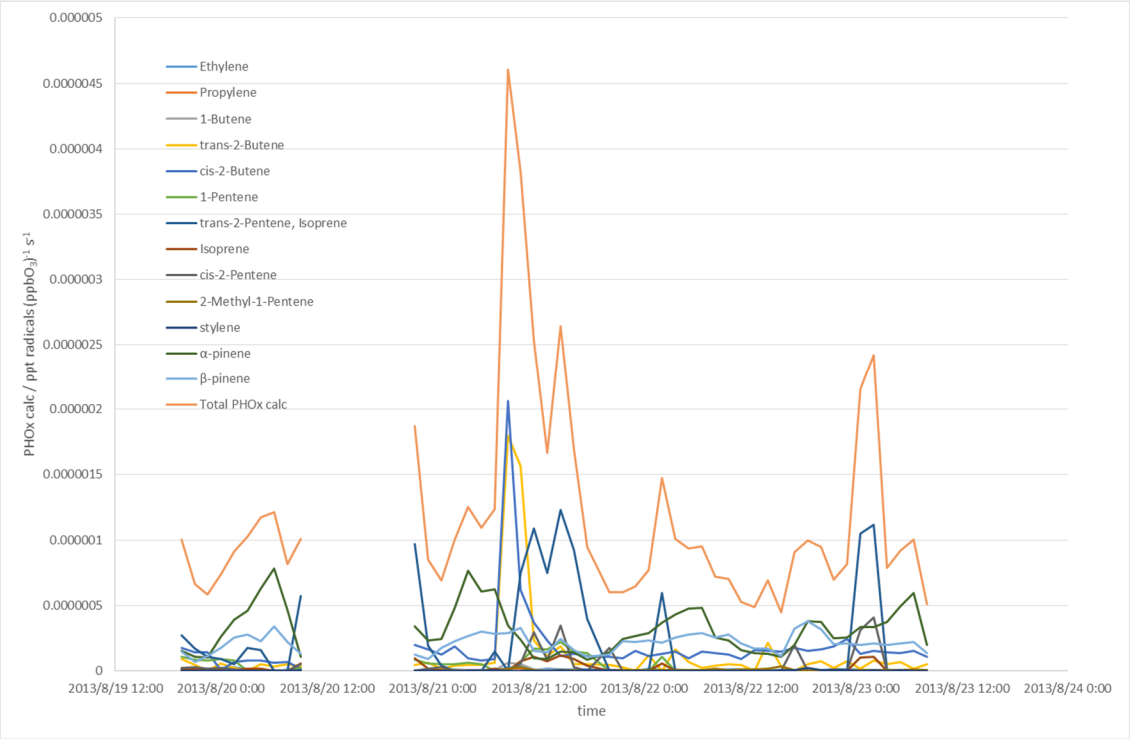

Fig.4-8 Calculated PHOx value from measured VOC species

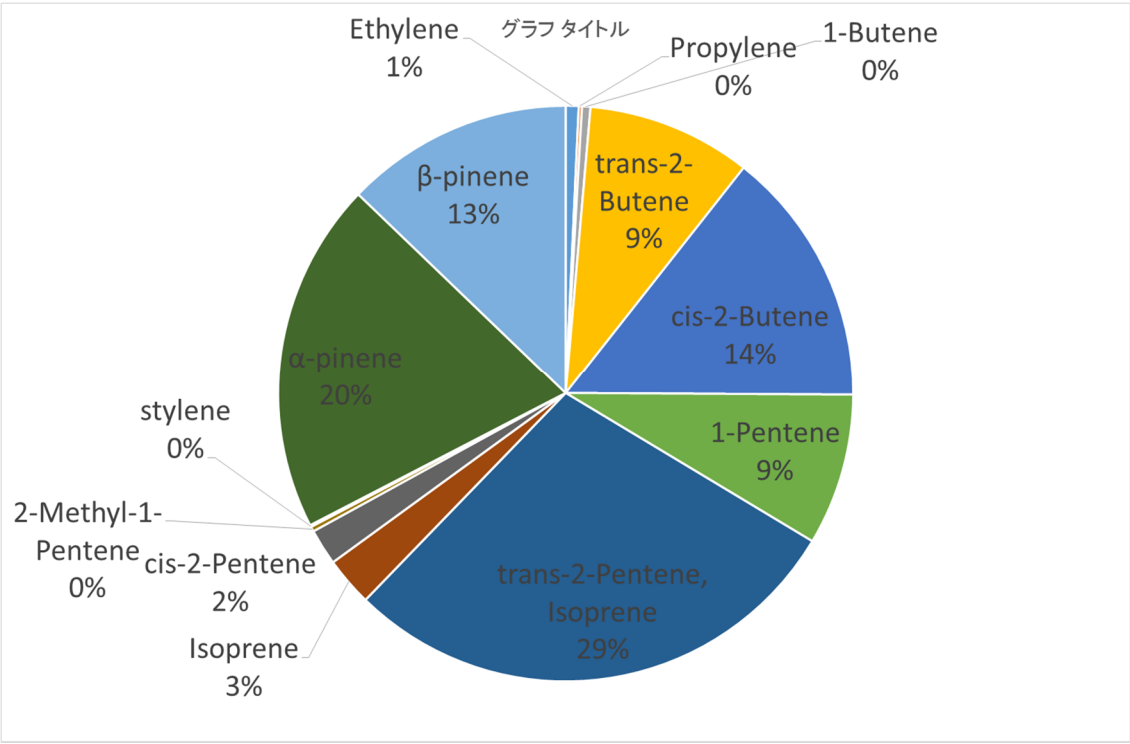

Fig.4-9 Contribution to PHOx by each measured VOC concentration

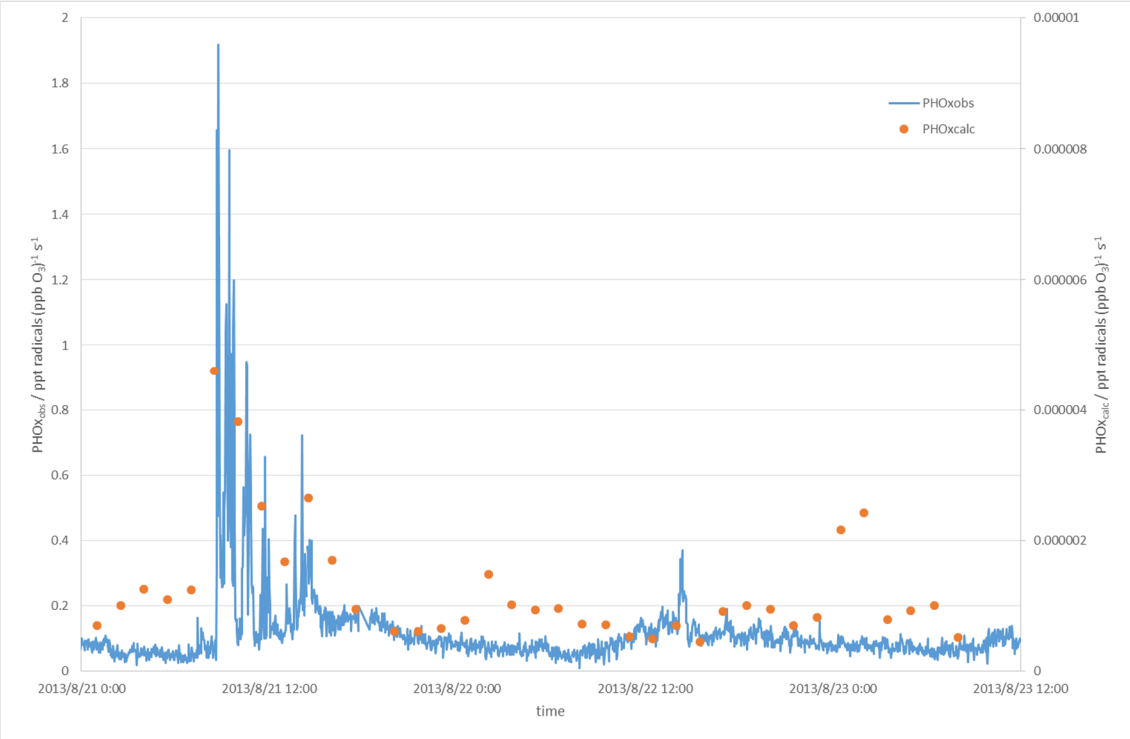

Fig.4-10 Time dependence of observed PHOx and calculated PHOx

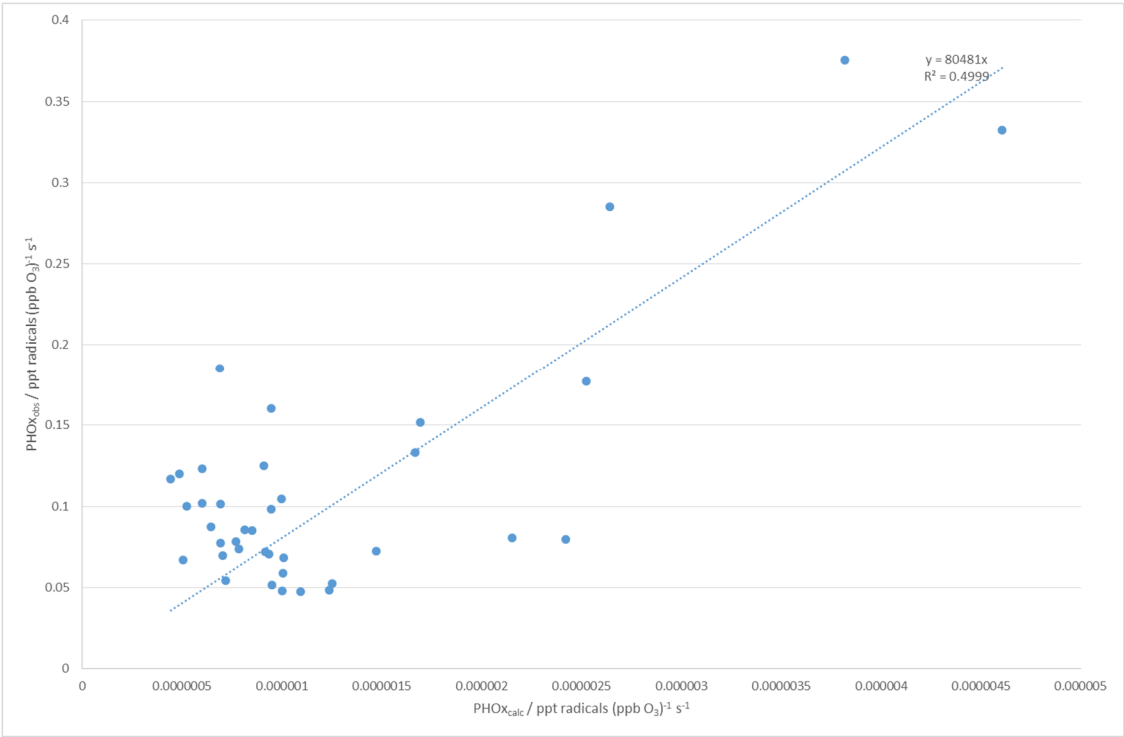

Fig.4-11 Scatter plot of observed PHOx and calculated PHOx

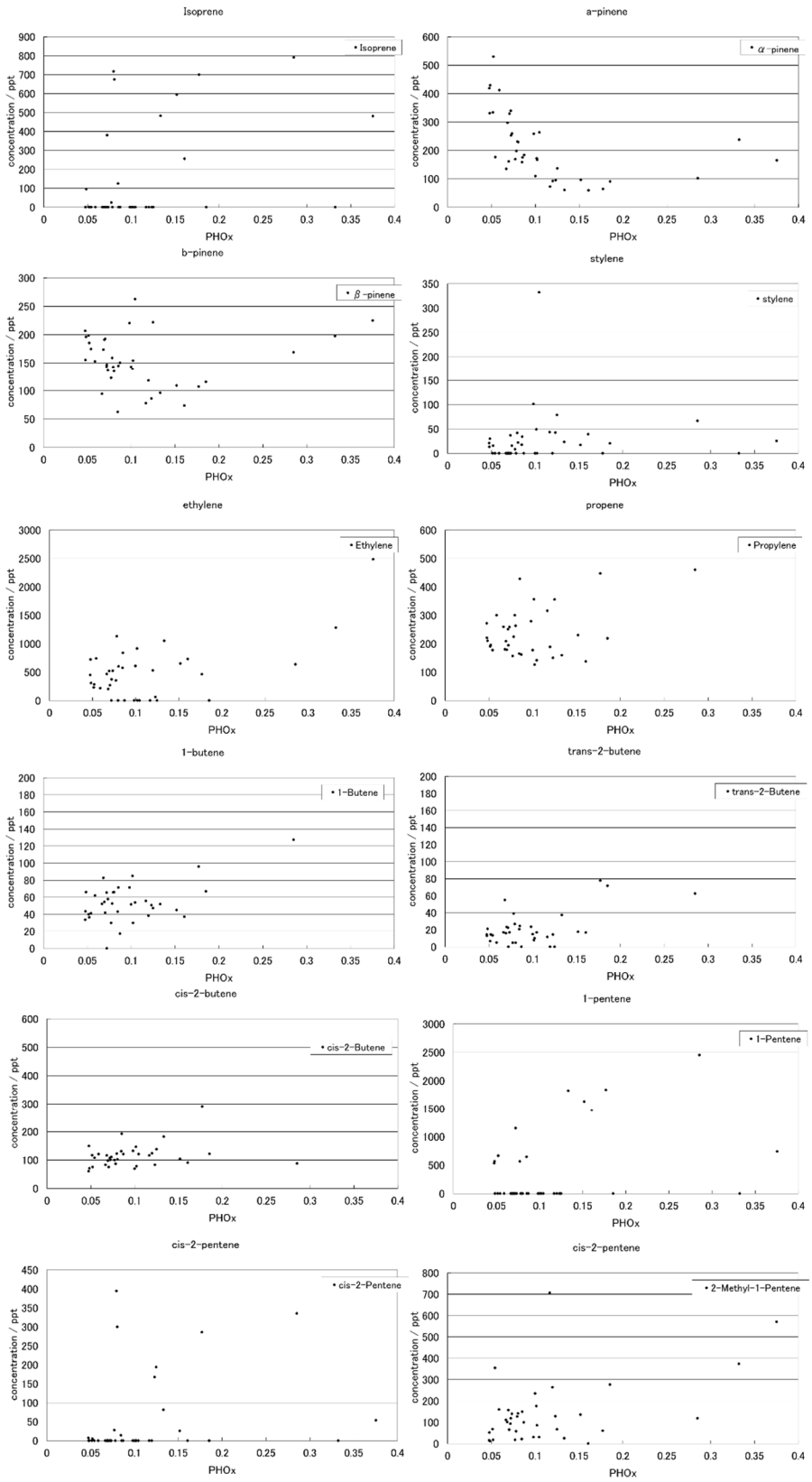

Fig.4-12 Scatter plot of each measured VOC concentration and PHOx

PHOx. Same scatter plot is held for each single measured VOC concentrate on and observed PHOx in Fig.4-12. Which has highest PHOx contribution, anthropogenic source has positive trend to observed PHOx value, but biogenic source such as α-pinene and β-pinene has clear negative trend to PHOx. Generally high reactive biogenic VOCs react O_3 and also OH radical rapidly during daytime compare than anthropogenic VOCs, concentration during daytime can be decline and reverse during nighttime. In contrast, anthropogenic VOCs are emitted from human activity, which can be higher during daytime. It suggests that total PHOx contribution by biogenic VOCs are comparable with anthropogenic VOCs, but if see VOC contribution in daytime and nighttime separately, anthropogenic VOCs are dominant in daytime HOx source, and biogenic VOCs are dominant in nighttime source.

4.1.3 2014/04/22 to 2014/04/28 at Kyoto University Yoshida South Campus

And also During 2014/04/22 to 2014/04/28, ambient measurement campaign of PHOx is held in Kyoto University Yoshida South campus. Measurement items and method is summarized in Table 4-3. Measured items are PHOx and ROx concentration, O_3, NOx and VOC concentration. VOC concentration is measured by using GC-FID, 58 speceis, 10 olefins are included. Measurement method of each items are same as previous measurement campaign.

Table 4-3 Measurement items and methods during 2014/04/22 to 2014/04/28

Measurement items	Measurement method
PHOx	PERCA-LIF technique
ROx concentration	PERCA-LIF technique
VOC concentration	GC-FID
O3 concentration	UV absorption
NOx concentraiton	NO+O3 chemiluminescence with photolytic converter
CO concentraion	IR absorption

PHOx and ROx concentration measurement result is shown in Fig.4-13. Successfully items are measured during campaign. Diurnal variation of PHOx and ROx concentration are shown in Fig.4-14 and O_3 and NOx are shown in Fig.4-15. O_3 and NOx concentration have similar diurnal trend to previous campaign, first NOx rise up before noon and after that O_3 has a peak afternoon. But in the case of PHOx and ROx have different trend that during daytime and also nighttime, two peaks can be seen clearly. As explained in section 4.1.4.2, RO_2 generation from NO_3 radical possibly effectible, but nighttime NO_2

concentration through campaign period is below than 10 ppb. It suggests nighttime ROx concentration peak is enhanced by VOC+O_3 reaction strongly, with small contribution from NO_3 radical.

Measured olefin concentrations during 2014/04/22 to 2014/04/28 are shown in Fig.4-16. During campaign period, 1-pentene and propene, anthropogenic olefin emissions are significantly high, but clear trend cannot be seen. Calculated PHOx from measured VOCs are compared with observed PHOx in Fig.4-17. Absolute value is not in same magnitude, but similar trend can be seen. Scatter plot between observed PHOx and calculated PHOx is shown in Fig.4-18. In this measurement, clear correlation cannot be seen.

From measured VOC concentration, calculated PHOx value is estimated. Time dependence of each VOC contribution to calculated PHOx is shown in Fig.4-19. In this period, trans-2-butene, α-pinene and limonene looks dominant for HOx generation from ozonolysis. Calculated PHOx contribution from each single VOCs is shown in Fig.4-20. In this campaign, trans-2-butene has dominant effect to PHOx and limonene has next. Same as previous measurement campaign, HOx generation from anthropogenic source is dominant in this area. Scatter plot of observed PHOx value and calculated PHOx contribution from single VOCs are shown in Fig. 4-21. In this period it is difficult to find contribution tendency from single component.

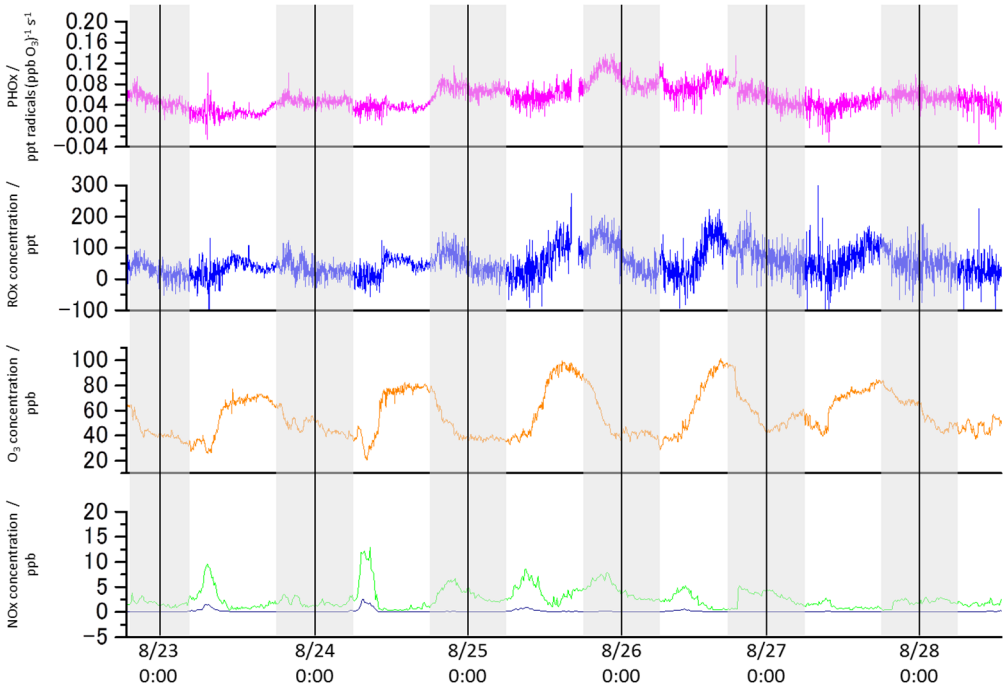

Fig.4-13 PHOx and ROx, O_3 and NOx concentration during 2014/04/22 to 2014/04/28

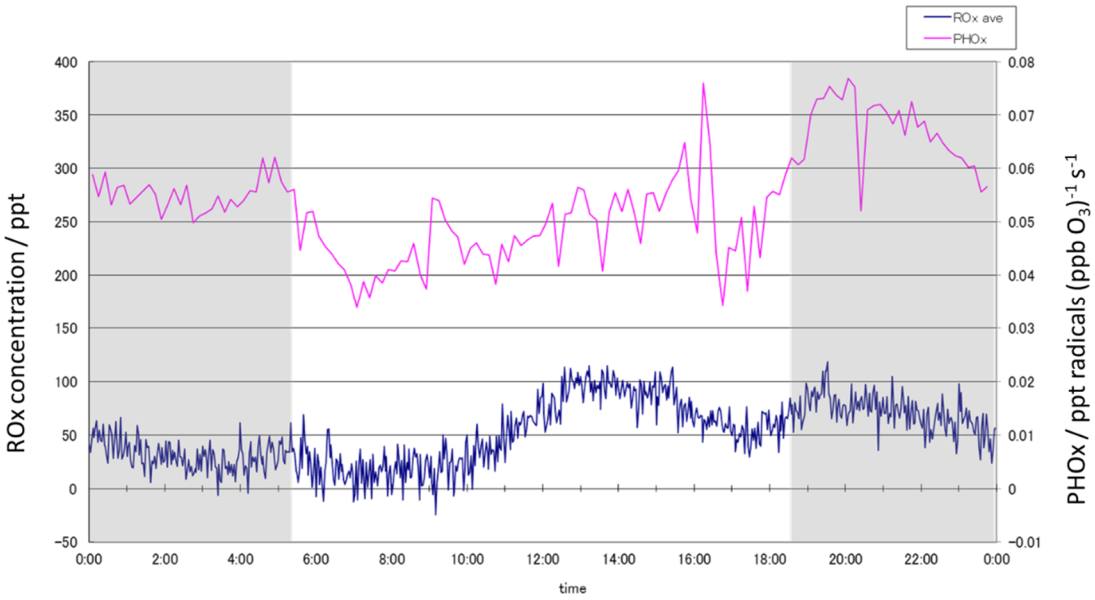

Fig.4-14 Diurnal variation of PHOx and ROx concentration

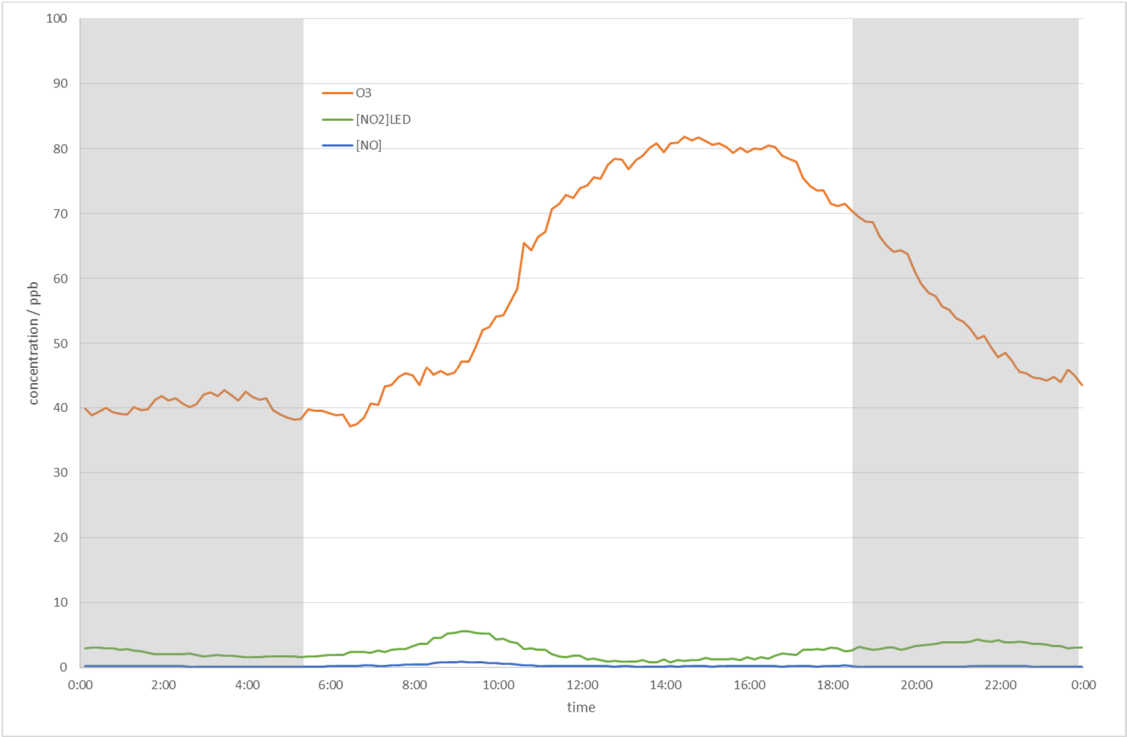

Fig.4-15 Diurnal variation of O_3 and NOx concentration

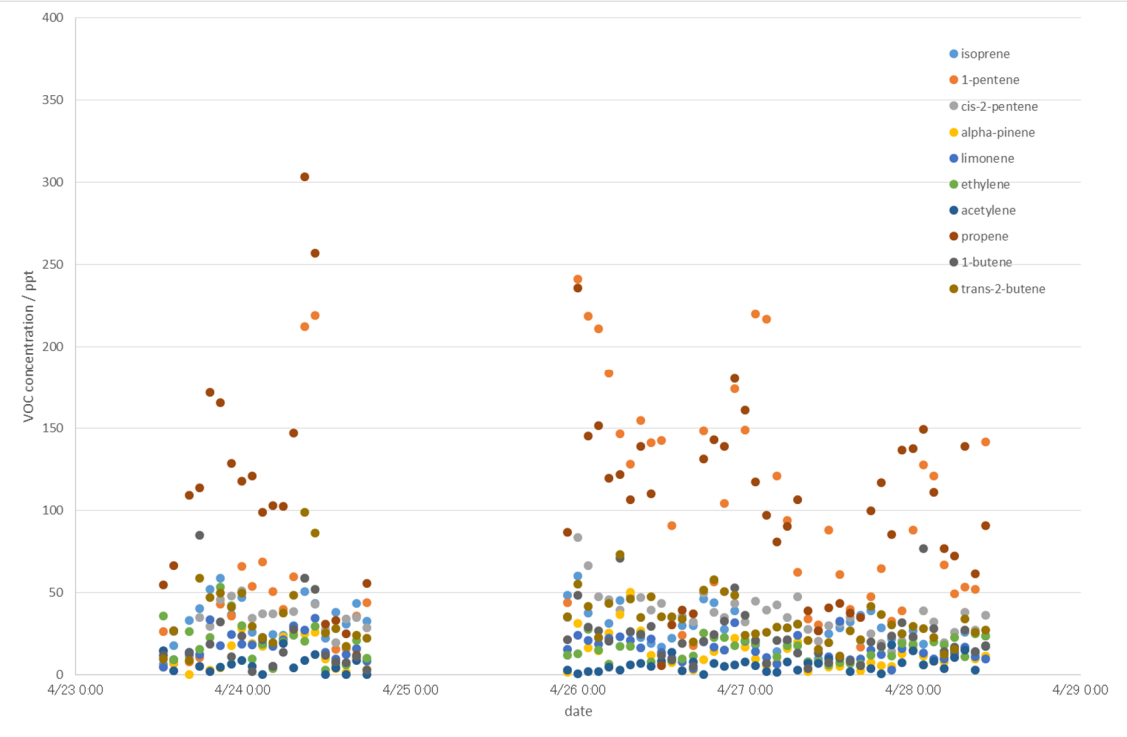

Fig.4-16 Measured olefin concentration during 2014/04/22 to 2014/04/28

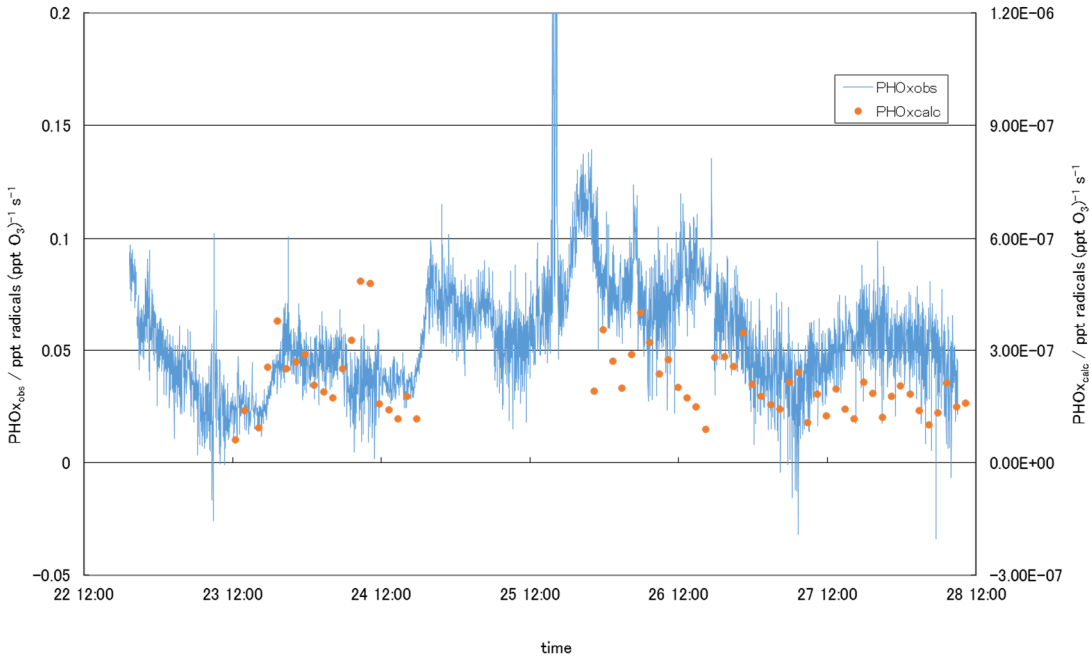

Fig.4-17 Time dependence of observed PHOx and calculated PHOx

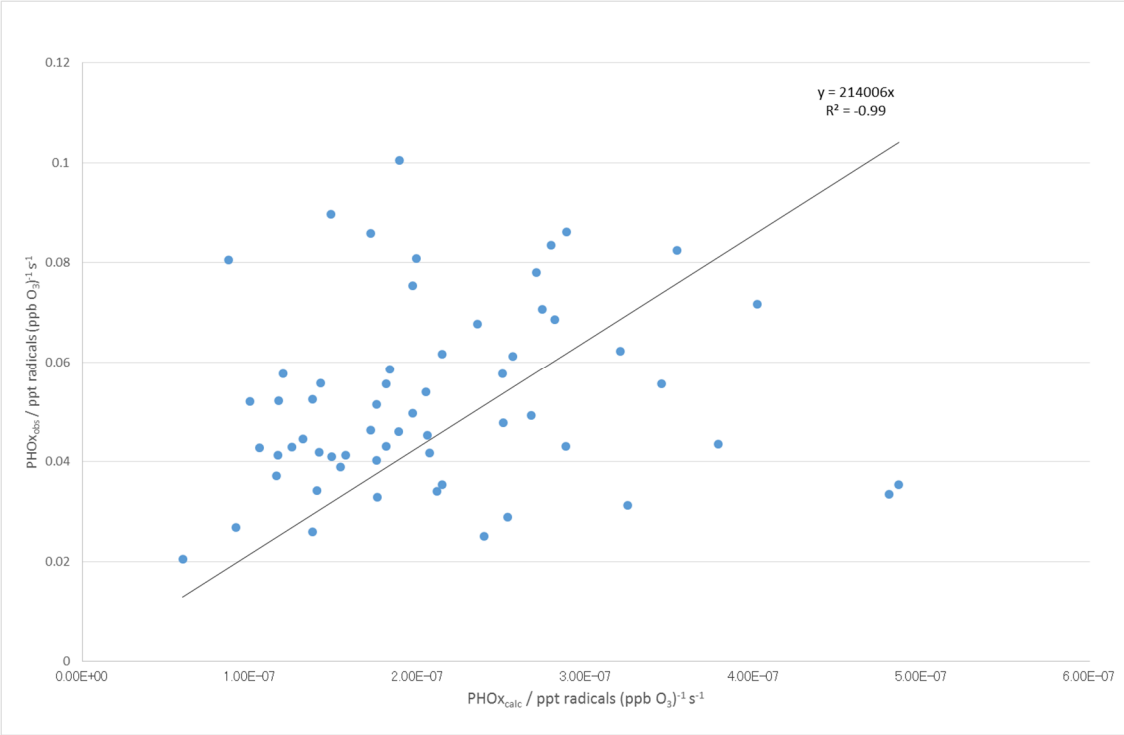

Fig.4-18 Scatter plot of observed PHOx and calculated PHOx

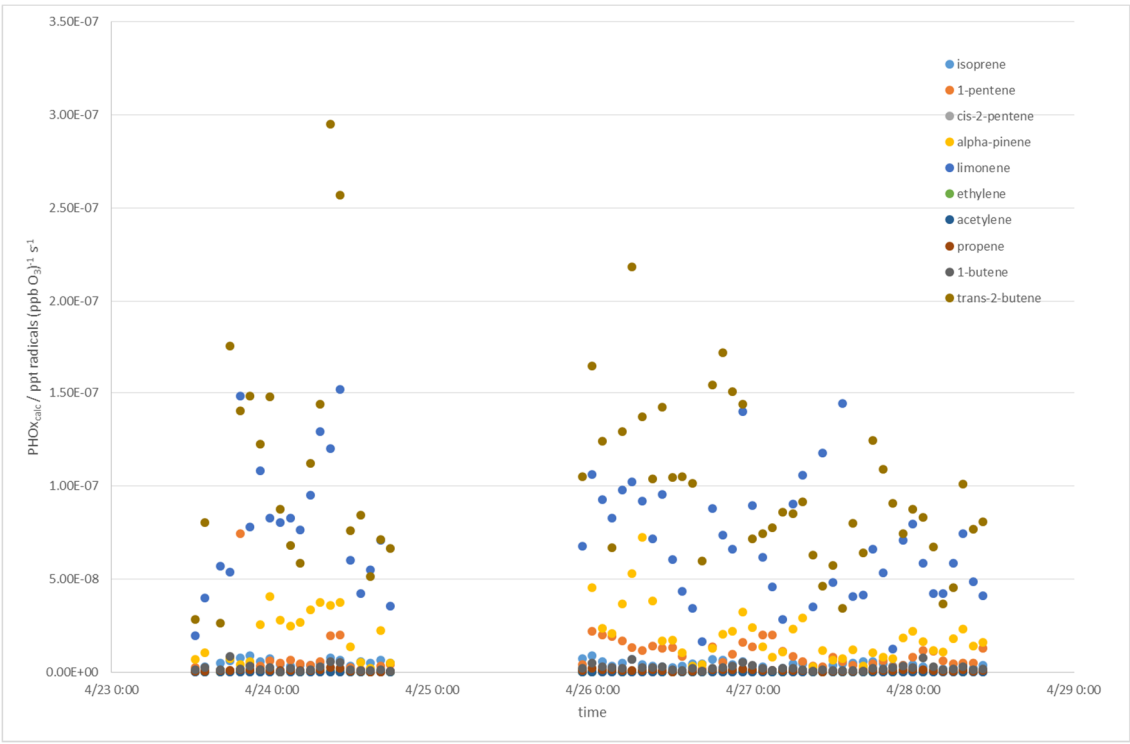

Fig.4-19 Time dependence of calculated PHOx value each VOC contribution

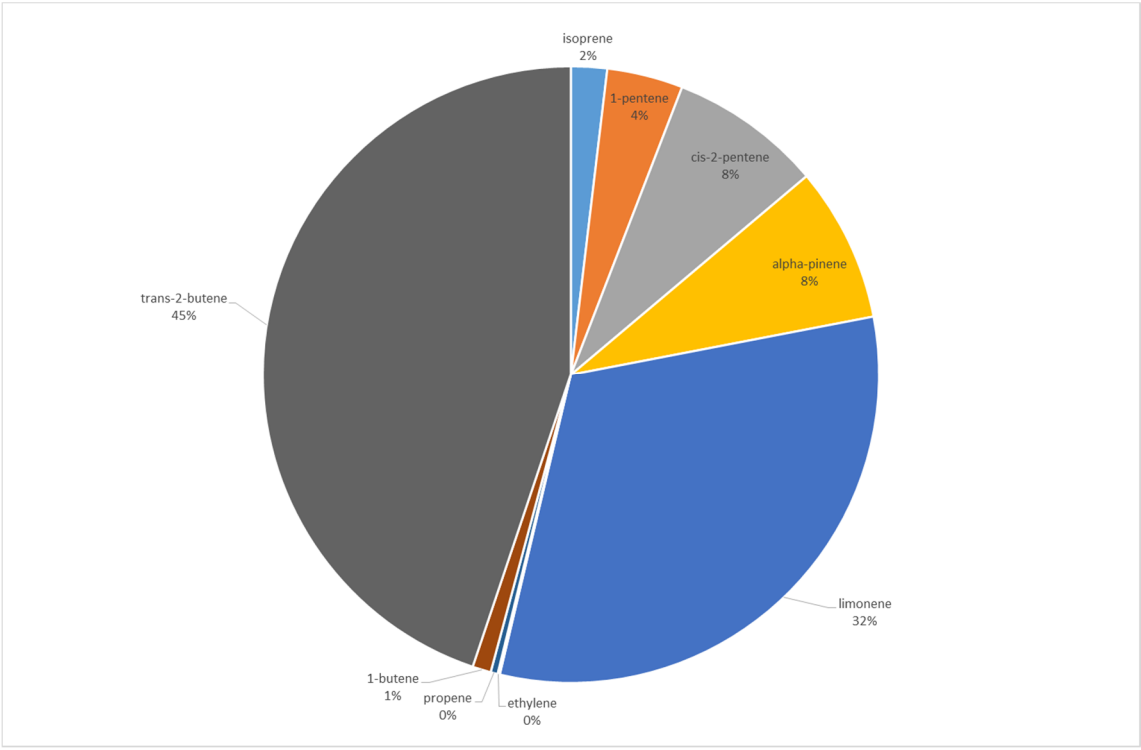

Fig.4-20 Calculated PHOx contribution from each single VOCs

Fig.4-21 Scatter plot of observed PHOx value and calculated PHOx from single species

4.1.4　2014/07/29 to 2014/28/28 at Kyoto University Wakayama Research Forest

During 2014/07/29 to 2014/08/09, PHOx measurement is held at Wakayama Research Forest. Measurement site is in middle of the mountain area where is from 32 km from Wakayama city, and 7.5 km from nearest town area. Extremely low anthropogenic NOx and VOCs are expected (Fig.4-22).

Measurement items are listed in Table 4-4. The purpose of this campaign is to focus on aerosol nuclear generation from biogenic source in rural area.

Some data is available but some analysis is going on. Time dependence of PHOx and ROx concentration is shown in Fig.4-23. Clear diurnal trend, high during daytime and rapidly fall to 0 after sunset can be seen in ROx concentration. In contrast, clear trend cannot be seen in PHOx but two times higher compare than previous ambient PHOx measurement. This high PHOx value possibly caused by high biogenic VOC emission from plants.

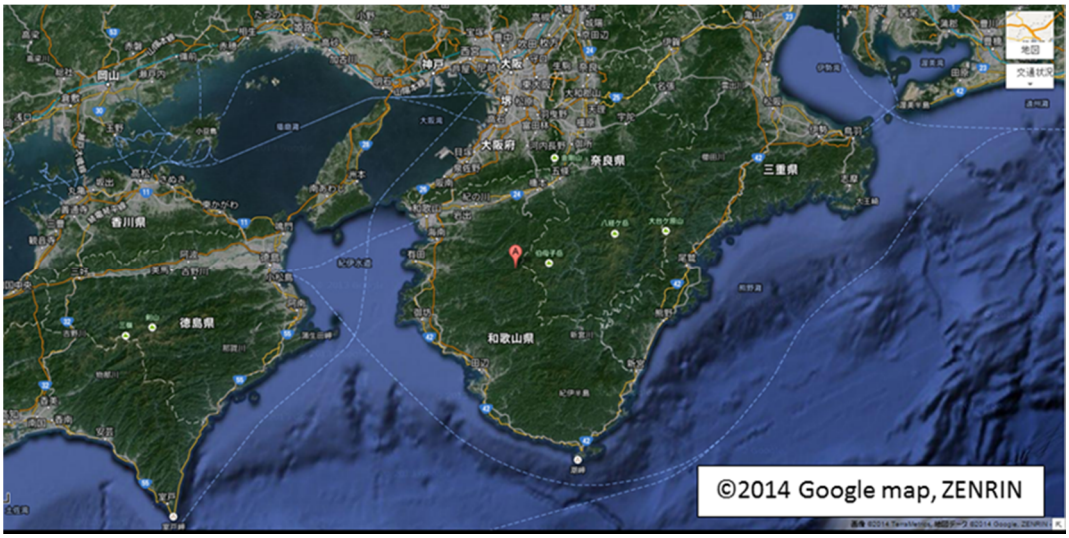

Fig.4-22 Wakayama research forest site description

Table 4-4 Measurement items in Wakayama research forest measurement campaign

Measuerment items	Measurement method	Intsitutuion
PHOx	PERCA-LIF technique	Kyoto University
ROx concentration	PERCA-LIF technique	Kyoto University
OH reactivity	LASER pump-probe technique	Kyoto University
O_3 production rate	LIF technique with quartz chamber	Osaka Prefecture University
VOC	GC-FID technique	Kyoto University
	Fast-GC	National Institute for Environmental Studies
	PTR-MS	Tokyo Metropolitan University
O_3 concentration	UV absorption	Kyoto University
NOx concentration	NO+O3 chemiluminescence	Kyoto University
NO_2 concentration	Cavity Attenuated Phase Shift spectroscopy	Osaka Prefecture University
NO_3 concentration	Broad-Band Cavity Enhanced Absorption Spectroscopy	Tokyo University of Agriculture and Technology
CO concentration	IR absorption	Kyoto University

Time dependence of O_3 and NOx concentration are shown in Fig.4-24. NOx concentration is around 1 ppb through all measurement campaign, with exception at 7/28 night. We have heavy rain in 8/2 and 8/3. Before and after rain event, tendency of O_3 is clearly changed. After rain event, O_3 concentration is up to 20 ppb, which is much lower than previous measurement campaign. Relatively high PHOx value but nighttime low ROx concentration is caused by low O_3 concentration.

VOC data is not available. Comparison between VOC and PHOx should be discussed in future work.

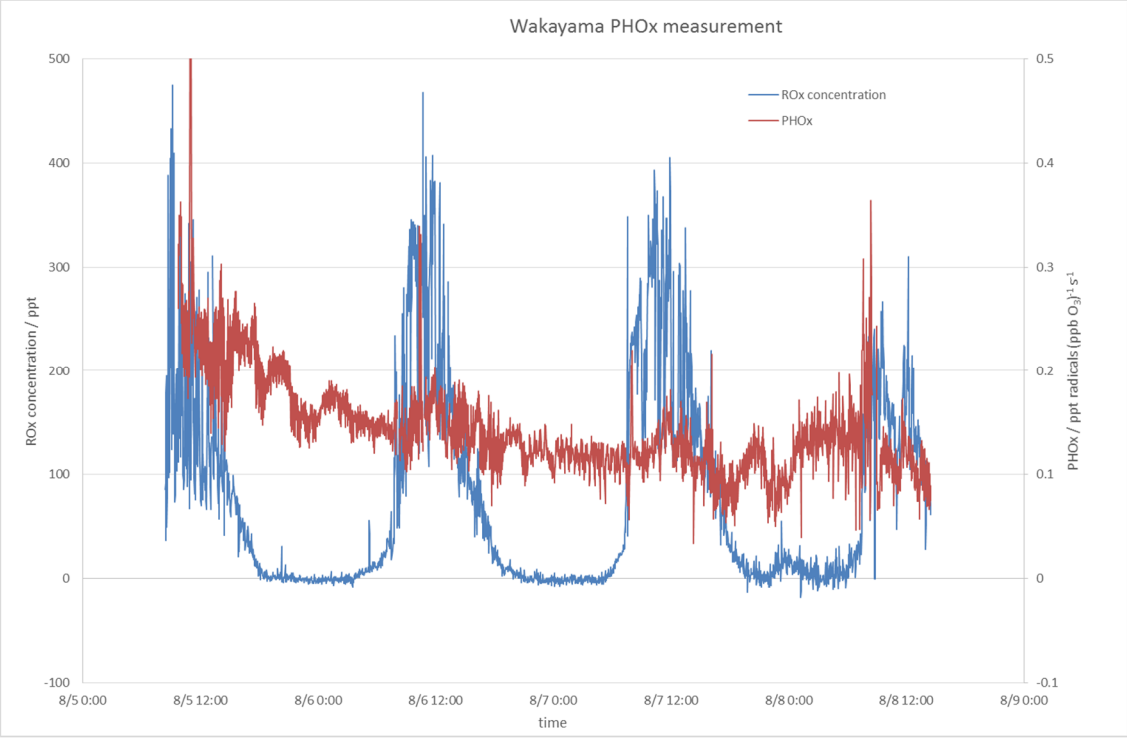

Fig.4-23 Time dependence of PHOx and ROx concentration during 2014/08/05 to 2014/08/08

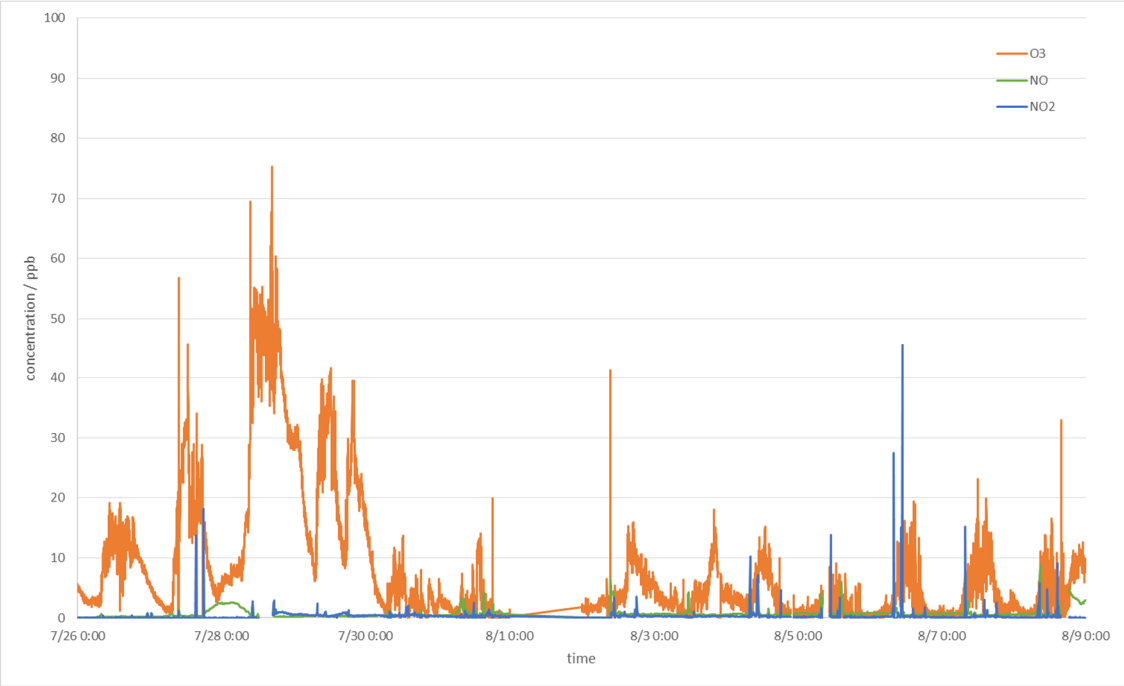

Fig.4-24 O_3 and NOx concentration during 2014/07/26 to 2014/08/08

4.2 Summary of ambient air measurement

Several places and seasons, PHOx measurement has been held successfully. But comparison between measured VOCs concentration was not comparable in absolute value. It can be considered that there are no contribution from oxygenated VOCs such as methyl vinyl ketone or methacrolein, which is main products from ozonolysis or OH-initiate reaction of isoprene are calculated. In this chapter, PHOx value is estimated by using Steady State Calculation.

From Eq (1-27), time variation of ROx concentration is assumed as constant, then ROx production rate equal to ROx loss rate. Loss rate of HOx is determined by reaction of ROx+NO_2 and wall reaction. Miyazaki et al (2013) measured HO_2 reactivity, which includes HO_2+NO_2 reaction and HO_2 wall loss and unidentified loss process. Direct measured HOx loss rate is two times higher than contribution of NO_2 through measurement campaign. By using this factor, PHOx from Steady State Calculation is estimated during 4 campaigns above.

Calculated ROx production rate from Steady State Calculation has near value to observed PHOx during ambient measurement campaign. In this chapter, by using photostationary state deviation and calculated HOx loss late, upper limit of HOx

production rate is estimated.

From Fig.4-25 to Fig.4-28, result of the comparison observed PHOx (PHOxObs), calculated PHOx from Steady State approximation (PHOxSS) and ratio of these two. In the case of 2013/07/10 to 2013/07/12 and 2013/08/21 to 2013/08/29, contribution of observed PHOx to total radical production rate, PHOxSS is quite low, below 10 %. But in the case of 2014/04/22 to 2014/04/28 and 2014/08/05 to 2013/08/08, contribution of observed PHOx is much higher. And also during 2014/04/22 to 2014/04/28, clear diurnal cycle, low at daytime and high at nighttime can be seen. It is not consistent with the importance of ozonolysis as night time HOx source. During 2014/08/05 to 2013/08/08 campaign in Wakayama research forest, which is in rural, low NOx and anthropogenic source area, contribution of PHOx to total HOx production ratio is much higher than other measurement campaign, around 50 to 60 % during daytime HOx generation, and most 100 % in nighttime. Sometime observed PHOx excess PHOxSS, because of the measurement error or approximation error.

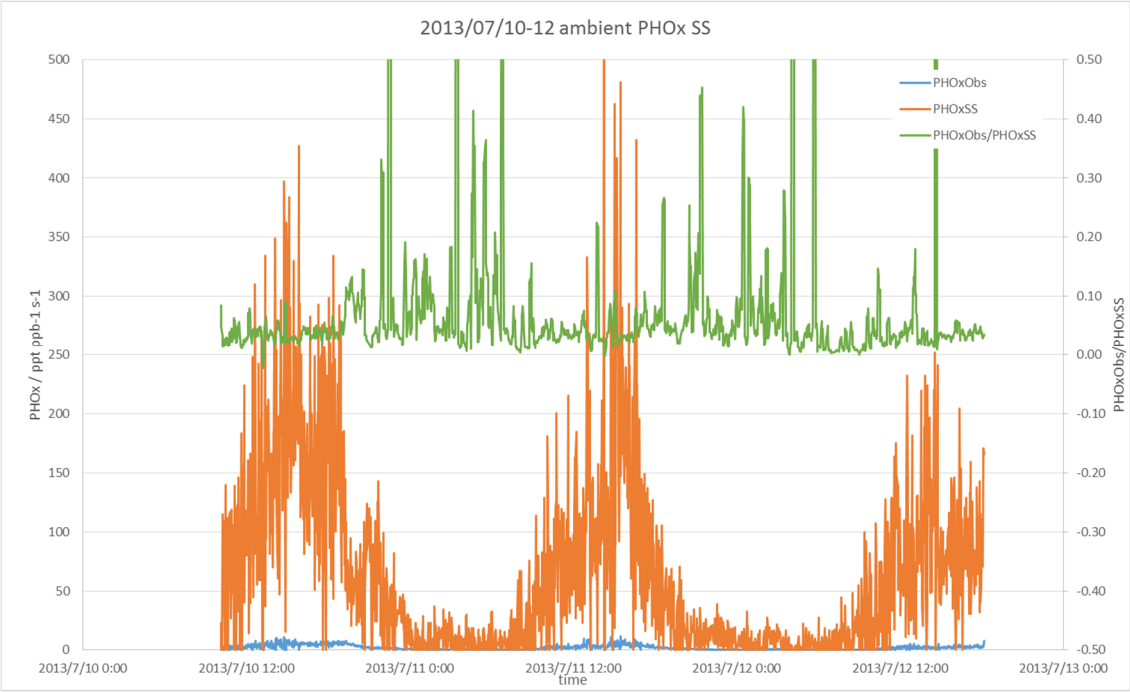

Fig.4-25 PHOx with Steady State calculation during 2013/07/10 to 2013/07/12

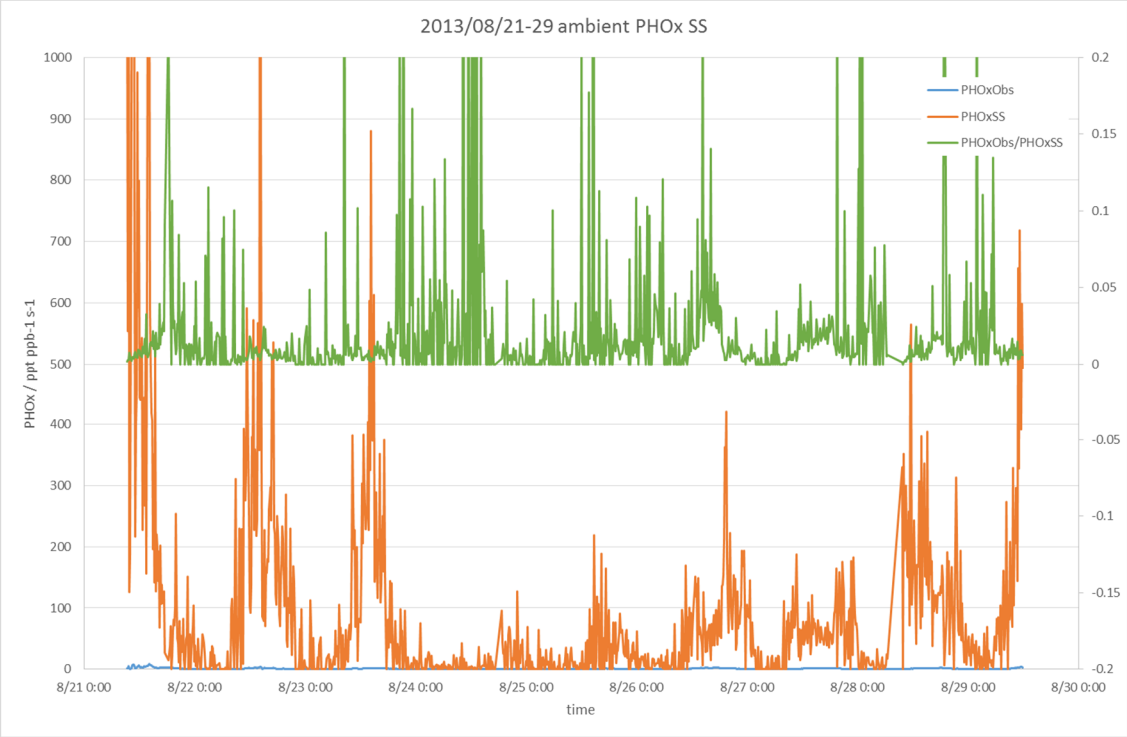

Fig.4-26 PHOx with Steady State calculation during 2013/08/21 to 2013/08/29

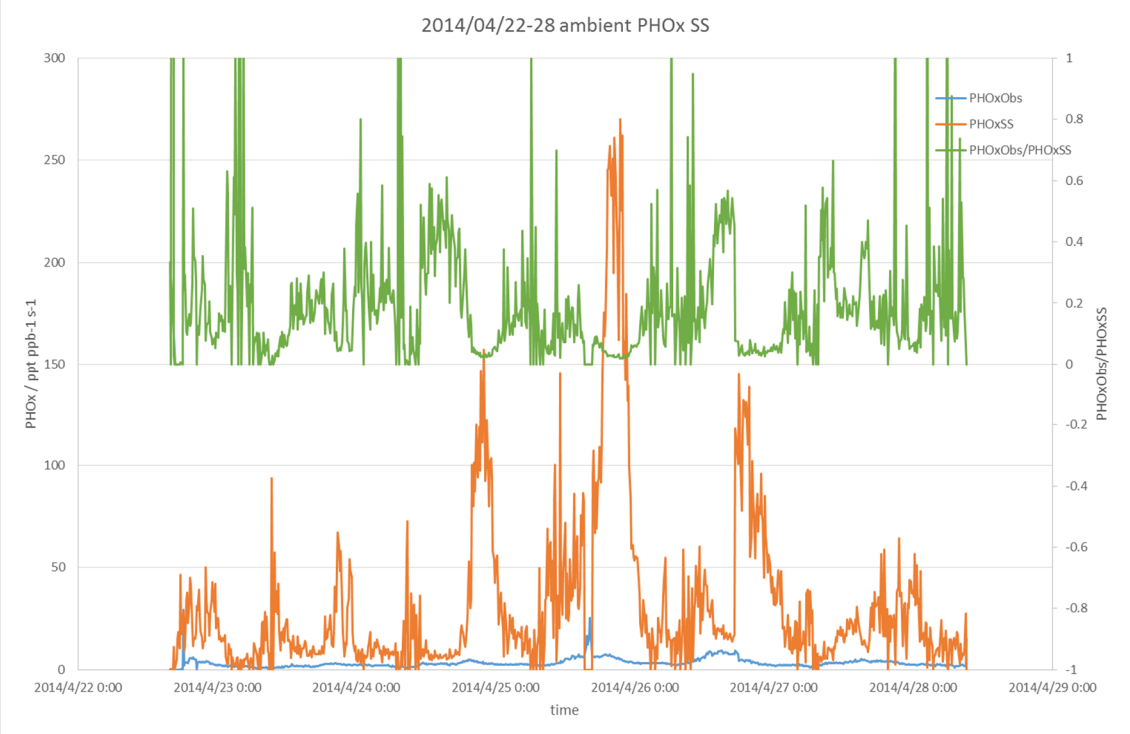

Fig.4-27 PHOx with Steady State calculation during 2014/04/22 to 2014/04/28

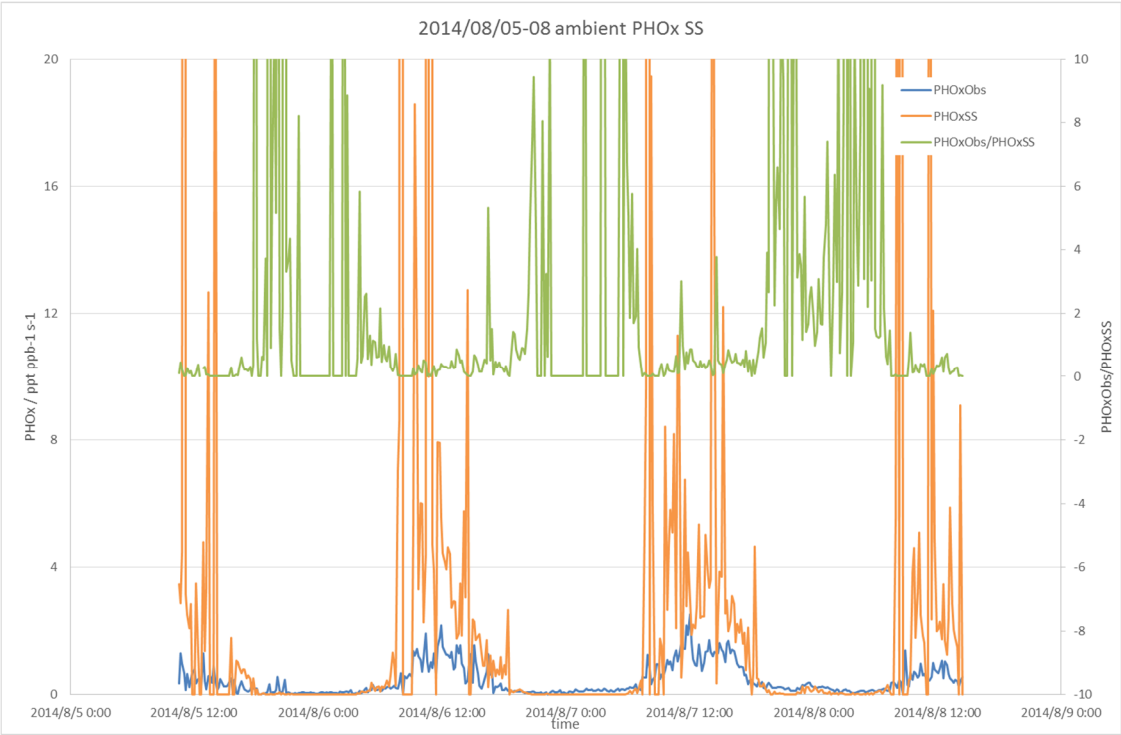

Fig.4-28 PHOx with Steady State calculation during 2014/08/05 to 2013/08/08

5 Summary and Conclusion

The direct measurement method of HOx(OH, HO_2) radical production rate from ozonolysis (PHOx) is developed. Ozonolysis is important nighttime HOx radical source also daytime, accurate ambient HOx radical production rate measurement method is needed to explain the behavior of HOx radicals in ambient air. First, fundamental experiments were held with single VOC, propene, isoprene, cyclohexene and limonene. Produced ROx radical concentration was increasing with increment of O_3 concentration, but not linear. It is caused by radical-radical self- or cross-reaction. It depends on not only O_3 concentration, rate constant with O_3 and HOx yield from ozonoylsis, also the characteristics of generated ROx. To avoid underestimation at high O_3 concentration period, PHOx was calculated from the slope of the generated ROx concentration at O_3 concentration close to 0 ppb. Each slopes of generated ROx concentration from fundamental experiments, observed value was corresponding with literature value. Based on fundamental experiment, ambient PHOx measurement has been held in Kyoto University Yoshida South campus and Wakayama Research Forest. PHOx was measured successfully with several conventional measurement items which relate to radical generation as precursor, and radical loss, mainly NOx compounds. Measured VOCs concentration and also calculated PHOx value had linear correlation with observed PHOx. Steady State Calculation have demonstrated that observed PHOx contributed to total HOx generation rate up to 60 % in Kyoto university measurement campaign, and 50 % at daytime, almost 100 % at nighttime in Wakayama research forest campaign. As a conclusion, construction of PHOx measurement technique can estimate the contribution of ozonolysis to total HOx production quantitatively which is including missing HOx source. And PHOx measurement technique is compared with calculated PHOx value from measured VOC concentration. This comparison suggests that the contribution of unidentified VOC will be revealed.

6 Acknowledgement

This research has been carried out as a doctoral courses of Graduate School of Global Environmental Study, Kyoto University.

At first, I would like to show my greatest appreciation to my academic supervisor, Prof. Yoshizumi Kajii (Kyoto University) for tolerant and supportive tutelage to this doctoral research and thesis.

I am deeply appreciate Prof. Masahito Sugiyama (Kyoto University) and Associate Prof. Shigeki Kiyonaka (Kyoto University) for accepting jury reporter and giving specific comments and advices to my doctoral thesis.

I would like to offer my special thanks to Associate Prof. Yasuhiro Sadanaga and Assistant Prof. Yoshihiro Nakashima for having discussion and giving specific comments to my doctoral thesis.

I am deeply grateful to Dr. Akira Ida and members of Kajii laboratory for having discussion about experiment at all times. I would also like to express appreciation to the secretary of Kajii laboratory, Ms. Rumi Ishida for her helps and encouragements.

I am deeply appreciate participants of measurement campaign in Kyoto University and Wakayama Research Forest.

At last I would like to appreciate my family for their supports and encouragements.

December, 2014

Hiroshi Tsurumaru

7 Reference

Alam, M. S., M. Camredon, A. R. Rickard, T, Carr, K. P. Wyche, K. E. Hornsby, P. S. Monks, W. J. Bloss, Total radical yields from tropospheric ethene ozonolysis, Phys. Chem. Chem. Phys., 13, 11002-11015, (2011).

Alam, M. S., A. R. Rickard, M. Camredon, K. P. Wyche, T. Carr, K. E. Hornsby, P. S. Monks, W. J. Bloss, Radical Product Yields from the Ozonolysis of Short Chain Alkenes under Atmospheric Boundary Layer Conditions, J. Phys. Chem. A, 117, 12468−12483, (2013).

Atkinson, R., Carter, W. P. L., Kinetics and Mechanisms of the Gas-Phase Reactions of Ozone with Organic Compounds under Atmospheric Conditions, Chemical Reviews, 84, 437-470, (1984).

Atkinson, R., S. M. Ashmann, J. Arey, B. Shorees, Formation of OH radicals in the gas phase reaction of O_3 with a series of terpenes, Journal of Geophysical Research, 97, 6065-6073, (1992).

Atkinson, R., S. M. Aschmann, OH radical production from the gas-phase reactions of O_3 with a series of alkenes under atmospheric conditions, Environ. Sci. Technol, 27, 1359-1361, (1993).

Atkinson, R., J. Arey, S. M. Aschmann, S. B. Corchnoy, Y. Shu., Rate constants for the gas-phase reactions of cis 3-hexenylacetate, trans-2-hexenal, and linalool with OH and NO_3 radicals and O_3 at 296 ± 2 K, and OH radical formation yields from the O_3 reactions, International Journal of Chemical Kinetics, 27, 941-955 (1995).

Atkinson. R., Gas-Phase tropospheric chemistry of volatile organic compounds: 1. Alkans and Alkenes, Journal of Physical Chemistry, 26, 215-290 (1997).

Ball, S. M., J. M. Langridge, R. L. Jones, Broadband cavity enhanced absorption spectroscopy using light emitting diodes, Chemical Physics Letters, 398, 68-74, (2004).

Bloss, C., Wagner, V., Jenkin, M.E., Volkamer, R., Bloss, W.J., Lee, J.D., Heard, D.E., Wirtz, K., Martin-Reviejo, M., Rea, G., Wenger, J.C., Pilling, M.J., Development of a detailed chemical mechanism (MCMv3.1) for the atmospheric oxidation of aromatic hydrocarbons, Atmospheric Chemistry and Physics 5, 641–664, (2005)

Campbell, M. J., J. C. Sheppard, B. F. Au, Measurement of hydroxyl concentration in boundary layer air by monitoring CO oxidation, Geophysical Research Letters, 6, 175-178, (1979).

Cantrell, C. A., D. H. Stedman, A possible technique for the measurement of atmospheric peroxy radicals, Geophysical Research Letters, 9, 846-849, (1982).

Cantrell, C. A., J. A. Lind, R.E. Shetter, J. G. Calvent, Peroxy radicals in the ROSE experiment: Measurement and Theory, Journal of Geophysical Research, 97, 20671-20686, (1992).

Chen, S., Ren, X., Mao, J., Chen, Z., Brune, W. H., Lefer, B, Rappenglück, B, Flynn, J., Olson, J., Crawford, J. H., A comparison of chemical mechanisms based on TRAMP-2006 field data, Atmospheric Environment, 44, 4116-4125, (2010).

Chen, X., K. Mopper, Determination of tropospheric hydroxyl radical by liquidphase scrubbing and HPLC: Preliminary Results, Journal of Atmospheric Chemistry, 36, 81-105, (2000).

Cheng. Y., X Wang, Z Liu, Y Bai J Li, A new method for quantitatively characterizing atmospheric oxidation capacity, Science in China Series B, 51, 1102-1109, (2008).

Chew, A. A., R. Atkinson, OH radical formation yields from the gas-phase reactions of O_3 with alkenes and monoterpenes, Journal of Geophysical Research, 101, 28649-28653, (1996).

Eisele, F. L., D. J. Tanner, Ion-assisted tropospheric OH measurements, Journal of Geophysical Research, 96, 9295-9308, (1991).

Elshorbany, B. Y., Barnes, I., Becker, K. H., Kleffman, J., Wiesen, P., Sources and cycling tropospheric hydroxyl radicals – An overview, Z. Phys. Chem., 224, 967-987, (2010).

Emmerson, K. M., Carslaw, N., Carpenter, L. J., Heard, D. E., Lee, J. D., Pilling, M. J., Urban Atmospheric Chemistry During the PUMA Campaign 1: Comparison of Modelled OH and HO_2 Concentrations with Measurements, Journal of Atmospheric Chemistry, 52, 143-164, (2005)

Emmerson, K. M., Carslaw, N., D. C., Lee, J. D., McFiggans, G., Bloss, W. J., Gravestock, T., Heard, D. E., Hopkins, J., Ingham, T., Pilling, M. J., Smith, S. C., Jacob, M., Monks, P. S., Free radical modelling studies during the UK TORCH Campaign in Summer 2003, Atmospheric Chemistry and Physics, 7, 167-181, (2007).

George, T. M., Hard, T. M., O'Brien, R. J., Measurement of free radicals OH and HO_2 in Los Angeles smog, Journal of Geophysical Research, 104, 11643-11655, (1999).

George, L. A., R. J. O'Brien, Prototype FAGE determination of NO2, Journal of Atmospheric Chemistry, 12, 195-209, (1991).

Guenther A., C. N. Hewitt, D. Erickson, R. Fall, C. Geron, T. Graedel, P. Harley, L. Klinger, M. Lerdau, W. A. McKay, T. Pierce, B. Scholes, R. Steinbrecher, R. Tallamraju, J. Taylor, P. Zimmerman, A global model of natural volatile organic compound emission, Journal of Geophysical Research, 100, 8873-8892, (1995).

Hanke, H., J. Uecker, T. Reiner, F. Arnold, Atmospheric peroxy radicals: ROXMAS, a

new mass-spectrometric methodology for speciated measurements of HO_2 and ΣRO_2 and first results, International Journal of Mass Spectrometory, 213, 91-99, (2002).

Hard, T. M., L. George, FAGE determination of tropospheric OH and HO_2, Journal of Atmospheric Science, 52, 3354-3372, (1995).

Hard, T. M., R. J. O'Brien, C. Y. Chen, A. A. Mehrabzadeh, Tropospheric free radical determination by FAGE, Environmental Science and Technology, 18, 768-777, (1984)

IPCC, IPCC Fourth Assessment Report: Climate Change 2007.

Jenkin, M.E., Saunders, S.M., Pilling, M.J., The tropospheric degradation of volatile organic compounds: a protocol for mechanism development, Atmospheric Environment 31, 81–104, (1997).

Kanaya, Y., Y. Sadanaga, J. Hirokawa, Y. Kajii, H. Akimoto, Development of an LIF-based instrument for measuring tropospheric HOx radicals: instrumentation and calibrations, Journal of Atmospheric Chemistry, 36, 73-110 (2001).

Kanaya, Y., Cao, R., Akimoto, H., Fukuda, M., Komazaki, Y., Yokouchi, Y., Koike, M., Tanimoto, H., Nobuyuki Takegawa, N., Yutaka Kondo, Y., Urban photochemistry in central Tokyo: 1. Observed and modeled OH and HO_2 radical concentrations during the winter and summer of 2004, Journal of Geophysical Research, 112, D21312, (2007).

Kim, S., Wolfe, G. M., Mauldin, L., Cantrell, C., Guenther, A., Karl, T., Turnipseed, A., Greenberg, J., Hall, S. R., Ullmann, K., Apel, E., Hornbrook, R., Kajii, Y., Nakashima, Y., Keutsch, F. N., DiGangi, J. P., Henry, S. B., Kaser, L., Schnitzhofer, R., Graus, M., Hansel, A., Zheng, W., Flocke, F. F., Evaluation of HOx sources and cycling using measurement-constrained model calculations in a 2-methyl-3-butene-2-ol (MBO) and monoterpene (MT) dominated ecosystem, Atmospheric Chemistry and Physics, 13, 2031-2044, (2013).

Levy, H., Normal atmosphere: large radical and formaldehyde concentrations predicted, Science, 173, 141-143, (1971).

Malkin, T. L., A. Goddard, D. E. Heard, P. W. Seakins, Measurements of OH and HO_2 yields from the gas phase ozonolysis of isoprene, Atmospheric Chemistry and Physics, 10, 1441-1459, (2010).

Martinez, M., Harder, H., Kovacs, T. A., Simpas, J. B., Bassis, J., Lesher, R., Brune, W. H., Frost, G. J., Williams, E. J., Stroud, C. A., Jobson, B. T., Roberts, J. M., Hall, S. R., Shetter, R. E., Wert, B., Fried, A., Alicke, B., Stutz, J., Young, V. L., White, A. B. Zamora, R. J., OH and HO_2 concentrations, sources, and loss rates during the Southern Oxidants Study in Nashville, Tennessee, summer 1999, Journal of Geophysical Research, 108, NO.D19, 4617, (2003).

Mather, J. H, P. S. Stevens, W. H. Brune, OH and HO_2 measurement using laser-induced fluorescence, Journal of Geophysical Research, 102, 6427-6436, (1997).

Mihelcic, D., D. H. Ehhalt, G. F. Kulessa, J. Klomfass, M. Trainer, U, Schmidt, H. Rohrs, Measurement of free radicals in the atmosphere by Matrix Isolation and Electron Paramagnetic Resonance, Pure and Applied Geophysics, 116, 530-536, (1978).

Mihele C. M., D. R. Hastie, The sensitivity of the radical amplifier to ambient water vapour, Geophysical Research Letters, 25, 1911-1913, (1998).

Miyazaki, K., A. E. Parker, C. Fittschen, P. S. Monks, Y. Kajii, A new technique for the selective measurement of atmospheric peroxy radical concentrations of HO_2 and RO_2 using a denuding method, Atmospheric Measurement Technique, 3, 1547-1554, (2010).

Miyazaki, K., Nakashima, Y., Schoemaecker, C., Fittchen, C., Kajii, Y., Note: A laser-flash photolysis and laser-induced fluorescence detection technique for measuring total HO_2 reactivity in ambient air, Review of Scientific Instruments, 84, 076106, (2013).

Monks, P. S., Gas-phase radical chemistry in the troposphere, Chemical Society Reviews, 34, 376-395, (2005).

Morrison, B. M. Jr., J. Heichken, The free radical oxidation of CH_2O in the presence of NO_2 and NO, Journal of Photochemistry, 15, 131-145, (1981).

Niki, H., Maker, P. D., Savage, C. M., Breitenbach, L. P., Atmospheric ozone-olefin reactions, Environmental Science and technology, 17, 312A-322A, (1983).

Ng, N. L., Kwan, A. J., Surratt, J. D., Chan, A. W. H., Chhabra, P. S., Sorooshian, A., Pye, H. O. T., Crounse, J. D., Wennberg, P. O., Flagan, R. C., Seinfeld, J. H., Secondary organic aerosol (SOA) formation from reaction of isoprene with nitrate radicals (NO_3), Atmos. Chem. Phys., 8, 4117-4140, (2008).

Paulson, S., J. H. Seinfeld, Development and evaluation of a photooxidation mechanism for Isoprene, Journal of Geophysical Research, 97, 20703-20715, (1992).

Perner, D., D. H. Ehhalt, H. W. Patz, U. Platt, E.P. Roth, A. Voltz, OH – radicals in the lower troposphere, Geophysical Research Letters, 3, 466-468, (1976).

Pitts, F., Pitts, J. Jr., Chemistry of the Upper and Lower Atmosphere. In: Theory, Experiment and Application. Academic Press, San Diego, CA; London: 1-969 (2000).

Ren, X., Hardera, H., Martineza, M., Lesher, R. L., Oliger, A., Simpas, J. B., Brune, W. H., Schwab, J. J., Demerjian, K. L., He, Y., Zhou, X., Gao, H., OH and HO_2 Chemistry in the urban atmosphere of New York City, Atmospheric Environment, 37, 3639-3651, (2003).

Ren, X., Brune, W. H., Mao, J., Mitchell, M. J., Lesher, R. L., Simpas, J. B., Metcalf, A. R., Schwab, J. J., Cai, C., Li, Y., Demerjian, K. L, Felton, H. D., Boynton, G., Adams, A., Perry, J., He, Y., Zhou, X, Hou, J., Behavior of OH and HO_2 in the winter atmosphere in New York City, Atmospheric Environment, 40, S252-S263, (2006).

Sadanaga, Y., J. Matsumoto, K. Sakurai, R. Isozaki, S. Kato, T. Nomaguch, H. Bandow,

Y. Kajii, Development of a measurement system of peroxy radicals using a chemical amplification/laser-induced fluorescence technique, Review of Scientific Instruments, 75, 864-872, (2004a)

Sadanaga, Y., Yoshino, A., Watanabe, K., Yoshioka, A., Wakazono, Y., Kanaya, Y., Kajii, Y., Development of a measurement system of OH reactivity in the atmosphere by using a laser-induced pump and probe technique, Review of Scientific Instruments, 75, 2648-2655, (2004b).

Schultz, M., M. Heitlinger, D, Mihelcic, A. Voltz-Thomas, Calibration source for peroxy radicals with built-in actinometry using H_20 and O_2 photolysis at 185 nm, Journal of Geophysical Research, 100, 18811-18816, (1995).

Shirley, T. R., Brune, W. H., Ren, X., Mao, J., Lesher, R., Cardenas, B., Volkamer, R., Molina, L. T., Molina, M. J. Lamb, B., Velasco, E., Jobson, T., Alexander, M., Atmospheric oxidation in the Mexico City Metropolitan Area (MCMA) during April 2003, Atmospheric Chemistry and Physics, 6, 2753-2765, (2006).

Stockwell, W.R., A homogeneous gas phase mechanism for use in a regional acid deposition model. Atmospheric Environment, 20, 1615–1632, (1986).

Stockwell, W.R., Middleton, P., Chang, J.S., Tang, X., The second generation regional acid deposition model chemical mechanism for regional air quality modeling, Journal of Geophysical Research, 95, 16343–16367, (1990)

Stockwell, W.R., Kirchner, F., Kuhn, M., Seefeld, S., A new mechanism for regional atmospheric chemistry modeling, Journal of Geophysical Research, 102, 25847–25879, (1997).

Stone, D., Whalley, L. K., Heard, D. E., Tropospheric OH and HO_2 radicals: field measurements and model comparisons, Chemical Society Reviws, 41, 6348-6404, (2014)

Su, F., J. C. Calvert, J. H. Shaw, Spectroscopic and kinetic studies of a new metastable species in the photooxidation of gaseous formaldehyde, Chemical Physics Letters, 65, 221-225, (1979)

Shu, Y., R. Atkinson, Rate constants for the gas-phase reactions of O3 with a series of terpenes and OH radical formation from the O3 reaction with sesuqioterpenes at 296± 2 K, International Journal of Chemical Kinetics, 26, 1193-1205, (1994).

Voigt, S., J. Orphal, J. P. Burrows, The temperature and pressure dependence of the absorption cross-sections of NO2 in the 250–800 nm region measured by Fourier-transform spectroscopy, Journal of Photochemistry and Photobiology A: Chemistry, 149, 1-7, (2002).

Watanabe, T., M, Yoshida, S, Fujiwara, K. Abe, A. Onoe, M. Hirota, S. Igarashi, Spin trapping of hydroxyl radical in the troposphere for determination by electron spin

resonance and gas chromatography/ mass spectroscopy, Analytical Chemistry, 54, 2470-2474, (1982).

Weinstock, B., Carbon Monoxide: Residence Time in the Atmosphere, Science, 166, 224-225, (1969).

Yarwood, G., Rao, S., Yocke, M., Whitten, G.Z., Updates to the Carbon Bond Mechanism: CB05. Final Report to the US EPA, RT-0400675. (http://www.camx.com/publ/pdfs/CB05_Final_Report_120805.pdf). (2005).